Ludwig-Maximilians-Universität München

Geomagnetic response from meteorite impacts

Dissertation
zur Erlangung des Doktorgrades
an der Fakultät für Geowissenschaften der
Ludwig-Maximilians-Universität München

vorgelegt von
Michael Eitel

München, den 18.12.2018

1. Gutachter: Prof. Dr. Stuart Gilder

2. Gutachter: Prof. Dr. Kai Wünnemann

Tag der mündlichen Prüfung: 06.05.2019

Contents

List of figures

List of tables

Summary

This work investigates the question whether shock waves generated by meteorite impacts can disturb the Earth's dynamo thereby triggering a geomagnetic field reversal or excursion. This hypothesis was originally proposed in the 1960s and 1970s with the discovery of tektite fields deposited around the same time as geomagnetic events. However, it is difficult to accurately resolve the timing of the impact with the lock-in of the magnetic remanence from sedimentary records. For this reason, melt rocks in impact craters were collected as a function of cooling time, e.g., from the margins toward the center of the melt sheets, to search for aberrations in the paleomagnetic record. This study investigated the Rochechouart (France) and Manicouagan (Canada) impact structures. The Rochechouart crater was chosen because an earlier study identified both normal and reversed directions in its melt rocks. The Manicouagan crater is one of the largest terrestrial craters that has thick (up to 1500 m) and accessible impact melts, making it a highly desirable candidate to search for impact-induced geodynamo effects.

The study at Rochechouart reported here identified samples that contain dual, nearly antipodal, paleomagnetic directions. The results from Curie point, hysteresis and paleointensity experiments, reflected-light microscopy, chemical analyses and Raman spectroscopy of the samples with normal and/or mixed polarities revealed magnetic mineralologies that typically possess self-reversal-type behavior. As samples with reversed polarity contained nearly stoichiometric hematite, which does not display self-reversal-type behavior, it was concluded that no geomagnetic field reversal or excursion was recorded in the Rochechouart impact melts – the presence of normal polarities was a rock magnetic artifact.

Impact melts and basement rocks collected at several localities on the surface of the ~85 km diameter Manicouagan crater, as well as samples from drill cores extending

up to 1500 m in depth, were studied for paleo- and rock magnetism. Neither paleomagnetic directions nor paleointensity data show significant deviation from expected values – they rather define variability typical of secular variation of the recent field. Impact melt samples with reliable directions span a thickness of 481 m, which corresponds to a maximum cooling time of 31,000 years. Since geomagnetic reversals last ca. 3-10 thousand years, such an event should have been recorded in the impact melts. Hence, a meteorite impact creating an 85 km diameter crater did not cause any observable disturbance of the geodynamo. Anisotropy of anhysteretic remanent magnetization experiments suggest the impact melts flowed radially from the center. Together with field observations, this is explained by outward flow of the impact melts away from the central uplift. Gravitational fractionation near the base of the thickest melt sheet produced an enriched layer in multidomain titanomagnetite that could be responsible for the presence of a distinct 2000-400 nT positive magnetic anomaly in the crater's center.

A summary is given on the magnetic characteristics of several terrestrial impact craters, with special focus on the Manicouagan (Canada), Mistastin (Canada), Ries (Germany), Rochechouart (France), and Vredefort (South Africa) craters. These craters share the communality of low to normal dispersion in paleomagnetic directions. None of the craters provided evidence for a geomagnetic event. It is also discussed how shock can permanently alter the magnetic mineralogy and/or remanence of ferromagnetic grains.

The fifth chapter of this thesis concerns an experimental study of the effects of heating on the acquisition of an anhysteretic remanent magnetization and on the coercivity spectrum of titanomagnetite-bearing impact melt rocks and obsidians. By comparing the sum of a pure thermal plus a high temperature anhysteretic remanence, it was found that the combination of thermal and anhysteretic remanence fulfills Thellier's law of additivity. Alternating field demagnetization experiments with and without prior heating show a positive correlation between Néel temperature and coercivity for the natural titanomagnetite-bearing rocks.

1 Introduction

Meteorite impacts are common events in the history of planets and moons, instantaneously changing the face of a celestial body from one moment to another. On Earth, due to erosion and tectonic processes, the larger or more recent impact craters can be recognized on the basis of their circular shapes. However, the classification of a circular structure as an impact crater is not straightforward, which is manifested by heated debate on their origin, whether they are internally (volcanic, kimberlitic, etc.) or externally derived. For example, the Highbury structure (Zimbabwe) was recognized from satellite images as a circular feature in 1985; however, its origin is still in doubt, not yet receiving the status of an accepted impact crater (Koeberl, 1994; Master et al., 1994; Reimold et al., 1994; Reimold and Koeberl, 2014). Other, now widely accepted impact craters (e.g., Sudbury, Canada) have for decades been called "cryptovolcanic" features due to their similarities with volcanic craters (see Stevenson and Stevenson [1980] for an overview). During impact, the target rocks are exposed to pressures up to several tens of GPa. Shock-metamorphic effects such as pseudotachylite, planar deformation features and shatter cones as well as high-pressure phases (e.g., diaplectic glass, mosaicism) give evidence for the impact origin of some craters (see Gucsik, 2009 and references therein), e.g., at Haughton, Canada (Robertson and Mason, 1975; Osinski and Spray, 2006) and Santa Fe, USA (Fackelmann et al., 2008; Cavosie and Lugo Centeno, 2014; Colón Lugo and Cavosie, 2014; Lugo Centeno and Cavosie, 2014).

Craters are also identified by gravity and magnetic data. Gravity anomalies over impact craters are mostly negative due to less dense sedimentary fill of the basin or by faulting and fracturing of the bedrock that decreases the density of the basement underlying the crater (Dence, 1964; Grieve and Pesonen, 1992; Elo, 1997). During me-

teorite impact events, new magnetic minerals can be created or the remanences in existing ferromagnetic grains can be overprinted. Magnetic field anomalies are positive or negative depending on the strength and direction of the present day magnetic field relative to the strength and direction of the magnetic remanence in the affected rocks, as well as the depth and dimensions of the magnetized material. Moreover, shock processes can lead to decomposition of magnetic minerals or induce a shock remanent magnetization in the target rocks (Beard, 2012; Plado et al., 2000).

One can also question whether meteorite impacts can influence the geodynamo. The temporal coincidence of the deposition of microtektite fields with geomagnetic events led several authors to propose an extraterrestrial origin for these events. Glass and Heezen (1967) associated the Australasian microtektite field with the Bruhnes-Matuyama reversal; Durrani and Khan (1971) and Glass and Zwart (1979) correlated the Ivory Coast microtektite field with the beginning of the Jaramillo subchron. However, due to differences in timing between the deposition of the microtectite fields and their respective proposed geomagnetic events, influences of meteorite impacts on the geodynamo were considered unlikely (Glass et al., 1991; Schneider and Kent, 1990; Schneider et al., 1992). In the Ries crater (Germany), Pohl (1977) discovered reversed polarities in the natural remanent magnetizations from the rocks created during the impact; magnetization directions in sediments deposited directly above the impact melts/suevites have normal magnetic polarities. These findings led Pohl (1977) to speculate that a field reversal, possibly caused by the impact, might have been recorded in the Ries lithologies.

The dipolar component of the geomagnetic field, which is responsible for about 90 % of the field intensity, is caused by the motion of the liquid iron in the Earth's outer core. This requires a mechanism to convert the energy released during the impact into disturbance of the magnetohydrodynamic regime in the outer core for an impact induced field reversal to take place. Several mechanisms linking meteorite impacts with changes of planetary magnetic fields have been proposed.

As an explanation for the statistical correlation found between periods of high cosmic flux and the frequency of geomagnetic reversals, Pal and Creer (1986) suggested

that during times of increased physical bombardment, additional turbulence would be introduced into the Earth's core and thus reverse the geomagnetic field. Muller and Morris (1986) presented a detailed model linking the correlation between impacts and geomagnetic reversals via redistribution of ocean water from low latitudes towards the poles where it is frozen as ice as a consequence of the cosmic winter caused by the impact. This process reduces the moment of inertia of the Earth's mantle, leading to an increase of the rotation rate of the mantle, while that of the Earth's inner core remains unaffected. In the case of a fast (a few centuries) sea level change, shear is introduced in the liquid outer core. For sea level changes of 10 m, Muller and Morris (1986) calculated a shear velocity of 0.3 mm/s at the bottom of the mantle. This value is comparable to the flow velocity in the outer core obtained from the actual drift of the non-dipole component of the geomagnetic field and is consistent with theoretical considerations. Burek and Wänke (1988) suggested that phase transitions are triggered from impact shock effects in the higher mantle. These phase transitions lead to a volume-decrease disturbing the morphology at the core-mantle boundary, thus leading to a geomagnetic field reversal.

On the other hand, a study by Loper and McCartney (1990) calculated that differences in the shear rate of the Earth's core and mantle are not possible since they are coupled too strongly to each other, leading them to exclude all of the above mentioned models. Rice and Creer (1989) showed that shock spallation from the inner core or from the mantle into the outer core cannot influence the geodynamo.

Roberts et al. (2009) suggested another mechanism how meteorite impacts can affect planetary magnetic fields by recalling that around 4.2 - 4.1 Ga, our solar system possessed an intense influx of meteorites. Roberts et al. (2009) proposed a sequence of large meteorite impacts that generated impact craters greater than 2500 km heated up the Martian mantle. This led to a reduction of the heat flux at the core mantle boundary, which resulted in the cessation of the Martian dynamo.

An alternative, perhaps more realistic model, was put forward by Won and Kuo (1973), who argued that seismic energy from an earthquake or impact travels through the Earth in form of shock waves that excite the inner core to oscillate (figure 1.1).

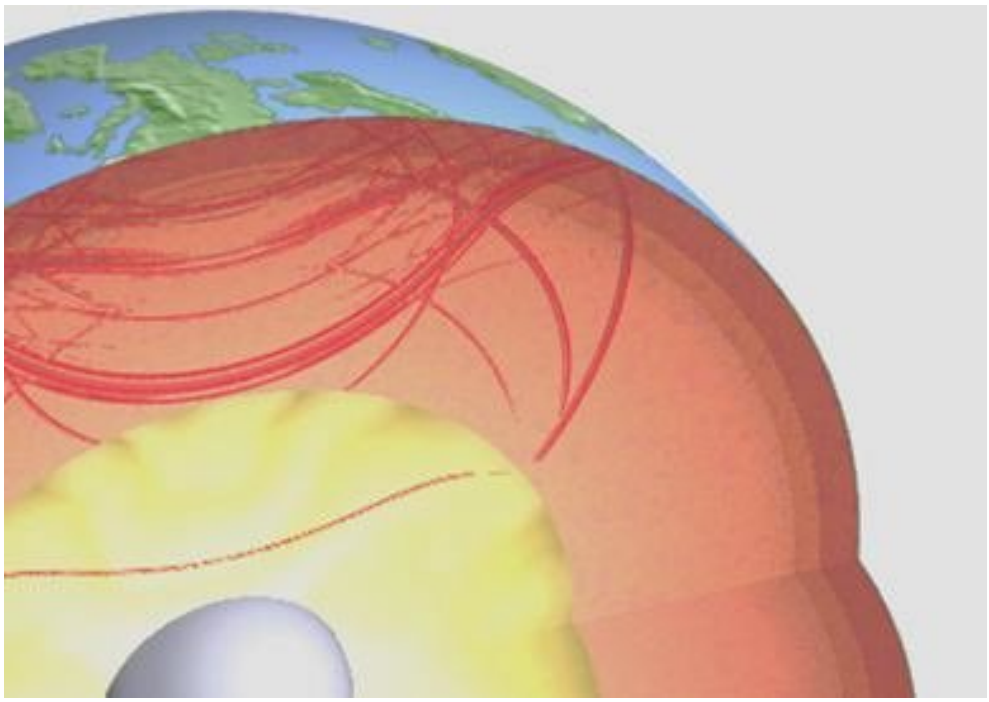

Figure 1.1: Model: Impact induced shock waves traveling through Earth cause the inner core to oscillate, hence perturbating the magnetic field and potentially causing a reversal or excursion (figure from Jahnke, 2010).

They calculated that a magnitude 8.5 earthquake releases 10^{18} J of energy, with about 4×10^{14} J being available to initiate inner core oscillation. This amount of energy leads to an oscillation amplitude of 58 cm with a period of 7.4 hours, which corresponds to an inner core oscillation velocity of 0.1 mm/s; the decay time is between 1000 and 10,000 years. The energy of large meteorite impacts exceeds earthquake energies by several orders of magnitude (e.g., 10^{22} J for Rochechouart, 10^{22} to 10^{23} J for Manicouagan and few 10^{23} J for Sudbury (Dence et al., 1977; Phinney and Simonds, 1977)). Although only $1/10^4$ of the impact energy is translated into seismic energy (Pierazzo and Melosh, 2013), the largest meteorite impacts still provide enough seismic energy to exceed the energy from large earthquakes by a few orders of magnitude. Once the Earth's inner core begins oscillating, it affects the outer core for thousands of years thereby disturbing the motion of the liquid iron, which could potentially result in a reversal or excursion of the geomagnetic field.

One of the main purposes of the current work is to investigate a potential influence of meteorite impacts on the geomagnetic field. Until present, most investigations were

carried out on sedimentary records. However, the magnetic field behavior after an impact is also recorded as a thermal remanent magnetization (TRM) in the rocks in craters that have been molten, or at least heated above their Curie temperatures. Moreover, as will be explained further below, a timeline of the geomagnetic field, is tracked by the cooling profile of the melt rocks and breccias created during impact. Thus, the link between meteorite impacts and abnormal behavior of the Earth's magnetic field can be tested using the TRM recorded in igneous rocks created by the impact and in the heated target rocks.

1.1 Crater Formation

Figure 1.2 shows the formation process of impact craters subdivided into three different stages (French, 1998; Gucsik, 2009). The contact/compression stage starts at the moment of the first contact of the bolide with the ground. From the point of contact, shock waves are transferred to the target rocks and are also reflected towards the back of the projectile. As soon as the shock wave reaches the bolide/target rock interface, which happens on the order of milliseconds up to a second, the contact/compression stage is finished. At that moment, depending on its size and energy, the meteorite is more or less entirely molten or vaporized due to the high shock pressures and temperatures.

During the excavation stage, the shock waves further propagate into the target rocks. This creates an outward flow of the material excavating the transient crater that expands until the shock waves become too weak to move more of the target rocks out of the cavity. The excavation stage ends after a few seconds to minutes when the transient crater reaches its maximum size (Grieve, 1991; French, 1998; Gucsik, 2009).

The excavation stage is followed by the modification stage, where mass redistribution occurs under the effect of gravity (French, 1998; Gucsik, 2009). The modification stage lasts on the order of minutes. It results, depending on the crater size, in a simple crater (bowl shaped, with diameters on Earth up to 2 to 4 km), a complex

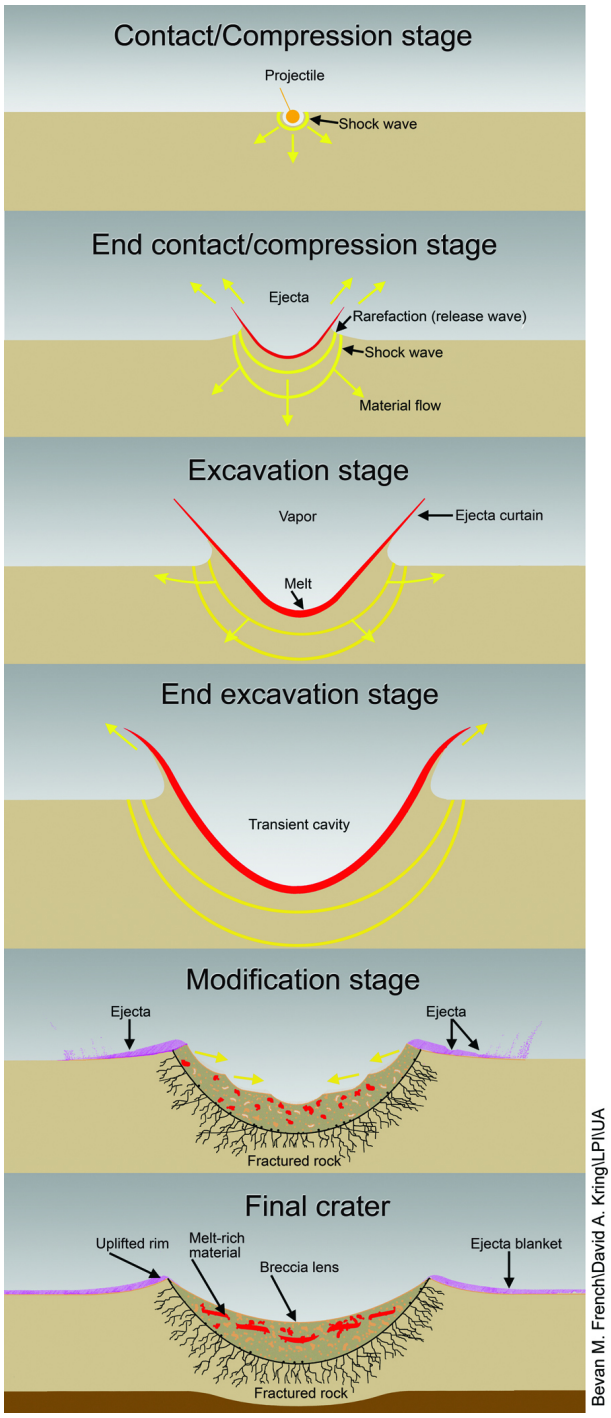

Figure 1.2: Stages of the formation of a meteorite impact crater. During the contact/compression stage, shock waves are transferred into the target rocks. Rock material is pushed away from the point of impact during excavation stage, forming a transient cavity. The modification stage contains the gravity driven collapse of the transient cavity and ends with the formation of the final crater. Figure courtesy of Kring, 2017.

crater (crater diameters up to ~100 km) including a central uplift in the form of a peak or ring, or in a multi-ring basin, when two or more inner rings exist (Dence et al., 1977; Grieve, 1991; French, 1998). Crater morphology depends on the size of the planet or moon, which dictate the gravitational acceleration at the surface.

1.2 Magnetic field recording in impact structures

Upon completion of crater formation, molten rocks may reside within the depression, forming an impact melt sheet. During cooling through the Curie temperatures of the ferrimagnetic minerals in the melt sheets, the ambient magnetic field is recorded. As the impact melt sheet cools from its margin towards the center, the geomagnetic field is recorded over time away from the margins of the melt body toward its center (figure 1.3). Thus, the impact melts provide a timeline of the geomagnetic field as a function of the cooling profile of the rocks.

To investigate the hypothesis of impact driven aberrations of the Earth's magnetic field, rocks were sampled from two meteorite impact craters for this thesis. To receive information from the longest possible time interval, and to maximize the chance of catching the record of a geomagnetic event, we sampled localities spanning the maximum possible vertical extent in the impact melts. Samples were collected at different altitudes assuming the melt sheets were emplaced horizontally and not tilted after their formation.

Among the limited amount of craters investigated for geomagnetic events is the 28 km-diameter Ries crater (Germany), which contains up to ~200 m of suevites and melt rocks. The paleomagnetic directions in the Ries suevites were extremely well grouped (Pohl, 1977) with very limited dispersion in geomagnetic field intensity (Koch et al., 2012), suggesting no significant change in geomagnetic activity proceeding impact. For the 28 km-diameter Mistastin crater (Canada), Hervé et al. (2015) came to the same conclusion based on tightly grouped directional variability of the magnetic remanences from multiple sampling sites. The strength of the ancient

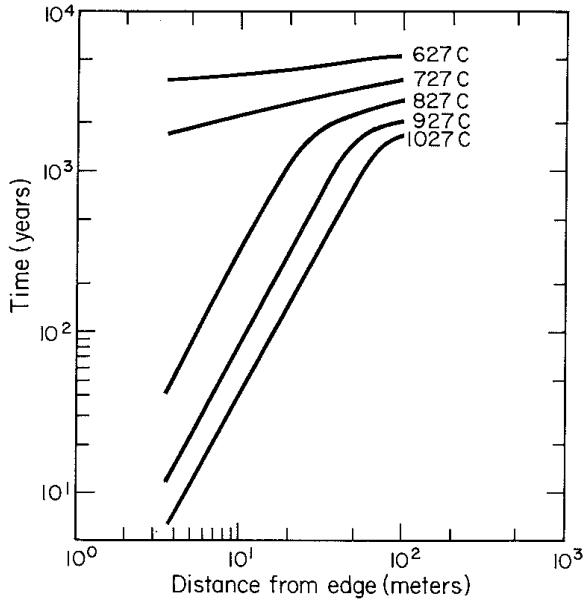

Figure 1.3: Cooling time of a 200 m thick impact melt sheet with a starting temperature of 1227°C to reach the indicated temperature as a function of the distance from the surface. Figure from Onorato et al., 1978.

geomagnetic field (paleointensity) was within uncertainty of the world-wide reference curve at the time of the impact (Biggin et al., 2010; Hervé et al., 2015).

In this work two craters were investigated for potential geomagnetic aberrations in the magnetic record of their impact melts. One of them was the Late Triassic Rochechouart crater (France), which today has a diameter of 26 to 28 km, of similar size as Ries and Mistastin (Kelley and Spray, 1997; Schmieder et al., 2010; Cohen et al., 2017), but has been highly eroded making its original diameter difficult to estimate – 40 to 50 km has been proposed (Lambert et al., 2010). Based on previous paleomagnetic studies, the Rochechouart crater is an appropriate case to study for an impact induced geomagnetic field reversal. Although Pohl and Soffel (1971) found solely reversed magnetization directions in the impact breccias, a study by Carporzen and Gilder (2006) also identified some suevites with normal polarities – antipodal to the reversed ones, which suggested that a geomagnetic field reversal occurred during cooling. Carporzen and Gilder (2006) speculated a geomagnetic reversal was recorded in the Rochechouart suevites and used the presence of both polarities to ar-

gue that enough time elapsed to sufficiently average secular variation. They did not consider the implications of finding a geomagnetic event in relation to the impact.

1.3 Original contributions from this thesis

Based on the findings in Carporzen and Gilder (2006), we carried out a new study on the Rochechouart crater to verify the existence of the reversal and determine its duration. I carried out paleomagnetic, rock magnetic, and microscopy experiments to identify the origin of the magnetizations in the Rochechouart impact melts. This work was published in *Earth and Planetary Science Letters* under the title, "Rochechouart impact crater melt breccias record no geomagnetic field reversal" (Eitel et al., 2014) and forms Chapter 2 of this dissertation.

The second impact crater I studied was Manicouagan (Québec, Canada). This Late Triassic impact structure was chosen because of its size and exceptionally thick impact melt sheet. With a rim-to-rim diameter of 85 km, Manicouagan is the sixth largest terrestrial crater listed in the Earth Impact Database (2018). Earlier paleomagnetic investigations on the Manicouagan melt sheet found only normal magnetization polarities with well-grouped directions (Larochelle and Currie, 1967; Robertson, 1967) although the thickness of the sampled rocks was not specified. The crater was considered volcanic in origin at that time. In our study, melt rocks spanning 481 m in thickness contained reliable paleomagnetic data. Assuming 100 m of the melt sheet was eroded, 481 m represents a total cooling time interval of 31,000 years, starting several hundred years after the impact. As geomagnetic field reversals last at least a few thousands of years and less than ca. 15 ka (Bogue and Merrill, 1992; Leonhardt and Fabian, 2007; Valet et al, 2012), if the impact at Manicouagan influenced the geodynamo, the effects should have been recorded in the Manicouagan impact melts.

Chapter 3 presents the paleomagnetic and rock magnetic results from the Manicouagan impact melts and basement rocks published in the *Journal of Geophysical Research* titled, "A paleomagnetic and rockmagnetic study of the Manicouagan impact structure: Implications for crater formation and geodynamo effects" (Eitel et al.,

2016). This paper was highlighted by the American Geophysical Union in its flagship journal, *EOS*. The manuscript includes anisotropy of magnetic remanence measurements in order to examine the flow direction of the impact melt during crater formation. I conducted all experiments and helped write the paper.

The following chapter (Chapter 4) comprises a book chapter that highlights our contributions of the Deutsche Forschungsgemeinschaft priority program *Planetary Magnetism* (SPP 1488) that funded my PhD work, "Magnetic Signatures of Terrestrial Meteorite Impact Craters: A Summary" (Gilder, Pohl and Eitel, 2018). As the title suggests, Chapter 4 gives an overview of terrestrial impact craters, the magnetic mineralogy of the rocks found in the craters and the magnetic anomalies of impact structures. It also discusses the effect of shock on magnetic minerals and their magnetic remanences. After compiling the paleomagnetic data from all the world's craters, we demonstrated that the paleomagnetic directions were consistent in each individual crater over the entire surface of the crater. This demonstrates that the craters were completely established over time scales less than it took the ferrimagnets to cool through their Curie temperatures and that no modification to the structures occurred thereafter. No evidence exists for a perturbation of the geomagnetic field in any terrestrial crater. I helped write this paper and drafted some of the figures.

The last chapter of this thesis combines thermal and alternating field (AF) demagnetization of natural titanomagnetite-bearing rocks to understand the behavior of the coercivity spectrum of titanomagnetite as a function of temperature. Dunlop and Bina (1977) published a similar study using artificial magnetite-bearing samples. We applied thermal fluctuation analysis (Néel, 1949; Dunlop, 1976) to our data.

This chapter also investigates the additivity of magnetic remanence (Thellier, 1938), which is valid for thermal remanent magnetization (TRM) of single domain (SD) particles. Experiments imparted a hybrid remanence with an anhysteretic remanent magnetization (ARM) at elevated temperature and a partial TRM through in-field cooling to room temperature to investigate whether the combined additivity of both types of remanences was fulfilled. Our study is the first to test the combined additivity of thermal and anhysteretic remanent magnetization. This chapter is currently in

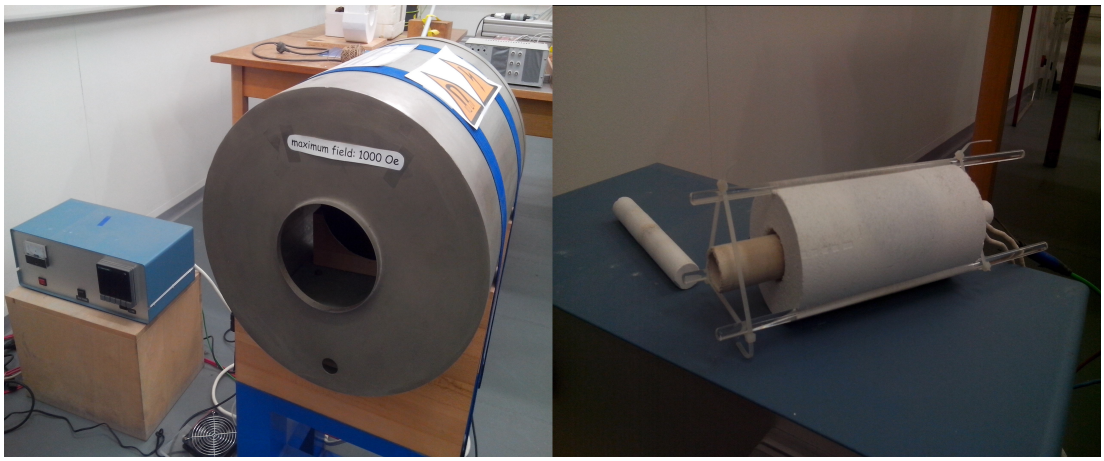

Figure 1.4: Magnetically shielded AF/ARM coil with temperature control unit and fan (not in place) (left) and high temperature insert (right).

preparation and will be submitted under the title, "AF demagnetization and ARM acquisition at elevated temperatures in natural titanomagnetite bearing rocks" to *Geophysical Journal International* (Eitel and Volk, in prep.). Michael Volk and I designed the experiment, conducted the research and wrote the manuscript. In order to be able to conduct the experiments, we had to design and build an oven that could be inserted into the AF-ARM coil (figure 1.4). A description of this unique instrumentation is provided in Chapter 5.

2 Rochechouart impact crater melt breccias record no geomagnetic field reversal

The following chapter (Eitel et al., 2014) was published under the title "Rochechouart impact crater melt breccias record no geomagnetic field reversal" in *Earth and Planetary Science Letters*.

2.1 Abstract

Impact melt breccias from the Rochechouart (France) meteorite crater possess paleomagnetic directions with both normal and reverse polarities, raising the question whether shock from the collision initiated a geomagnetic field reversal. Stepwise thermal demagnetization together with a suite of rock magnetic experiments, optical microscopy, Raman spectroscopy and electron microprobe analyses identify adjacent, multiphase, titanohematite in the samples containing normal and mixed polarities – typical of lithologies bearing self-reversal behavior stemming from magnetic exchange interaction. Melt breccias possessing mostly titanium-free hematite as the magnetic remanence carrier have solely reverse-polarity directions, leading to the conclusion that the Rochechouart meteorite impact did not spawn a geomagnetic event. Samples displaying paleomagnetic directions with normal or mixed polarity yield unreliable paleointensity data. 30 samples with reverse polarity that pass stringent data selection criteria from Thellier-Thellier paleointensity experiments with alteration, tail and additivity checks define an average field value of 12.8 ± 3.7 μT. This translates into a virtual dipole moment of $2.7 \pm 0.8 \times 10^{22}$ Am^2, which is relatively low, but within uncertainty of other Mesozoic paleointensity data.

2.2 Introduction

Meteorite impact craters form common topographic features on several planets and moons in our solar system. They are also found throughout the geologic record on Earth. The energy released during an impact can exceed that of the strongest terrestrial earthquakes by several orders of magnitude, leading one to question whether such events can perturb the magnetohydrodynamic regime in planetary interiors and influence the magnetic field generation process.

Glass and Heezen (1967) first argued that the Australasian microtektite field was deposited during the period coinciding with the last known reversal (Bruhnes-Matuyama) thereby linking changes in the geomagnetic field to a meteorite impact event. Durrani and Khan (1971) suggested that the slightly older Ivory Coast microtektite field was deposited just above the base of a brief magnetic chron known as the Jaramillo event. Further drilling in the Atlantic Ocean led Glass and Zwart (1979) to conclude that the Ivory Coast microtektite field was four times larger than previously thought. They correlated the tektite layer with the beginning of the Jaramillo event.

The association of meteorite impacts with geomagnetic field reversals led several workers to explore how an impact event could perturb the geodynamo (see Schwarzschild, 1987, for an overview). Won and Kuo (1973) worked out the conditions for which the solid inner core begins oscillating from translational motion due to an earthquake. They found that a magnitude 8.8 earthquake (10^{18} J of energy released) would provoke an inner core oscillation with an amplitude of 58 cm. The amount of inner core oscillation required to modify the magnetohydrodynamic regime in the outer core is unknown.

Muller and Morris (1986) postulated that the link between impacts and geomagnetic perturbation occurred through climate change. They calculated that if sea level fluctuations were large (≥10 m) and rapid (few hundred years) enough before adjustments in the moment of inertia could take place, then shear would occur between the Earth's mantle and its solid core, which would deform convection cells in the liquid

outer core and influence the Earth's magnetic field. Their scenario predicts that the dipole component of the geodynamo would diminish with a concomitant increase in multipole components, which are characteristics of field reversals and transitions. Pal and Creer (1986) performed a statistical analysis of field reversals and found a correlation with episodes of bombardment. Like Muller and Morris (1986), and later Burek and Wänke (1988), Pal and Creer (1986) postulated that meteorite impacts would create turbulence in the outer core leading to lower field strength and a departure from axial symmetry, consistent with reversal models. Roberts et al. (2009) proposed that bombardment by very large meteorites producing craters >2500 km in diameter could have completely stopped the Martian dynamo.

Loper and McCartney (1990) computed that dynamical coupling between the core and mantle is too strong to allow large angular displacements to occur and thus refuted the extraterrestrial origin models for field reversals of Muller and Morris (1986) and Pal and Creer (1986). Rice and Creer (1989) calculated that shock spallation, either at the core-mantle or inner-outer core boundaries, would not provide enough energy to significantly disturb the geomagnetic field. More detailed work on the Australasian and Ivory Coast microtektite fields, including a more detailed examination of sedimentation rates, led to further pessimism. Schneider and Kent (1990) and Glass et al. (1991) found the Ivory Coast field was laid down at least 8 kyr after the Jaramillo event started and 40 kyr before it ended, indicating that the impact responsible for the Ivory Coast tektites was not causally related to the Jaramillo polarity subchron. Burns (1990), de Menocal et al. (1990) and Schneider et al. (1992) placed the deposition of the Australasian microtektite layer 12-15 kyr before the Bruhnes-Matuyama polarity reversal, leading Schneider et al. (1992) to conclude against a casual link between impacts and geomagnetic reversals. Hartl and Tauxe (1996) subsequently found a global decrease in paleointensity approximately 15 kyr prior to the Bruhnes-Matuyama reversal, suggesting that it may have commenced earlier than previously thought – precisely at the time when the Australasian microtektites were deposited.

Tektite production represents only a small fraction of the material created/expulsed during meteorite impacts, whereas a much larger volume of the target rocks is heated, often melted, and deposited near the crater. For this reason, a more straightforward test for a relationship between meteorite impacts and geomagnetic field changes can be performed by examining the thermal remanent magnetization of the melt rocks and impact breccias (suevites) acquired during cooling through the Curie temperatures of the magnetic minerals after the impact. In a study of the ca. 15 Ma Ries crater (Germany), Pohl (1977) found that suevites had reverse polarities while sediments deposited on top of the suevites had normal polarities, leading to the suggestion that the impact may have triggered a field reversal. Paleointensity determinations on the suevite and impact melts from Ries yielded a virtual dipole moment of $3.2 \pm 0.2 \times 10^{22}$ Am^2 (Koch et al., 2012). Although relatively low, it is indistinguishable from the global paleointensity database between 20 and 10 Ma. A very small dispersion in magnetization directions (Pohl, 1977), together with limited variation in paleointensity, led Koch et al. (2012) to conclude that either the energy released from the Ries impactor was too small to affect the geodynamo, the Ries impactites cooled too fast to record any effect on the geodynamo and secular variation was not averaged, or the Ries impactites cooled slowly enough to record secular variation, but the geodynamo was remarkably stationary over secular variation time scales, either naturally or due to the impact.

In order to further examine the potential connection between geomagnetic disturbances and impact events, we now focus on the Rochechouart (France) meteorite crater where Carporzen and Gilder (2006) previously identified antipodal (normal and reverse) magnetization directions in the impact breccias. We collected new samples specifically to test the existence of a geomagnetic field reversal. In addition to stepwise thermal demagnetization, the samples were subjected to a suite of rock magnetic analyses and Thellier-Thellier paleointensity experiments.

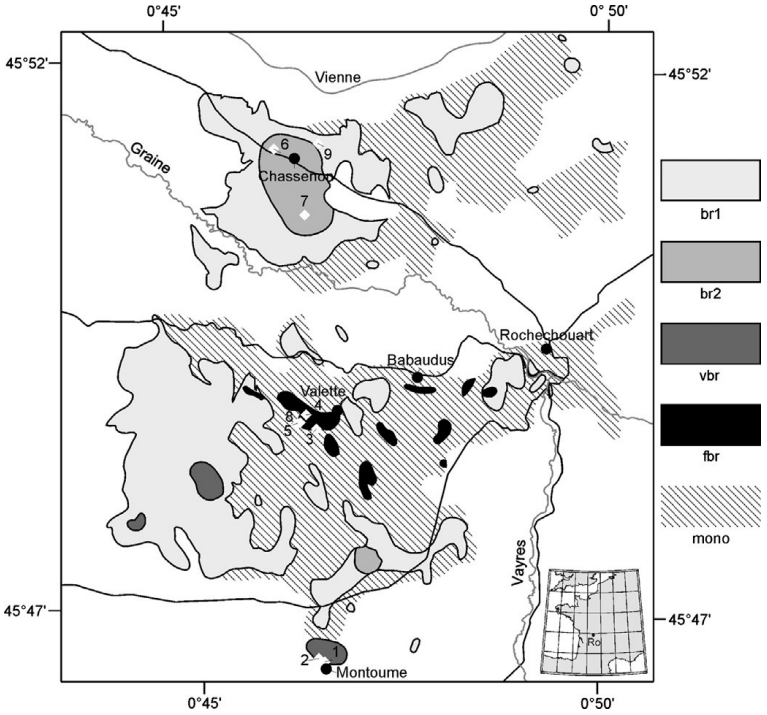

Figure 2.1: Locality and geologic map of the Rochechouart crater region (after Chèvremont et al., 1996) in western France (Ro in inset). Numbers are the sampling sites from this study. Abbreviations for the geologic units are: br1 – polymict, lithic breccia with no glass; br2 – polymict, lithic, glass-bearing breccia (Chassenon type suevite); vbr – red, melt-rich breccia (Montoume type suevite); fbr – polymict breccia with high degree of melting (Babaudus type suevite); mono – momomict breccia and cataclastite.

2.3 Geological setting and sampling

Located in west-central France (figure 2.1), the Rochechouart structure is a heavily eroded crater with no morphological expression, yet possesses a negative Bouguer anomaly 26-28 km in diameter centered on the impact-related lithologies (Pohl and Ernstson, 1994). Its maximum possible original size was estimated by Lambert (2010) in the 40-50 km-diameter range based on comparison with other craters. The presence of impact breccias, planar deformation features and shatter cones all attest that the area was struck by a bolide (Kraut and French, 1971; Lambert 1974, 1977a, 1977b; Reimold et al., 1984; Bischoff and Oskierski, 1987). Diaplectic quartz glass found in the crater indicates maximum shock pressures exceeded 35 GPa (Trepmann, 2008). Assuming a minimum diameter of 26-28 km for the Rochecouart crater, the

impact energy would be on the order of 10^{22} J, which translates into a radiated seismic magnitude of 9.0 based on the relation that the seismic energy equals 10^{-4} of the impact energy (Pierazzo and Melosh, 2013).

Several workers have dated the structure, yet those using the Ar-Ar technique are likely the most precise. $^{40}Ar/^{39}Ar$ laser spot fusion dating of pseudotachylite from the Champagnac quarry yielded a matrix age of 214 ± 8 Ma (Kelley and Spray, 1997). $^{40}Ar/^{39}Ar$ step heating of potassium feldspar from shocked gneiss yielded two plateau ages of 201 ± 2 Ma (Schmieder et al., 2010). Three types of impact breccia (suevite), classified by increasing degrees of melting, are identified at Rochechouart: Chassenon, Montoume and Babaudus (Lambert, 1974, 1977b; Chèvremont et al., 1996), with thicknesses ranging from a few meters up to 50-70 m (Lambert, 2010). Pohl and Soffel (1971) reported paleomagnetic results from the Chassenon and Montoume type suevites, while Carporzen and Gilder (2006), from the Montoume and Babaudus types. Chassenon and Montoume suevites yielded reverse-polarity magnetizations and Babaudus, normal-polarity magnetizations.

We collected 71 cores from nine sites with a gas-powered drill and oriented them using magnetic and, whenever possible, sun compass measurements with an automated orientation sensor linked to a small portable computer (Wack, 2012). The average measured magnetic declination anomaly of -0.3° ± 2.2° (N = 31) conforms well to that predicted by the international geomagnetic reference field (0.8°). Only nine samples from the Fonceverane Forest (near the village of Valette, figure 2.1) were found to possess normal polarities by Carporzen and Gilder (2006), so we specifically chose to augment the number of samples from there. At Montoume, we collected samples over the largest possible vertical extent (3 m) to see whether we could detect differences as a function of distance (cooling time) from the margin. For the Chassenon suevites, we obtained samples from the Roman quarry where Pohl and Soffel (1971) collected their samples and added two additional sites. All sampling was carried out under the auspices and kind hosting of Marie-France Yserd, Claude Marchat and François Mazeaufroid from the Association Pierre de Lune (http://www.espacemeteorite.com) in April 2010.

2.4 Experimental results

2.4.1 Stepwise demagnetization

Stepwise demagnetization experiments were performed on cylindrical specimens measuring 2.5 cm in diameter and 2.2 cm in height. The three components of the natural remanent magnetization (NRM) were measured with a three axis, 2G Enterprises Inc., cryogenic magnetometer situated in a magnetically shielded room at Ludwig Maximilians Universität (University of Munich) using the program of Wack (2010). Samples were stepwise thermally demagnetized using 15 temperature steps up to a maximum temperature of 680°C. Figure 2.2 shows orthogonal projections and normalized magnetization decay plots of representative samples. Remanent magnetization directions were determined with principle component analysis (Kirschvink, 1980); site-mean directions and confidence ellipses were calculated using Fisher statistics (Fisher, 1953).

All samples from Montoume have a single reversed magnetization component that trends univectorially to the origin on orthogonal demagnetization diagrams from the first demagnetization step until complete loss of magnetization at 670–680°C (figure 2.2a). The site-mean direction (Table 2.1) is indistinguishable at 95% confidence limits with that of Carporzen and Gilder (2006). Samples from Chassenon also exhibit reversed magnetization components (figures 2.2b to 2.2d), except the maximum unblocking temperatures are noticeably lower (625–650°C) than at Montoume. Of note is that, for all samples from site 9, the magnetization increases slightly after the 425°C step and then begins decreasing at the 575°C step (figure 2.2d).

The samples from Valette exhibit complicated demagnetization trajectories, being strongly dependent on the individual sampling site or outcrop within a site. A few samples, like R0_60 from site 8, possess a single reversed magnetization component (figure 2.2e). Samples from site 5 have solely normal-polarity directions (figure 2.2f), very similar to that found in sites 6 and 7 of Carporzen and Gilder (2006 – compare with their figure 1c). New to this study is that several samples, especially

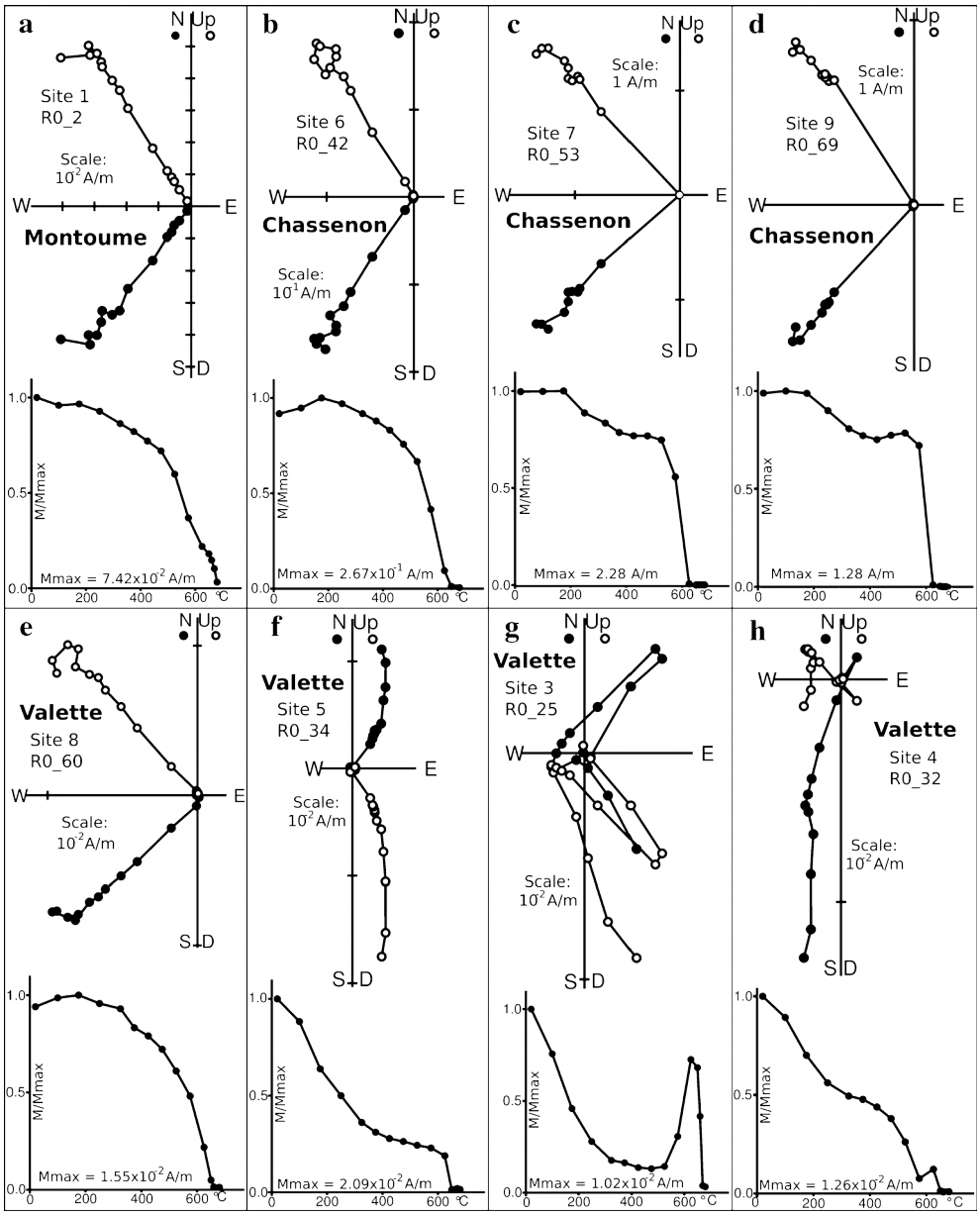

Figure 2.2: Orthogonal demagnetization diagrams and normalized magnetic moments of representative samples from the Rochechouart impact crater.

those from sites 3, 4 and 8, display multi-component demagnetization trajectories with both normal and reverse-polarity magnetization components (figures 2.2g and 2.2h). Often the sequence of magnetization components goes normal-reverse-normal, with the reverse segment being isolated between 425° and 625°C; complete demagnetization occurs around 650-660°C. The demagnetization behavior of the Valette

samples strongly resembles self-reversal behavior produced by antiferromagnetic exchange interaction from two magnetic minerals (e.g., Prévot et al., 2001).

Table 2.1 lists the mean directions and Fisher statistics for the sites that yield reverse-polarity directions excluding those from Valette. The precision parameter estimates (k) are generally high (>200) – typical of lava flows, with the exception of site 6 from Chassenon that deserves further comment. Each of the seven demagnetized samples yields trajectories that decay linearly to the origin from the beginning step to the end (figure 2.2b). The average direction agrees within 95% confidence limits of the other sites except k is about ten times lower than the other sites. The low k arises from two samples that have similar inclinations but more westerly declinations than the 5 others. These two samples lie 50 m apart from each other, yet less than 1 m from other samples. Excluding these two results in a much higher k, yet the site mean no longer clusters with the other sites (table 2.1). Whether all seven samples or just five are considered in the average has potential consequence on interpretations of secular variation. A study of the magnetic fabric on the same samples shows no correlation between the anisotropy ellipsoid and paleomagnetic direction, so we use the average direction based on all samples.

Table 2.1
Site-mean paleomagnetic directions from this study.

Site	Location	N/n	Dec (°)	Inc (°)	k	α_{95} (°)	Slat (°N)	Slon (°E)
1 + 2	Montoume	10/10	220.5	-41.1	357.5	2.6	45.776	0.775
3	Valette	0/9					45.811	0.772
4	Valette	0/6					45.813	0.770
5	Valette	0/7					45.812	0.769
8	Valette	0/8					45.812	0.768
6	Chassenon	7/7	222.3	-45.5	23.5	12.7	45.853	0.762
		5/7	209.2	-45.7	202.0	5.4		
7	Chassenon	4/6	222.8	-38.3	281.0	5.5	45.844	0.769
9	Chassenon	4/6	222.4	-46.9	403.6	4.6	45.854	0.771

Abbreviations are: N/n, number of samples used in the calculation/number of samples stepwise demagnetized; Dec., declination; Inc., inclination; k, best estimate of the precision parameter; α_{95}, the radius of the cone where the true mean direction lies with 95% confidence; Slat, site latitude in degrees north; Slon, site longitude in degrees east.

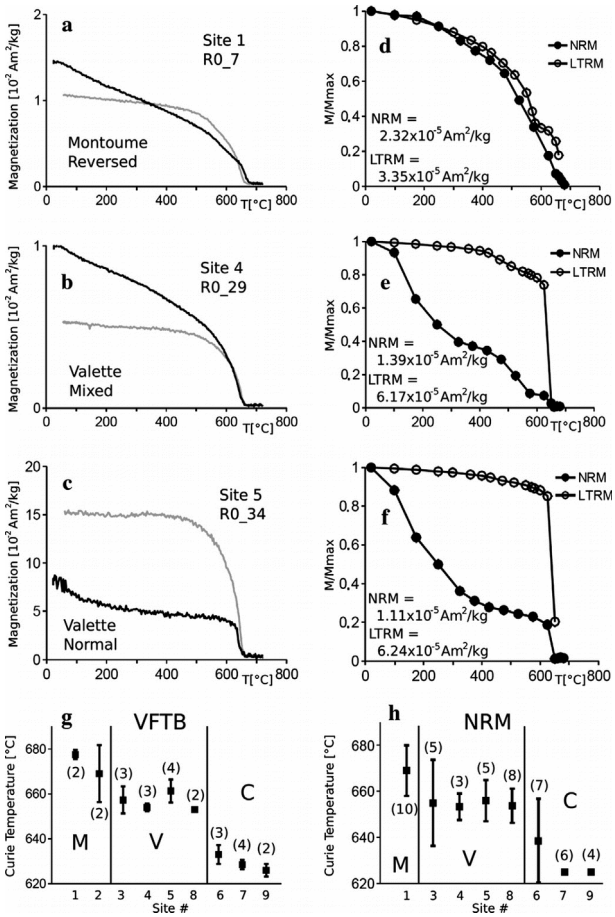

Figure 2.3: (a–c) Thermomagnetic curves of three samples from the Rochechouart crater measured in a 320 mT applied field with a Petersen Instruments, variable field translation balance (VFTB). The black (grey) curve represents the heating (cooling) cycle. (d–f) Corresponding normalized decay plots of the remanent magnetization. Solid circles denote the decay of the natural remanent magnetization (NRM), open circles denote the decay of a laboratory-imposed (50 μT) thermal remanent magnetization (LTRM). Normalized factors are provided in the plots. (g) Site-mean and single standard deviation of the Curie temperatures obtained from the thermomagnetic curves. (h) Site-mean and single standard deviation of the Curie temperatures obtained from stepwise thermal demagnetization of the NRM. Numbers above the uncertainties represent the number of samples used to calculate the mean; M is for Montoume, V, Valette and C, Chassenon.

2.4.2 Curie point experiments

Figures 2.3a to 2.3f show the temperature dependence of the magnetization for samples exhibiting normal, reversed and mixed polarities. Thermomagnetic curves (magnetization measured at the indicated temperature) were measured with a Petersen In-

struments, variable field translation balance (VFTB) with an applied magnetic field of 320 mT (figures 2.3a to 2.3c). Magnetomineralogic alteration during the experiments is evident when comparing the heating (black) and cooling (grey) curves. Site-averaged Curie temperatures reveal a conspicuous correlation with suevite type (figure 2.3g), yielding the following averages: Montoume 673° ± 9°C, Valette 656° ± 5°C and Chassenon 630° ± 4°C, suggestive of titanohematite with titanium concentrations of 0.4, 2.4 and 5.3%, respectively. That these Curie temperatures do not correspond to non-stoichiometric maghemite will be confirmed below.

Figures 2.3d to 2.3f plot the relative magnetization from the stepwise demagnetization experiments. As opposed to the VFTB data, stepwise demagnetization of the natural remanent magnetization (NRM) often show inflections at temperatures <600°C in addition to one in the 620°C to 680°C range. Site-averaged Curie temperatures for the high unblocking phase agree well with the VFTB measurements (figure 2.3h), yielding the following averages by suevite type: Montoume 669° ± 11°C, Valette 655° ± 10°C and Chassenon 631° ± 13°C.

To further explore the nature of the magnetic remanence carriers, we heated 29 samples from Montoume and Valette to 700°C, cooled them to room temperature in a 50 μT artificial field and then stepwise demagnetized the laboratory-imposed, thermal remanent magnetization (LTRM) (figures 2.3d to 2.3f). Magnetization directions parallel the applied field with no trace of self-reversal in each case. The normalized magnetization intensities for the Montoume samples are comparable between NRM and LTRM with the exception that a phase with a Curie temperature around 580°C, likely magnetite, becomes more pronounced (figure 2.3d). For the two samples from Valette suspected of harboring self-reversal behavior, the normalized intensity curves are quite different (figures 2.3e to 2.3f), with LTRM unblocking spectra that decay in a limited temperature range, yet the final unblocking temperatures are quite similar between LTRM and NRM.

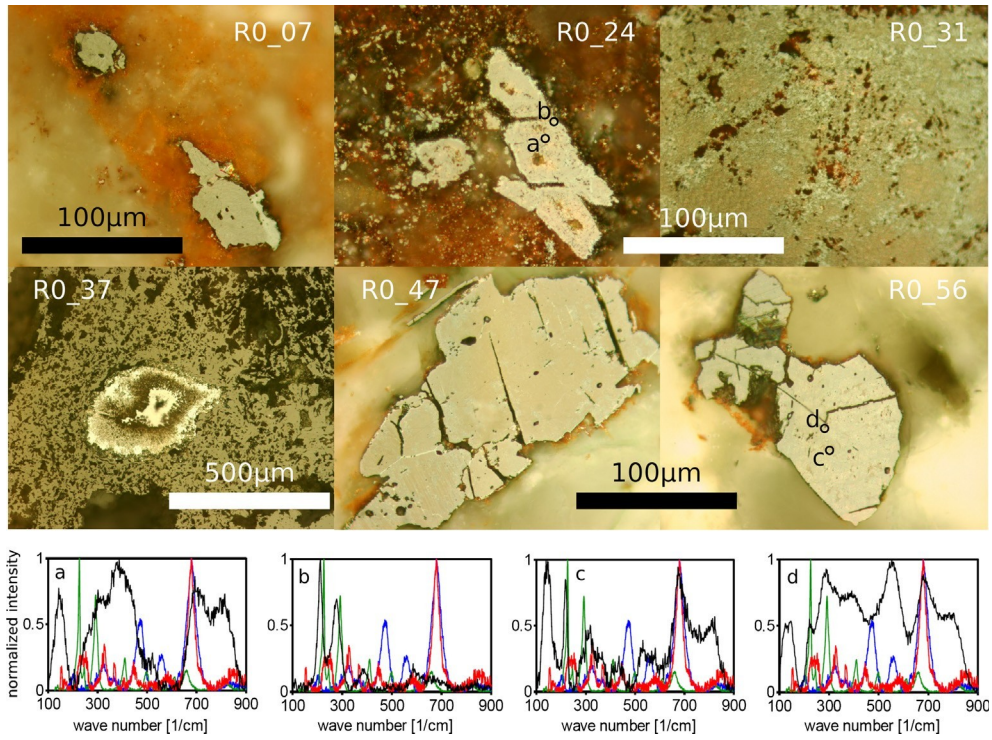

Figure 2.4: Upper part: Reflective light microscope images of iron oxides from impact melt breccias from the Rochechouart crater. Lower part: Raman spectra (black line) of samples R0_24 and R0_56. Circles and letters within the images denote the spots where the Raman spectra were taken. Reference Raman spectra from Downs (2006) are provided for hematite (green), magnetite (blue) and ilmenite (red). The samples come from the following sites and suevite types: R0_07 – site 1, Montoume; R0_24 – site 3, Valette; R0_31 – site 4, Valette; R0_37 – site 5, Valette; R0_47 – site 6, Chassenon; R0_56 – site 7, Chassenon.

2.4.3 Optical microscopy, Raman spectroscopy and electron microprobe analyses

Figure 2.4 presents reflected light optical microscope images of iron oxide grains in samples from six localities. The image of sample R0_07, red suevite from Montoume, shows two crystals included in a silicate matrix. Electron microprobe (Cameca SX100, University of Munich) analyses using an electron beam voltage of 15 kV and beam current of 40 nA show lamella of ilmenite adjacent to more iron-poor/titanium-rich lamella (30–40% FeO, 50–60% TiO_2; 1–4% MgO). We ascribe the latter to armalcolite [$(Mg,Fe)Ti_2O_5$], which has only been found at a few places on Earth, including the Ries crater in Germany (El Goresy and Chao, 1976) and in the

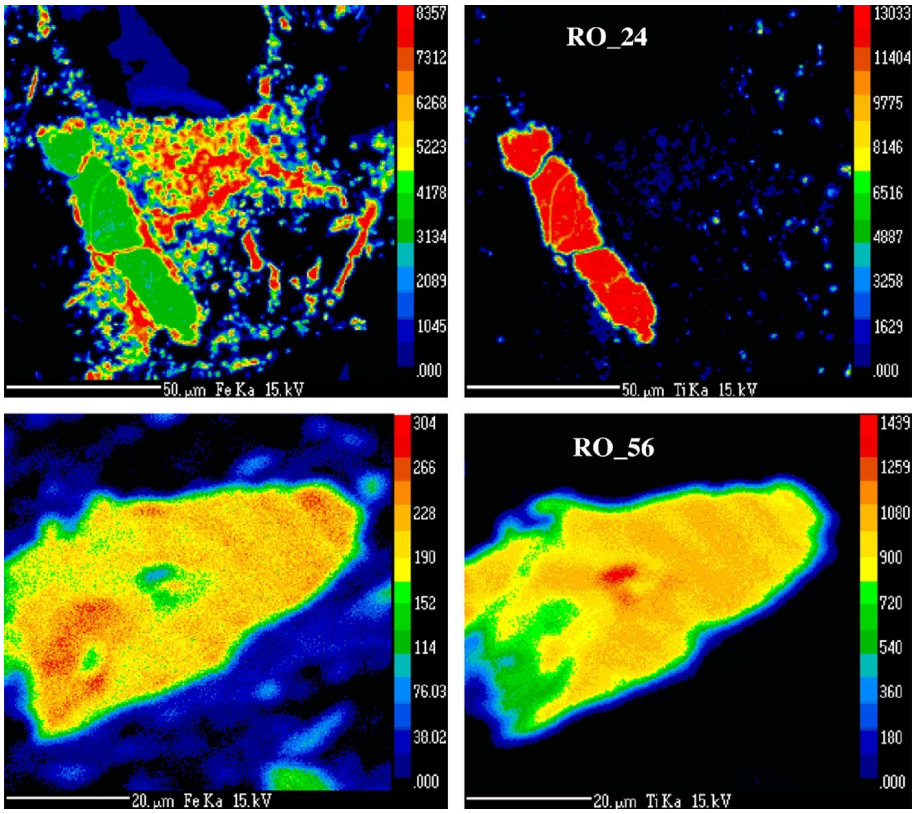

Figure 2.5: Electron microprobe concentration maps of two samples with multiple magnetization components (R0_24, from Valette) and (R0_56, from Chassenon). Relative iron (titanium) abundances are shown in the left (right) column; scale units are counts per second. The grain in sample R0_24 is an iron–titanium oxide surrounded by titanium-poor (∼2 mol%) titanohematite. The titanohematite grain in sample R0_56A contains a titanium-rich core.

Dhofar meteorites in Oman (Cohen et al., 2004). Hematite lies at the grain margins. The periodicity of the lamella is about 3 to 6 µm.

The Babadus-type suevites from Valette (figure 2.4, R0_24, R0_31 and R0_37) are riddled with vesicles. Large opaque grains are often fractured, with the cracks in between the pieces filled with silicate host rock material. Magnetic grains in R0_24 are sometimes zoned with a dark iron oxide phase at the center surrounded by a lighter iron oxide phase, which seems to have been produced via alteration of the darker phase. Raman spectra of the lighter phase indicate a chemical gradient with a more titanium-rich titanohematite toward the interior and less titanium-rich titanohematite toward the margins (figure 2.4: spots a and b). Chemical mapping of R0_24 (figure 2.5) coincides well with the Raman spectra, showing regions of titanium-rich

($Fe_{1.1}Ti_{0.9}O_3$) and titanium-poor ($Fe_{1.98}Ti_{0.02}O_3$) titanohematite. Titanium-poor, iron-rich material is also observed in a diffuse region away from the grain (figure 2.5). The Ti concentration of the Ti-poor phase matches well with the measured Curie temperatures.

Opaque minerals in Valette samples R0_31 and R0_37 lack sharp crystal faces due to severe alteration (figure 2.4). Because no present day field magnetization component was identified, the alteration likely occurred during suevite formation and not from recent weathering, consistent with the findings of Lambert (2010), who found that the Rochechouart impactites were metasomatized during post-impact hydrothermal activity. Magnetic minerals from Chassenon (R0_47 and R0_56) are less altered than at Valette, with those from site 8 (R0_56) being more altered than from site 6 (R0_47). Raman spectra of R0_56 (figure 2.4: spots c and d) reflect titanohematite, similar to R0_24 from Valette. Iron-titanium oxide grains from Chassenon are fractured. Chemical mapping of a grain in sample R0_56 (figure 2.5), reveals a high Ti, low-Fe titanohematite core surrounded by titanohematite with lower Ti and higher Fe titanohematite. In general we can conclude that the samples contain titanohematite with variable Ti concentration. Such magnetomineralogy is consistent with the measured Curie temperatures as well as being characteristic of rocks carrying self-reversed magnetizations (e.g., Nagata, 1953; Fabian et al., 2011; Swanson-Hysell et al., 2011).

2.4.4 Paleointensity

We carried out absolute paleointensity experiments following the Coe (1967a, 1967b) modified version of the Thellier-Thellier (Thellier and Thellier, 1959) method with alteration, tail and additivity checks using cylindrical cores with diameters of 5 and 8 mm. Heating was done in a Shaw oven with a 30 μT applied field. Figure 2.6 shows typical examples of Arai plots (Arai, 1963) and corresponding orthogonal demagnetization diagrams. Higher scatter in the declination component results from inaccuracies in orienting the small samples in the sample holder. Paleointensity data

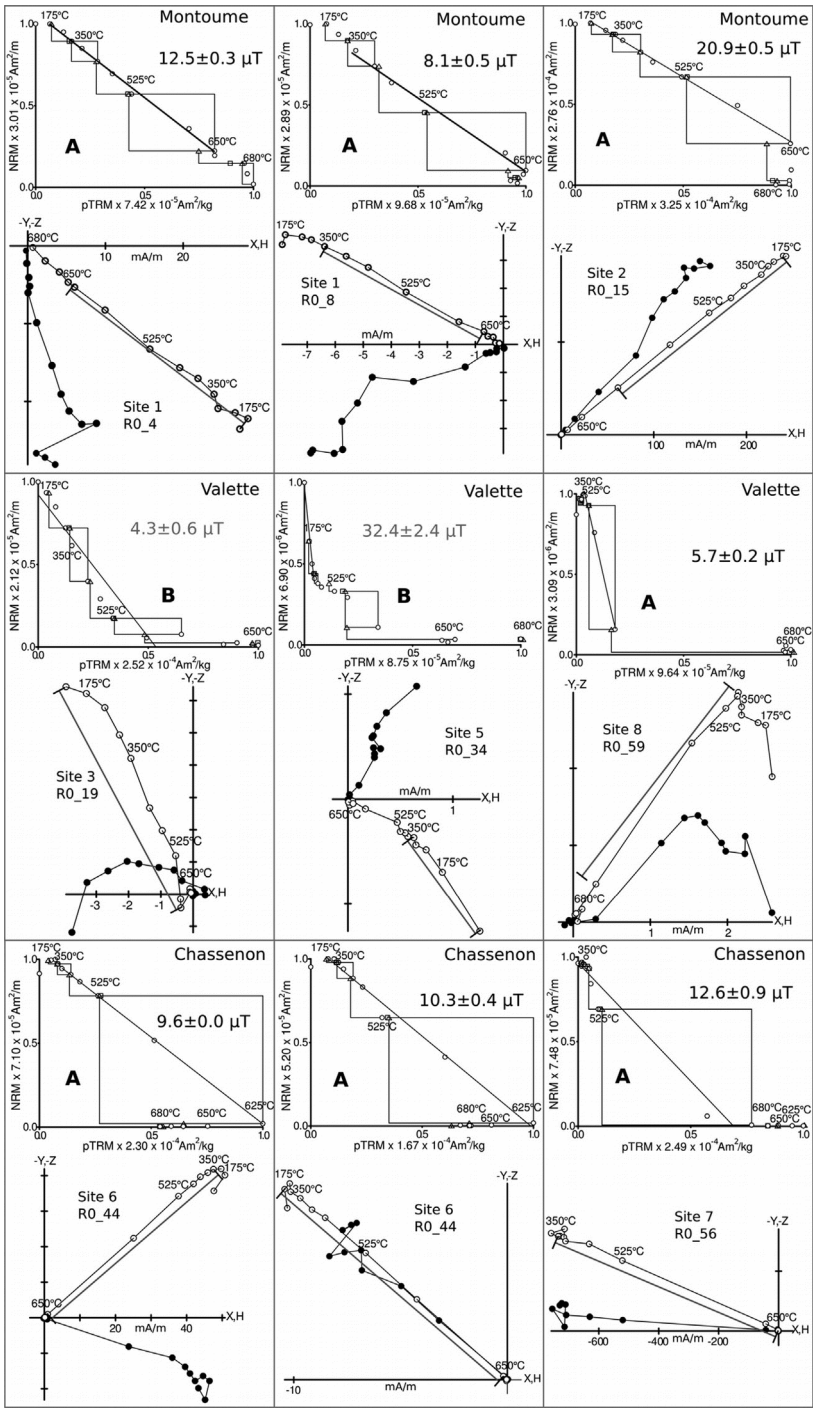

Figure 2.6: Arai plots and orthogonal demagnetization diagrams from the Thellier-Thellier paleointensity experiments. Three representative examples per suevite type are shown. The squares (triangles) in the Arai plots denote additivity (pTRM) checks. Paleointensity values are shown in black (gray) for samples that pass the Class A (Class B) criteria. In the orthogonal component diagrams, open (solid) circles denote the projection on the vertical (horizontal) plane, and the thick lines mark the temperature range used for the paleointensity determination.

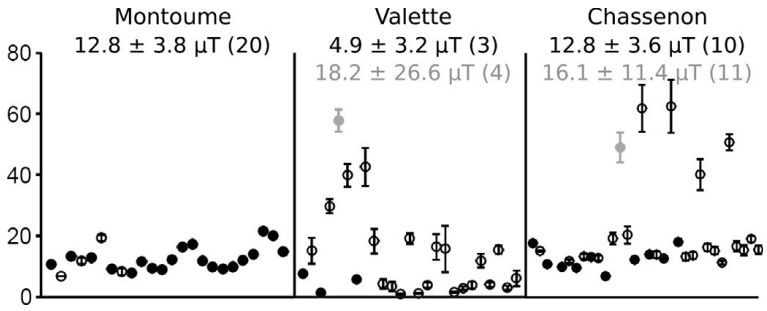

Figure 2.7: Paleointensity results from the Rochechouart impact crater. Solid circles represent samples that pass Class A acceptance criteria of the MT4 Thellier-Thellier paleointensity experiments (Leonhardt et al., 2004). Two outliers in gray (58 µT and 49 µT) did not pass the Class A criteria before check correction. Open circles are from non-Class A results. One Class B data point from Chassenon (131 µT) was removed. Average paleointensity values and single standard deviations are given for each suevite type, with the number of samples in parentheses. The overall mean paleointensity is 12.1 ± 4.3 µT (n = 33) for all Class A samples with two outliers removed, 15.8 ± 13.1 µT based on all fits (n = 80), and 12.8 ± 3.7 µT for Class A results from Montoume and Chassenon excluding one outlier.

were analyzed with the Thellier-Tool (Leonhardt et al., 2004). We ranked the best quality (Class A) results based on the following criteria: ≥5 consecutive temperature steps that comprise ≥50% of the NRM intensity, with an allowable difference of ≤10% between the NRM and LTRM intensity remaining at a given demagnetization step; ≤10% standard deviation on the linear fit with a maximum angular deviation of ≤6°; a quality factor (q) of ≥5 (Coe et al., 1978); ≤5% cumulative difference between pTRM* values (the partial thermal remanent magnetization acquired when cooling from a given temperature to room temperature in a field) and checks from room temperature up to the maximum temperature step; normalized tail parameters [Δ(t*)] of ≤3%; ≤5% relative intensity difference on the additivity check.

The Arai plots in figure 2.6 give examples of fits fulfilling Class A criteria, together with the paleointensity values; two Class B fits are shown for comparison. 20 of 24 samples from Montoume meet Class A requirements, for an average paleointensity of 12.8 ± 3.8 µT (figure 2.7; Table 2.2). Samples from Valette often have curved Arai plots and some, especially those with mixed polarity, have segments with positive slopes. Only 4 of 25 Valette samples attain Class A designation (figure 2.7) with an average of 18.2 ± 26.6 µT and 4.9 ± 3.2 µT after removing one outlier which did not

pass the Class A criteria before check correction (Table 2.2). All paleointensity results from Valette, regardless of class, are bimodally-distributed with one population around 4 μT and a second around 17 μT, which likely arises from the curvature of the Arai plots. Of concern is that the Class A paleointensities lie within this distribution. Several samples from Chassenon display linear slopes to 625°C, whereafter little of the original NRM remains, in agreement with the demagnetization and VFTB experiments. Paleointensity segments never exceeded 625°C. The average, Class A paleointensity (N = 11) for the Chassenon suevites is 16.1 ± 11.4 μT and 12.8 ± 3.6 μT after omitting one outlier that did not pass the Class A criteria before check correction (Table 2.2). Counting only data from Montoume and Chassenon and excluding the sole outlier leads to an average paleointensity of 12.8 ± 3.7 μT for the Rochechouart crater.

2.4.5 Anisotropy of TRM

To investigate the reason for the variability in paleointensity values, we measured TRM anisotropy for 16 samples from Montoume and Chassenon that yielded A class results following the procedure of Selkin et al. (2000) and Leonhardt et al. (2006). Samples were cooled from 700°C to room temperature in a 30 μT field in 6 directions (+x, -x, +y, -y, +z, -z), and then a final experiment in the +x direction was repeated to check for consistency. Only 5 of 16 samples met the consistency requirement with a <15% difference in total moment from the first step to the last. Of the five samples, all from Montoume (sample numbers 5, 8, 15, 16, 17), two samples with the lowest corrected anisotropy degrees (P' of Jelinek, 1981, both 1.04) have slightly oblate fabrics (shape parameter T of Jelinek, 1981 = 0.15 and 0.20), while the three with P' of 1.12, 1.21 and 1.28 have prolate fabrics with T = -0.54, -0.56 and -0.62. The average difference in anisotropy-corrected paleointensity is -0.9 ± 0.7 μT (n = 5), so slightly less than the original values (ranging from 10-21 μT), but there is no systematic change depending on original paleointensity or anisotropy parameters. Below we consider only non-anisotropy-corrected paleointensity estimates.

Table 2.2
Summary of the Class A paleointensity data from this study.

Site	Loc	Sample	D (mm)	T_{min} (°C)	T_{max} (°C)	N	f	g	q	Pint (μT)
1+2	M	R0_01	5	250	625	8	0.68	0.78	18.6	12.7 ± 0.4
1+2	M	R0_02	5	175	650	10	0.77	0.84	13.9	*13.2 ± 0.6
1+2	M	R0_02	8	300	625	7	0.58	0.78	10.2	17.8 ± 0.8
1+2	M	R0_03	5	175	660	11	0.90	0.84	44.2	13.4 ± 0.2
1+2	M	R0_04	5	175	575	8	0.66	0.79	30.3	9.4 ± 0.2
1+2	M	R0_04	8	175	625	9	0.73	0.83	24.7	12.5 ± 0.3
1+2	M	R0_05	5	175	575	8	0.51	0.80	16.8	8.2 ± 0.2
1+2	M	R0_05	8	175	625	9	0.74	0.84	25.4	10.0 ± 0.2
1+2	M	R0_06	5	175	575	8	0.60	0.77	21.5	10.1 ± 0.2
1+2	M	R0_07	5	175	625	9	0.75	0.76	21.0	9.1 ± 0.2
1+2	M	R0_07	8	250	625	8	0.72	0.78	15.9	9.3 ± 0.3
1+2	M	R0_08	5	350	625	6	0.73	0.74	9.1	8.1 ± 0.5
1+2	M	R0_08	8	300	680	11	0.94	0.80	18.0	*9.9 ± 0.4
1+2	M	R0_09	8	175	625	9	0.72	0.83	20.1	11.7 ± 0.3
1+2	M	R0_10	5	0	625	10	0.89	0.82	19.5	12.6 ± 0.5
1+2	M	R0_11	8	175	650	10	0.80	0.84	41.7	13.8 ± 0.2
1+2	M	R0_13	5	0	625	10	0.76	0.82	10.9	18.0 ± 1.0
1+2	M	R0_15	8	175	625	9	0.70	0.81	26.2	20.9 ± 0.5
1+2	M	R0_16	8	300	625	7	0.67	0.79	20.0	19.9 ± 0.5
1+2	M	R0_17	8	0	680	14	1.00	0.83	24.8	*14.8 ± 0.5
3	V	R0_19	5	175	525	7	0.75	0.81	10.8	*7.7 ± 0.4
3	V	R0_23	8	250	680	12	0.96	0.62	7.7	1.4 ± 0.1
5	V	R0_34	8	0	425	6	0.60	0.77	7.5	*57.8 ± 3.6
8	V	R0_59	8	425	625	5	0.69	0.48	8.3	5.7 ± 0.2
6	C	R0_41	5	350	625	6	0.77	0.68	108.1	17.6 ± 0.1
6	C	R0_43	5	250	625	8	0.75	0.80	11.1	12.5 ± 0.7
6	C	R0_44	5	175	625	9	0.92	0.73	16.4	10.3 ± 0.4
6	C	R0_44	8	350	625	6	0.88	0.61	144.8	9.6 ± 0.1
6	C	R0_45	8	175	625	9	0.88	0.73	10.4	15.3 ± 0.9
6	C	R0_46	8	350	625	6	0.88	0.63	26.0	6.4 ± 0.1
6	C	R0_47	8	0	680	14	0.96	0.85	8.2	*49.0 ± 4.9
6	C	R0_48	8	300	625	7	0.89	0.63	15.6	11.7 ± 0.4
7	C	R0_54	8	0	660	12	0.99	0.55	13.1	*14.0 ± 0.6
7	C	R0_54	8	0	625	10	1.00	0.51	6.8	12.8 ± 0.9
9	C	R0_70	8	0	625	10	1.00	0.51	6.3	18.1 ± 1.5

*Abbreviations are: Loc, locality; M, Montoume; V, Valette; C, Chassenon; D, core diameter; T_{min} and T_{max}, minimum and maximum temperature step for the paleointensity calculation; N, number of temperature steps used; f, the fraction of NRM; g, gap factor; q, quality factor; P_{int}, paleointensity value and standard deviation – *check corrected.*

2.5 Interpretation and conclusions

Stepwise demagnetization experiments reveal samples with normal, reversed or mixed (normal and reverse) polarity, which raises the question whether the rocks recorded a geomagnetic field reversal during cooling or whether one of the polarities and the mixed polarities arise from a rock magnetic self-reversal. An important new finding in this new study, not seen by Carporzen and Gilder (2006), is the presence of samples with mixed polarity, so the consequences of self-reversal behavior must be considered. Moreover, rocks containing titanohematite, like those from Rochechouart, are those that commonly exhibit self-reversal behavior (e.g., Hoffmann and Fehr, 1996; Prévot et al., 2001; Krása et al., 2005; Fabian et al., 2011).

Nagata (1953) first observed a self-reversal in a dacitic pumice from Mount Haruna, Japan. This finding led to a long-standing debate whether reverse-polarity magnetizations in rocks are not geomagnetic in origin, but rather due to an intrinsic property of the magnetomineralogy. Different mechanisms can account for self-reversal behavior (e.g., Néel, 1951; Verhoogen, 1956; Schult, 1968). One can be found in a single ferrimagnetic mineral whose two antiferromagnetically-coupled magnetic sublattices have different temperature dependencies such that in one temperature range, one of the sublattices has a larger net moment and in another temperature range, the other sublattice has a larger net moment (Néel, 1951). In these so-called N-type ferromagnets, a self-reversal occurs at the temperature where the two magnetic sublattices are equal and opposite in intensity.

Another self-reversal mechanism is caused by magnetostatic interaction between two decoupled magnetic phases (A + B) that have different Curie temperatures and spontaneous magnetizations; commonly the phase (A) with the higher Curie temperature has a lower spontaneous magnetization (Néel, 1951). During cooling, phase A acquires a magnetization parallel to the ambient field. Upon further cooling, when the remanence is blocked in phase B, the local field from mineral A exceeds the ambient field, which may induce a magnetization in the opposite direction as the ambient field depending on the geometrical arrangement of the two minerals, leading to a self-re-

versal because the magnetization of phase B is much higher than that of phase A. A third self-reversal mechanism via exchange interaction also requires two magnetic phases. In this case, the boundaries of the magnetic crystals are directly coupled with each other by sharing O^{2-} ions, which leads to negative magnetic interaction between the two phases. This phenomenon is common in titanohematite ($Fe_{2-x}Ti_xO_3$) with $0.53 \leq x \leq 0.71$ (Fabian et al., 2011).

That the Rochechouart suevites possessing mixed polarity also contain titanohematite supports self-reversal behavior as a likely explanation. The reversed polarity Montoume suevites possess relatively Ti-free hematite, whereas the normal-polarity samples from Valette contain titanohematite, which favors a reversed state of the geomagnetic field when the impact occurred. Moreover, demagnetization trajectories of the normal-polarity samples are systematically curved, whereas trajectories of the reversed polarity samples from Montoume decay univectorally toward the origin. None of the normal-polarity samples yield reliable paleointensity data, and even those few samples from Valette with Class A designations appear suspect. The stepwise demagnetization and paleointensity experiments as well as the rock magnetic investigations lead us to conclude that the Rochechouart suevites do not contain the record of a geomagnetic reversal, but rather strongly suggest a self-reversal mechanism acts in the samples with normal and mixed polarity; the geomagnetic field was likely in a reversed state when impact occurred.

The overall mean direction calculated from the four site-mean directions where self-reversal behavior is absent or limited (Montoume and Chassenon only) is declination 222.4° and inclination 43.0°; the radius of the cone where the true mean direction lies with 95% confidence (α_{95}) is 4.7° and the precision parameter (k) is 390. The corresponding virtual geomagnetic pole (VGP) lies at 107.5°E longitude and 50.3°N latitude ($A_{95} = 3.8°$), comparable to the VGPs found by Pohl and Soffel (1971) and Carporzen and Gilder (2006). The VGP from our study lies $9.4 \pm 5.0°$, $5.7 \pm 4.7°$ and $8.6 \pm 4.3°$ from the 200, 210 and 220 Ma VGPs for the European-plate apparent polar wander path (APWP) of Torsvik et al. (2008) (figure 2.8a), being clockwise rotated yet with negligible paleolatitudinal difference from the 210 Ma or 220 Ma

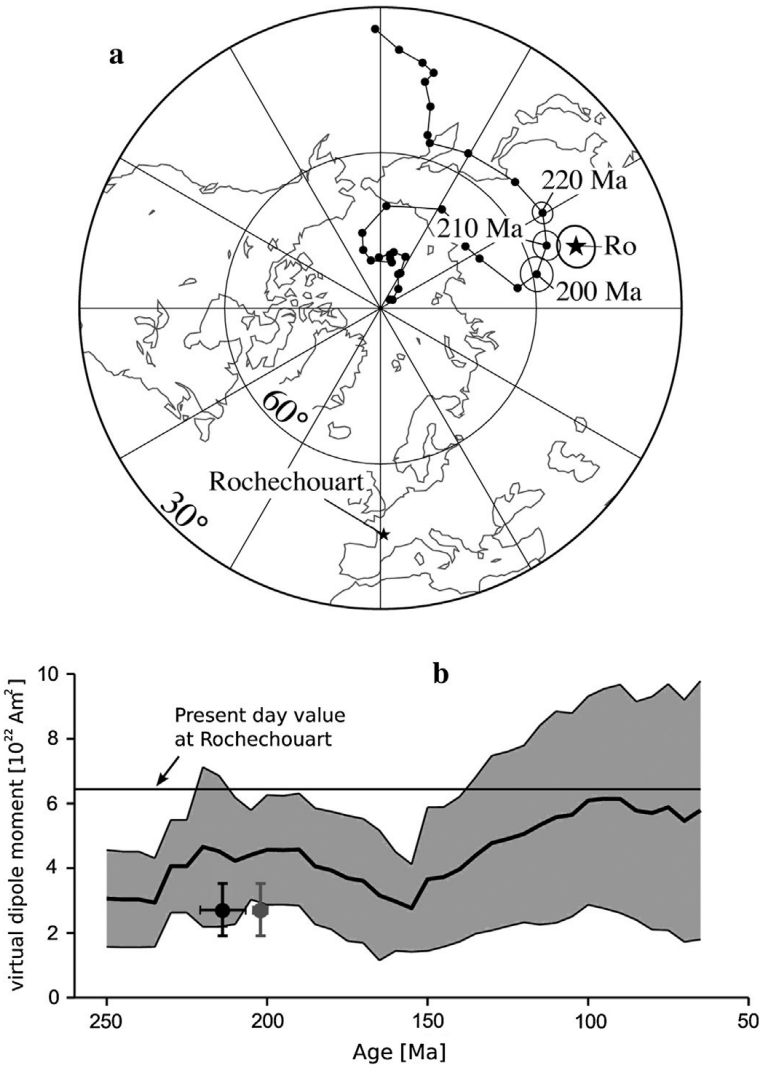

Figure 2.8: (a) Comparison of the Rochechouart (Ro) pole from this study with the apparent polar wander path for Europe (Torsvik et al., 2008). (b) Evolution of the virtual dipole moment in the Mesozoic using a running average (thick black line) with a window size of 20 Ma; the grey region represents the single standard deviation (PINT database of Biggin et al., 2010). The black circle with black uncertainties denotes the virtual dipole moment from the Rochechouart crater ($2.7 \pm 0.8 \times 10^{22}$ Am^2, n = 30) for 214 ± 8 Ma (Kelley and Spray, 1997) and in grey for 201 ± 2 Ma (Schmieder et al., 2010).

poles, whereas the comparison with the 200 Ma pole requires both clockwise rotation and latitudinal displacement. Hence, the paleomagnetic results better match the 214 ± 8 Ma age determination (Kelley and Spray, 1997) than that of 201 ± 2 Ma (Schmieder et al., 2010); however, it is entirely possible that the Rochechouart pole did not average secular variation, and thus its comparison with an APWP as a dating tool would not be valid.

Based on coeval ages between Rochechouart (214 ± 8 Ma) and the Manicouagan (214 ± 1 Ma; Hodych and Dunning, 1992) crater in Canada, Kelley and Spray (1997) proposed both formed from the fragmentation of a single meteorite. The concordance between the paleomagnetic poles of both craters at the 95% confidence level after accounting for opening of the Atlantic Ocean supported this hypothesis (Carporzen and Gilder, 2006). This assumed that the Rochechouart pole averaged secular variation because the presence of two polarities suggested that enough time lapsed during cooling among the various sites. However, if the Rochechouart pole does not average secular variation, and recalling that Rochechouart and Manicouagan have opposite magnetization polarities (Kent, 1998), the coherency between the Rochechouart and Manicouagan poles could be fortuitous. Further radiometric dating is surely needed for Rochechouart, especially from facies containing impact melts.

The overall mean paleointensity of the 30 Class A results is 12.8 ± 3.7 μT when omitting the Valette data and one outlier from Chassenon. From this value and the mean inclination of 43°, the virtual dipole moment for Rochechouart is $2.7 \pm 0.8 \times 10^{22}$ Am^2. Figure 2.8b compares the virtual dipole moment of Rochechouart with the Mesozoic database of Biggin et al. (2010). Rochechouart lies at the lower end, but still within one standard deviation of the reference data, similar to the virtual dipole moment obtained from the ca. 15 Ma Ries (Germany) crater, which was also low ($3.2 \pm 0.2 \times 10^{22}$ Am^2) but within uncertainty of the paleointensity data from 20 to 10 Ma (Koch et al., 2012). On the other hand, Rochechouart exhibits a much larger relative variability in paleointensity (standard deviation/mean) than at Ries. This is likely not attributed to a bias by magnetic fabric, but possibly due to longer time averaging during the cooling of the impact melts.

At the Rochechouart crater, we observe no evidence for a change in the geomagnetic field caused by the meteorite impact. One reason for this could be that the energy released by the impact was too low to influence the geodynamo. Keeping in mind that the melt sheets at Rochechouart are relatively thin (a few to several 10s of meters), it could be that the suevite cooled too quickly to leave a trace of a geomagnetic disturbance in the paleomagnetic record. It would be worthwhile to test this hypothesis at

larger impact craters where higher impact energies have been produced and where thicker impact melt sheets cooled over a longer time interval.

2.6 Acknowledgments

We thank Marie-France Yserd, Claude Marchat and François Mazeaufroid from the Association Pierre de Lune for their kind hosting and logistical help. Jérôme Gattacceca and an anonymous reviewer provided insightful reviews. Editorial handling by Lars Stixrude and financing by Deutsche Forschungsgemeinschaft project GI712/6-1 under the auspices of SPP1488 are also much appreciated.

3 A paleomagnetic and rock magnetic study of the Manicouagan impact structure: Implications for crater formation and geodynamo effects

The following chapter (Eitel et al., 2016) was published under the title "A paleomagnetic and rockmagnetic study of the Manicouagan impact structure: Implications for crater formation and geodynamo effects" in *Journal of Geophysical Research: Solid Earth*.

3.1 Abstract

We report rock magnetic and paleomagnetic data from the ~214 Ma Manicouagan (Canada) impact crater based on 25 widely distributed sites of impact melt and basement rocks collected at the surface as well as from boreholes drilled to depths ≤1.5 km. Titanomagnetite and titanohematite carry the magnetic remanence in impact melts above 320 m elevation and in most basement rocks. Impact melts below 320 m contain solely titanomagnetite. Magnetic susceptibility and saturation magnetization, proxies for titanomagnetite concentration, increase more than tenfold toward the base of the thickest impact melt that underwent fractional crystallization. The titanomagnetite-enriched zone partially contributes to a 2000 nT magnetic anomaly in the crater's center. Stepwise demagnetization reveals a single, normal polarity magnetization component in all samples regardless of the magnetic phases present. Coeval lock-in remanence times for titanomagnetite and titanohematite indicate that the titanohematite formed >570°C during oxi-exsolution. The average paleomagnetic direction and intensity coincide well with 214 Ma reference values. We find no evidence for an aberration of the geomagnetic field over the several thousands of years

it took to cool a 481 m thick portion of the impact melt body. Hence, the energy released by the Manicouagan impact that created one of the 10 largest known craters on Earth provoked no measurable disturbance of the geodynamo. Magnetic anisotropy of clast-free impact melts define magnetic lineation directions that are, in places, radially oriented with respect to the crater's center. Centrifugal flow of the melt within the evolving transient crater probably generated the fabric.

3.2 Introduction

Meteorite impact craters are common morphologic features in the solar system. The energy released during impact events can exceed that of the largest terrestrial earthquakes by several orders of magnitude. Some of this kinetic energy penetrates deep within the planet, potentially influencing the magnetohydrodynamic regime in the core, which could in turn perturb the dynamo generation process (see Eitel et al. (2014) for a more detailed discussion). Evidence linking meteorite impacts to anomalous magnetic field behavior arises from correlating tektite layers with the paleomagnetic records in marine sediments (Glass and Heezen, 1967; Durrani and Khan, 1971; Glass and Zwart, 1979; Hartl and Tauxe, 1996); however, the correlations are highly debated (Burns, 1990; deMenocal et al., 1990; Schneider and Kent, 1990; Glass et al., 1991; Schneider et al., 1992).

To test the link between dynamo perturbation and high-energy shock events, we initiated a paleomagnetic study of rocks within meteorite craters whose ferromagnetic minerals cooled through their Curie temperatures after impact. The objective is to sample impact lithologies as a function of cooling time, e.g., from the margins toward the interior of impact melt sheets, to identify potential changes in magnetic field direction and/or intensity. To date we have carried out such work in the Ries (Germany (Koch et al., 2012)), Rochechouart (France (Eitel et al., 2014)), and Mistastin (Labrador, Canada (Hervé et al., 2015)) craters. Anomalous field behavior has not been observed in any of them – possibly because the energy released from these impact events was insufficient to have an influence or because the rocks cooled too

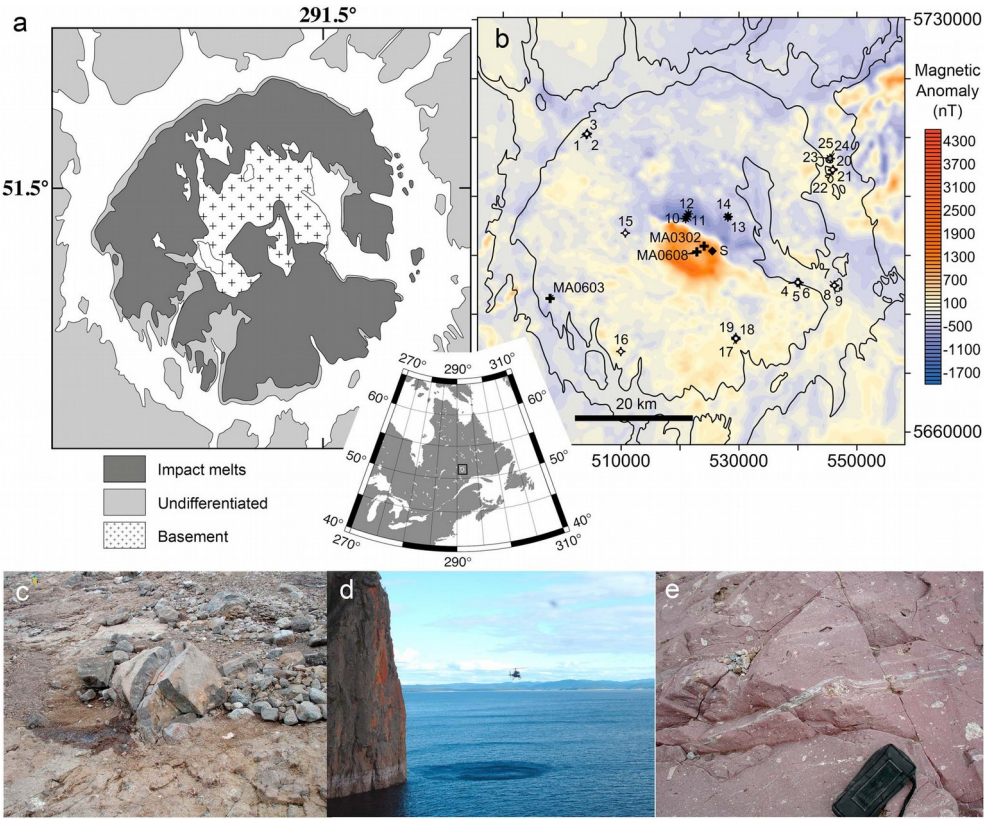

Figure 3.1: (a) Simplified geologic map of the Manicouagan impact crater (after Spray et al., 2010) with regional geographic location map (inset). (b) Magnetic anomaly map (Natural Resources of Canada, Geoscience Data Repository for Geophysical Data, 2014: http://gdr.agg.nrcan.gc.ca/gdrdap/dap/search-eng.php) including paleomagnetic sampling sites (numbered open symbols are impact melts, and filled symbols are basement rocks); drill cores used in this study are represented by pluses (e.g., MA0608); S is the drill core analyzed by Scott et al. (1996). Field photos of (c) site 5 showing melt-bearing breccias with highly rounded basement clasts with diameters ranging from centimeters to meters; (d) impact melts near sites 8 and 9 – annular lake and helicopter in view to south; and (e) basal, clast-laden impact melt near site 24 showing a flow fabric.

fast after impact and "missed" the event. The amount of time captured by the magnetic record in these craters did not exceed 400 years.

We now focus on the Manicouagan crater (Québec, Canada; figure 3.1), whose rim-to-rim diameter of 85 km ranks it as one of the ten largest impact craters on Earth (Earth Impact Database, 2015) – 2 to 3 times larger in diameter than the craters we previously studied. Estimates of the energy released from this event range between 10^{22} and 10^{23} J (Dence et al., 1977; Phinney and Simonds, 1977). Moreover, recent drilling results reveal melt thicknesses up to 1500 m at Manicouagan, which, except

for Sudbury, exceed other known terrestrial impact melt bodies nearly tenfold (Spray and Thompson, 2008), potentially allowing us to sample a much longer record of field behavior following the impact event. Cooling rate calculations, which have inherent uncertainties, such as the original thickness and initial temperature of the melt, suggest that the paleomagnetic remanence archives up to several thousand to tens of thousands of years succeeding the impact event (i.e., over similar time scales as expected for geodynamo activity resulting in excursions or reversals). Here we report the paleomagnetic results from impact melt and crystalline basement rocks collected from a wide spatial area within the crater, as well as those obtained from three drill cores penetrating the impact melt body. We also present the results of a wide range of rock magnetic experiments (Curie temperature, anisotropy of magnetic remanence, etc.) and paleointensity data. All experiments were performed in laboratories at Ludwig-Maximilians-Universität (Munich).

3.3 Geological setting and sampling

The Manicouagan structure in Québec (Canada, 51.4°N, 68.7°W; figure 3.1) formed when a 4 - 6 km diameter projectile impacted Proterozoic crystalline bedrock at hypervelocity. Several isotopic methods define a Late Triassic age for the impact. The K-Ar method applied to the impact melt yielded 210 ± 8 (2σ) Ma (Wolfe, 1971), which was recalculated at 214 ± 8 Ma using revised decay constants (Steiger and Jäger, 1978; Grieve, 2006). Jahn et al. (1978) obtained an Rb-Sr isochron age of 214 ± 5 Ma, while U-Pb dating on zircons defined a concordant age of 214 ± 1 Ma (Hodych and Dunning, 1992). An initial strontium $^{87}Sr/^{86}Sr$ value of 0.7099 supports the interpretation that the impact melts were derived from the Proterozoic basement (Jahn et al., 1978; O'Connell-Cooper et al., 2012). Zircons extracted from the melt sheet yielded 213.2 ± 5.4 Ma based on (U-Th)/He (van Soest et al., 2011); (U-Th)/He applied to titanite separated from anorthosite in the central uplift yielded 208.9 ± 4.1 Ma (Biren et al., 2014). Diaplectic glass from basement rocks lying 10–12 km from the crater's center is suggestive of shock pressures ~35 GPa (Grieve and

Head, 1983), while stishovite and maskelynite in the central uplift connote peak shock pressures from 12 to 30 GPa (Biren and Spray, 2011).

The Manicouagan structure is one of the best preserved and well-exposed impact craters on Earth (Spray et al., 2010). Impact melt sheet occurrences are restricted to the central 55 km diameter island (Île René Levasseur), with rim collapse features occurring on the mainland at ~65 km diameter and beyond. The central island is separated from the mainland by the Manicouagan reservoir, which is part of a hydroelectric program initiated in the 1960s. From 1994 through to 2006, a number of drilling operations took place on the island to appraise the structure as a potential analogue for the Sudbury impact structure of Ontario – a crater renowned for its world-class Cu-Ni sulfide and platinum group element deposits. While no significant economic indicators have been found to date, the drilling programs furnished ~18 km of core, 10 km of which is now held by the Planetary and Space Science Centre at the University of New Brunswick. Moreover, four holes exceed 1.5 km in depth, thus providing an unprecedented window into the deeper structure of the crater stratigraphy (Spray and Thompson, 2008). Specifically, the 1.5 km deep M0608 drill hole, situated close to the geometric center of the structure, penetrated >1 km of clast-free, differentiated impact melt and a further 400 m of clast-laden impact melt before encountering footwall basement rocks. Thicker (~500 m) sections of clast-free impact melt were also present in two other holes, drilled to the north and south of M0608. Other centrally located drill holes to the east and west, with only a thin layer of impact melt, or none at all, aid in delineating a probable fault controlled N-S trough of impact melt and demonstrate a locally castellated structure to the crater floor at Manicouagan (Spray and Thompson, 2008). Previous estimates, based on surface mapping and sampling, placed the melt sheet thickness at 200–300 m (Floran et al., 1978).

In August 2010, we drilled and oriented 198 cores at 25 sites in impact melts and basement rocks throughout the crater; most basement rocks come from near the central uplift (figure 3.1b). Cores were oriented either manually with a magnetic compass or with an automated system (Wack, 2012). The average declination anomaly

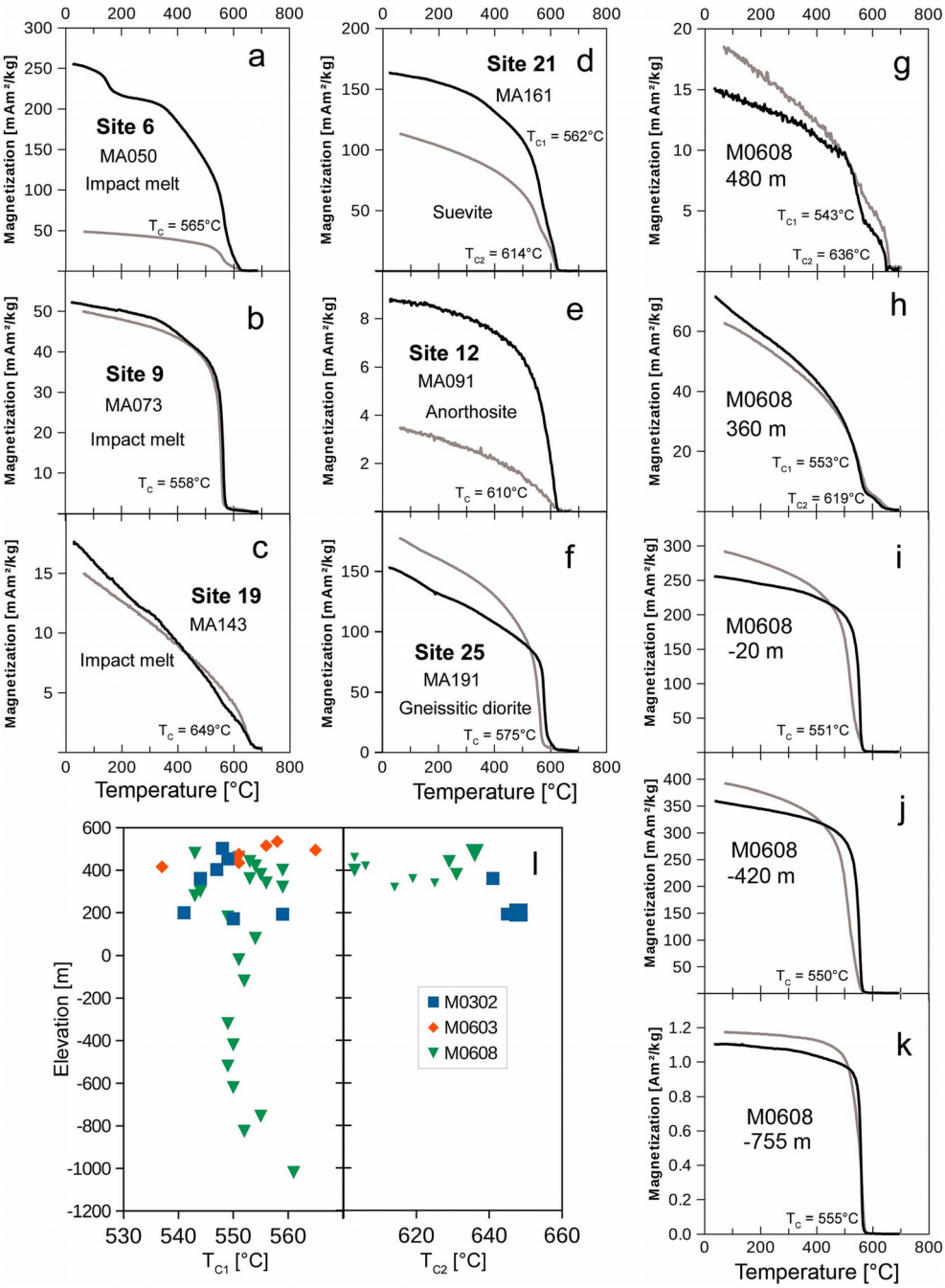

Figure 3.2: Thermomagnetic curves of samples collected (a–f) on the surface and (g–k) from drill core M0608 as a function of depth. Heating curves are shown in black, cooling curves in gray. (l) Low (T_{C1}) and high (T_{C2}) Curie temperatures from the three drill cores as a function of depth relative to sea level. In M0608, minerals carrying T_{C2} are only found relatively close to the surface. The size of the data points indicates the relative proportion of the magnetization for each of the two populations.

from 78 Sun compass readings is -19.8° ± 2.5°, which coincides well with that expected from the international geomagnetic reference field (-20.2°). We also studied the impact melts from three drill holes (M0302, M0603, and M0608; figure 3.1b) that penetrated 702 m, 322 m, and 1529 m below the surface, respectively. These deep cores stem from a commercially driven drilling program by three mining companies at 38 locations in the crater. The text below reports depths relative to sea level. Further details surrounding these cores are reported in Spray and Thompson (2008), Spray et al. (2010), and O'Connell-Cooper and Spray (2011).

3.4 Experimental results

3.4.1 Curie temperature

We measured the temperature dependence of the magnetization with a Petersen Instruments variable field translation balance in an applied field of 30 mT (surface cores) or 37 mT (deep drill cores) (figure 3.2). Most impact melt and melt-bearing breccia samples collected near the surface exhibit one or two deflections in the temperature ranges between 530 and 570°C and/or between 600 and 650°C, which are indicative of relatively Ti-poor titanomagnetite and titanohematite, respectively (figures 3.2a–3.2d). Anorthosite basement rocks have Curie temperatures similar to the impact melts, lying generally in the range from 526 to 565°C and around 610°C (figure 3.2e). Gneissose diorite from site 25 has Curie temperatures either close to that of stoichiometric magnetite (575°C) or higher (>600°C) (figure 3.2f). One observes a high degree of reversibility between the heating (black) and cooling (gray) curves, meaning that heating in air produces insignificant oxi-exsolution or chemical alteration. In core M0608, the relative contribution of titanohematite in the impact melt samples disappears with depth to where only a single magnetic phase exists with a Curie temperature in the 545–570°C range (figures 3.2g–3.2l). As shown below, samples containing both magnetic mineral phases possess identical magnetization directions, which indicates that both formed during primary cooling in the Late Triassic.

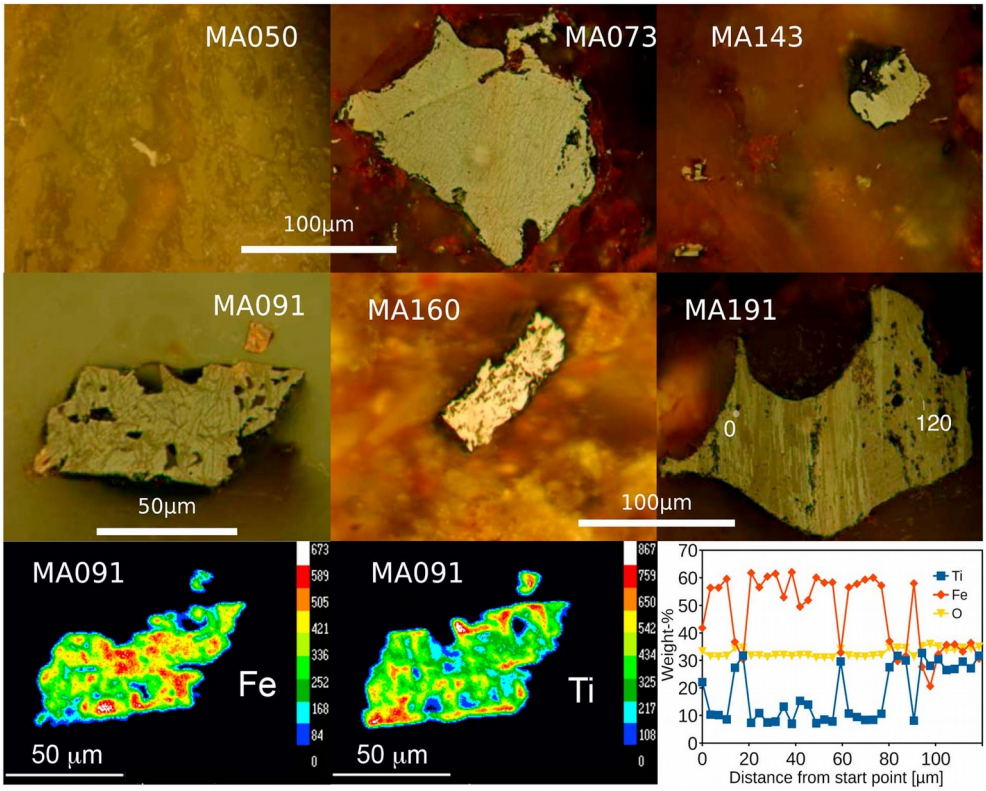

Figure 3.3: (top and middle rows) Reflected light microscopy images of iron oxide grains from impact melt samples MA050 (site 6), MA073 (site 9), and MA143 (site 13); anorthosite MA091 (site 12); melt-bearing breccia MA160 (site 21); and gneissic diorite MA191 (site 25). (bottom left and middle) Relative Fe and Ti concentrations of an opaque grain from sample MA091 shown in the microscope image above (electron microprobe units in counts per second). Ti-rich, Fe-poor areas correspond to darker phases of the grain. (bottom right) Line profile from electron microscopy of the exsolved grain from sample MA191; start and end points are marked by a circle and a bar in the microscope image; numbers are distances from start point in micrometers. Note that the highly rounded grain morphology in MA191 is also typical of the basement rocks from the Vredefort, South Africa crater (S. Gilder, unpublished data).

3.4.2 Reflective light microscopy and electron microprobe analyses

Figures 3.3 (top row) and 3.3 (middle row) show reflective light images of iron oxide grains from surface samples. Opaque phases rotated in polarized light go extinct, typical of optically isotropic minerals like magnetite. Opaque grain sizes in the impact melts vary by orders of magnitude and show no evidence for shock damage (figure

3.3, top row and MA160) – the same observation holds for the basement rocks (figure 3.3, middle row MA091 and MA191).

Electron microprobe (Cameca SX100) analyses of all samples reveal exsolved titanium-iron oxides with Ti-rich and Ti-poor zones. Fe and Ti concentration mapping was carried out on an anorthosite sample collected from the central uplift (Mont de Babel) (MA091, figure 3.3, bottom left). Total Fe contribution (Fe^{3+} versus Fe^{2+} in wt %) more closely matches titanohematite than titanomagnetite, which coincides with a Curie temperature at 610°C (figure 3.2e). Gneiss sample MA191 (site 25) contains grains with optically visible (tens to hundreds of micrometers wide) lamellae where Ti concentrations average either ~8 wt % or ~30 wt % (figure 3.3, bottom right). Fe concentration varies inversely with Ti; oxygen is higher in the zones with higher Ti. The bulk sample has a well-defined Curie temperature of 575°C (figure 3.2f), suggestive of nearly pure stoichiometric magnetite. As discussed in the following section, a deflection at 118 K (figure 3.4d) matches the Verwey transition of a nearly stoichiometric, yet slightly oxidized, magnetite compatible with a Curie temperature of 575°C. Thus, both titanohematite and titanomagnetite likely coexist in the gneissose diorite.

3.4.3 Bulk susceptibility, magnetic hysteresis, and low-temperature characteristics

We measured bulk magnetic susceptibility with a Bartington Instruments MS2B sensor. The most striking data are found in core M0608, where susceptibility increases with depth in a few discrete steps (figure 3.4a and table A1 in the appendix). Above 300 m, the mass normalized susceptibility averages 0.5×10^{-6} m^3/kg, then 7×10^{-6} m^3/kg from 300 m to -620 m, and then jumps to 20–60 $\times 10^{-6}$ m^3/kg below -620 m. Saturation magnetization obtained from hysteresis loops (Petersen Instruments, variable field translation balance) mimic the pattern displayed by susceptibility (table A1). As the mass susceptibility of titanomagnetite is orders of magnitude greater than titanohematite and paramagnetic, iron-bearing minerals like pyroxene

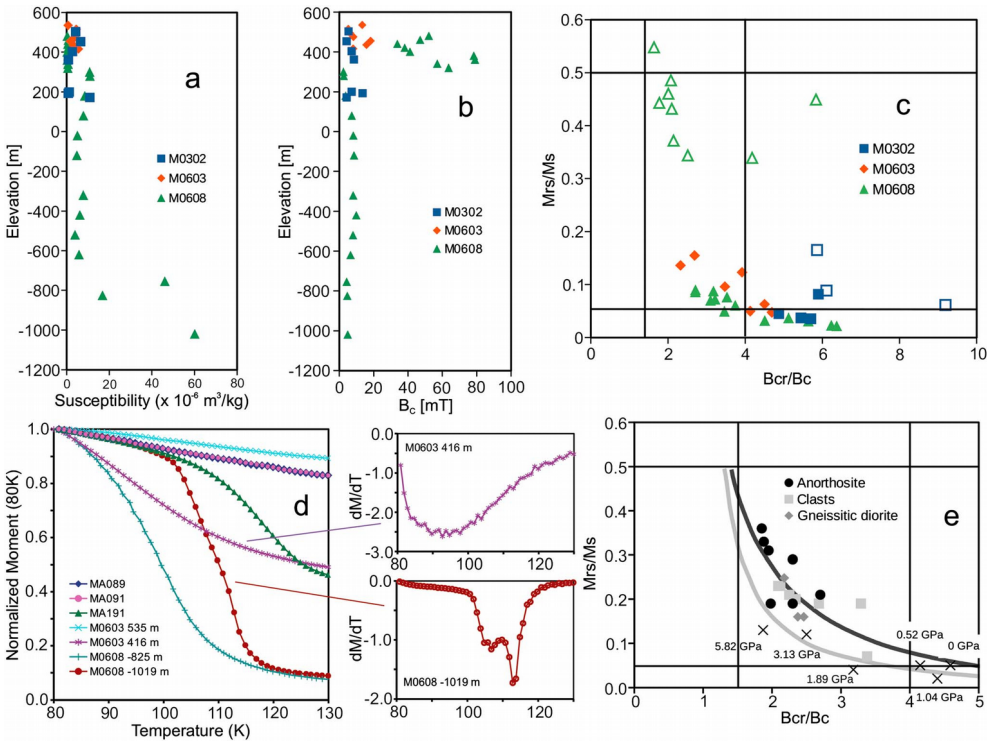

Figure 3.4: (a) Bulk susceptibility and (b) bulk coercive force (B_c) versus depth with respect to sea level for the samples from the three drill cores. In core M0608, as for the surface cores, samples with the lowest susceptibilities possess Curie temperatures >600°C (titanohematite) as well as higher coercive forces. (c) Day et al. (1977) plot of impact melts from the cores. Samples with a significant fraction of Curie temperatures in the 600–650°C range (titanohematite) lie toward the single-domain (SD) field (unfilled triangles), while the rest lie closer to the multidomain (MD) field. Hysteresis loops for the former do not fully saturate in 800 mT fields. Samples from core M0302 that are displaced away from the stoichiometric SD-MD magnetite mixing line (Dunlop, 2002) also have a component with Curie temperatures >600°C (titanohematite). (d) Thermoremanence curves of a 1 T field applied at 80 K, then warmed in an ambient field to 130 K to measure variations related to the Verwey transition. Data are normalized to the moment at 80 K. MA089 and MA091 are anorthosites from Mont de Babel; MA191, gneissic diorite (site 25); the rest are impact melts from two cores with depths as indicated. Plots on right are the derivatives of the curves on the left. (e) Day et al. (1977) plot of basement rocks from the Manicouagan crater that have only titanomagnetite-like Curie temperatures (<580°C). Anorthosite samples are from Mont de Babel (sites 10 to 12), clasts were entrained in melt-bearing breccia from site 5, and gneissic diorite is from site 25. Crosses denote data points from Carporzen and Gilder (2010) for slightly oxidized magnetite measured at ambient conditions after decompression from the indicated pressure. Gray and black mixing lines are from Dunlop (2002).

(Dunlop and Özdemir, 1997), one can use susceptibility as a proxy for titanomagnetite concentration.

Bulk coercive force (Bc) defines two discrete populations in M0608 with average values of 54 mT above 320 m and 6 mT below (figure 3.4b). Together with the Curie temperature data, this behavior is attributed to a profusion of titanohematite in the upper part of the impact melt sheet. Below, titanomagnetite is present as the only carrier of the magnetization with an increasing abundance toward the base. As expected, titanohematite-bearing samples plot closer to the single-domain field on a Day plot (figure 3.4c) (Day et al., 1977), with the caveat that not all samples above 320 m were fully saturated by 800 mT. The rest do reach saturation and lie closer to the multidomain field. For this population, titanohematite-bearing samples depart from the pure-stoichiometric magnetite mixing line of Dunlop (2002). These observations suggest that oxidation was prevalent above 320 m, where titanohematite is readily observed in the surface samples (tables 3.1 and A1). However, oxidation at the surface is heterogeneous, as some sites (3, 22, and 24) contain no, or minimal traces of, titanohematite. We found no spatial correlation for the occurrence of titanohematite. Because the solely titanomagnetite-bearing impact melts lie near or within the multidomain field, erosion must have removed the uppermost layers that cooled fast enough to produce smaller, single-domain-sized grains.

The prevalence of oxidation toward the surface can also be seen in the thermomagnetic curves measured with a Lakeshore MicroMag 3900 vibrating sample magnetometer (figure 3.4d). The samples were cooled in the ambient field to 80 K, exposed to a 1 T field at 80 K, and then warmed from 80 to 130 K in the ambient field. For core M0603, the sample lying closest to the surface at 535 m has a Curie temperature of 558°C (table A1), which corresponds to a Ti concentration of 0.9 wt % (Akimoto, 1962); thus, it should possess a visible Verwey transition. Oxidation likely explains the absence. The sample at 416 m has a broad Curie temperature averaging 537°C, which corresponds to an average Ti concentration of 1.8 wt %. A diffuse Verwey transition at ~93 K is consistent with the Ti concentration (Kakol et al., 1994). However, the drop in moment in the 80–130 K window is not as substantial as one would expect if the sample possessed a high fraction of multidomain grains, as expected from the hysteresis parameters (table A1), and that over 95% of the remanence was

demagnetized by an alternating field with a peak field of 75 mT (see below, figure 3.7d). Thus, the titanomagnetite in this sample is also likely oxidized, albeit not enough to completely erase the expression of the Verwey transition as in the sample 119 m above.

Samples from the deepest levels of M0608 at -825 and -1019 m also show Verwey transitions typical of multidomain grains owing to the significant drop in magnetization (Moskowitz et al., 1993). The Curie temperatures of these samples are 552 and 561°C, respectively (Ti concentrations of 1.2 and 0.8 wt %), so we should expect a lower Verwey transition temperature for the sample at -826 m than at -1019 m, which is consistent with the data (figure 3.4d). Interestingly, the deepest sample shows two distinct low-temperature transitions yet only a single Curie temperature in the titanomagnetite range (table A1).

The sum of these observations is entirely compatible with Mössbauer spectra on Manicouagan impact melts, which show that hematite dominates the mineral phases with the highest ferric iron concentrations (Morris et al., 1995; note that this study only considered end-member Fe compositions, i.e., no Ti). Morris et al. (1995) likewise found that hematite and magnetite can coexist in the same rock in widely varying proportions; the lack of iron hydroxide or maghemite led them to conclude that the oxidation occurred above 250°C. We also find no evidence for either iron hydroxide or maghemite. O'Connell-Cooper and Spray (2011) found higher ferric oxide (hematite) concentrations toward the top of core M0608. This coincides with our findings that titanohematite, likely caused by high-temperature oxidization, disappears by a depth of 320 m in core M0608. That titanomagnetite increases with depth is consistent with their finding that fractional crystallization occurred in the lower portion of the core. Moreover, the melt sheet must have cooled slowly enough to create multidomain-sized grains. On the other hand, O'Connell-Cooper and Spray (2011) report a decrease in magnetite with depth, which is at odds with the susceptibility and hysteresis (saturation magnetization) data. We find only the presence of titanomagnetite in core M0603, consistent with O'Connell-Cooper and Spray (2011),

who detected no appreciable ferric iron component. It is noteworthy that the basement rocks and impact melts have similar magnetic mineralogies.

Figure 3.4e shows a Day plot of the basement rocks (including basement clasts entrained in melt-bearing breccia or in impact melt at the base of the impact melt sheet) for samples that only have a dominant Curie temperature below 580°C. Titanomagnetite-bearing, deep-seated plutonic rocks like anorthosite and diorite would typically plot in the multidomain field on this graph, yet the samples from Manicouagan lie well within the pseudo single-domain field. There are three potential explanations. One unlikely scenario is that titanohematite, clearly present in many surface samples, is not expressed in the Curie temperature measurements but influences the remanence and coercivity ratios. Although minor amounts of titanohematite could alter the coercivity ratio, it should not raise the remanence ratio. Second is that high-temperature oxidation reduced the grain size fraction, displacing preimpact titanomagnetite grains that would originally lie in the multidomain field toward the single-domain field on the Day plot. Such an effect was observed at the Mistastin crater, where baked anorthosite within 1 m of the contact with impact melt has higher coercivity than nonbaked anorthosite lying farther away from the contact (Hervé et al., 2015, Figure 6). Third, pressure cycling of slightly oxidized multidomain magnetite makes it more single-domain-like (Gattacceca et al., 2007; Carporzen and Gilder, 2010). Figure 3.4e superimposes the pressure-cycled data on the Day plot, which shows the evolution that multidomain magnetite undergoes when pressurized up to 5.8 GPa. As the pressures involved at Manicouagan exceed 30 GPa, it is not surprising that some samples plot well above the experimental result at 5.8 GPa. Moreover, Hervé et al. (2015) found that the anorthosite basement rocks at Mistastin trend from multidomain to single domain when approaching the center of the crater where pressures were greater. In sum, we interpret that the higher than expected remanence ratios and lower than expected coercivity ratios of the titanomagnetite-bearing basement rocks at Manicouagan reflect both pressure and temperature effects related to the impact.

Table 3.1
Site Mean paleomagnetic directions for Manicouagan[a]

Site	Rock Type	Slat (°N)	Slon (°W)	Alt (m)	N/n	Dec (°)	Inc (°)	k	α_{95} (°)	NRM (Am^2/kg)	χ (m^3/kg)
1	Impact melt	51.545	68.941	653	7/8	356.1	39.1	147.6	5.0	$1.3 \pm 0.6 \times 10^{-4}$	$6.8 \pm 1.3 \times 10^{-7}$
2	Impact melt	51.547	68.939	608	6/6	356.3	42.0	316.1	3.8	$9.6 \pm 0.3 \times 10^{-5}$	$7.7 \pm 0.4 \times 10^{-7}$
3	Impact melt	51.547	68.939	586	6/6	7.5	43.9	389.3	3.4	$8.3 \pm 0.6 \times 10^{-5}$	$1.5 \pm 0.1 \times 10^{-6}$
4	Suevite	51.318	68.428	359	11/11	15.4	45.0	182.4	3.4	$4.4 \pm 2.5 \times 10^{-4}$	$1.2 \pm 0.4 \times 10^{-6}$
5	Impact melt/clasts	51.318	68.423	359	14/14	13.7	47.7	96.8	4.1	$0.9 \pm 1.4 \times 10^{-3}$	$1.3 \pm 0.6 \times 10^{-6}$
6	Impact melt	51.319	68.426	359	7/7	6.1	49.2	72.6	7.1	$1.5 \pm 0.5 \times 10^{-4}$	$3.0 \pm 1.2 \times 10^{-6}$
7	Impact melt	51.314	68.337	361	6/6	17.1	31.4	202.9	4.7	$8.9 \pm 1.9 \times 10^{-5}$	$1.9 \pm 1.5 \times 10^{-6}$
8	Impact melt	51.313	68.337	384	6/6	19.6	34.1	393.9	3.4	$5.8 \pm 2.3 \times 10^{-5}$	$7.9 \pm 0.9 \times 10^{-7}$
9	Impact melt	51.313	68.337	394	6/6	12.4	38.3	80.1	7.5	$8.1 \pm 4.1 \times 10^{-5}$	$7.0 \pm 5.3 \times 10^{-7}$
10	Anorthosite	51.417	68.699	844	5/6	11.3	39.0	104.5	7.5	$2.4 \pm 3.0 \times 10^{-4}$	$1.9 \pm 0.3 \times 10^{-7}$
11	Anorthosite	41.420	68.696	898	6/6	21.2	41.8	104.3	6.6	$1.9 \pm 1.1 \times 10^{-4}$	$4.5 \pm 2.0 \times 10^{-7}$
12	Anorthosite	51.424	68.692	947	6/6	19.5	38.8	416.1	3.3	$1.3 \pm 0.7 \times 10^{-4}$	$5.6 \pm 3.9 \times 10^{-7}$
13	Anorthosite	51.419	68.596	939	3/6	25.6	39.0	72.6	14.6	$5.5 \pm 4.4 \times 10^{-6}$	$6.3 \pm 3.7 \times 10^{-8}$
14	Anorthosite	51.420	68.595	945	5/6	20.6	43.5	226.7	5.1	$1.8 \pm 1.1 \times 10^{-6}$	$2.7 \pm 1.0 \times 10^{-8}$
15	Impact melt	51.395	68.846	510	6/6	13.2	34.6	382.4	3.4	$3.0 \pm 1.3 \times 10^{-4}$	$6.8 \pm 9.4 \times 10^{-7}$
16	Impact melt	51.215	68.856	470	6/6	16.3	38.7	104.5	6.6	$4.4 \pm 0.8 \times 10^{-5}$	$9.0 \pm 4.8 \times 10^{-7}$
17	Impact melt	51.232	68.577	360	6/6	15.9	39.9	202.9	4.7	$8.2 \pm 3.9 \times 10^{-5}$	$2.0 \pm 0.6 \times 10^{-6}$
18	Impact melt	51.235	68.578	361	6/6	30.5	39.7	923.4	2.2	$4.0 \pm 0.2 \times 10^{-4}$	$6.4 \pm 0.2 \times 10^{-7}$
19	Impact melt	51.235	68.578	356	6/6	18.6	41.8	757.1	2.4	$1.7 \pm 0.5 \times 10^{-4}$	$4.6 \pm 1.8 \times 10^{-7}$
20	Impact melt	51.490	68.338	360	6/6	13.7	36.6	168.2	5.2	$3.1 \pm 0.6 \times 10^{-4}$	$6.1 \pm 1.2 \times 10^{-6}$
21	Suevite	51.490	68.339	353	6/6	6.5	46.6	180.5	5.0	$8.7 \pm 1.4 \times 10^{-4}$	$4.4 \pm 0.5 \times 10^{-6}$
22	Impact melt	51.489	68.339	352	6/6	11.4	44.0	145.1	5.6	$1.1 \pm 0.9 \times 10^{-3}$	$1.2 \pm 0.5 \times 10^{-5}$
23	Impact melt	51.507	68.344	355	6/6	21.3	38.3	277.6	4.0	$2.5 \pm 0.5 \times 10^{-4}$	$3.0 \pm 1.3 \times 10^{-6}$
24	Impact melt	51.507	68.344	363	6/6	11.6	39.1	252.3	4.2	$2.4 \pm 0.5 \times 10^{-4}$	$8.1 \pm 3.0 \times 10^{-6}$
25	Gneissic diorite	51.507	68.345	361	5/6	9.6	47.8	682.4	2.9	$6.8 \pm 2.0 \times 10^{-4}$	$3.2 \pm 0.5 \times 10^{-6}$

[a]*Slat, site latitude in degrees north; Slon, site longitude in degrees west; Alt, altitude in meters; N/n, number of samples used in the calculation/number of samples stepwise demagnetized; Dec., declination; Inc., inclination; k, best estimate of the precision parameter;* α_{95}*, the radius of the cone where the true mean direction lies with 95% confidence; NRM, average and single standard deviation of the mass normalized, natural remanent magnetization;* χ*, average and single standard deviation of the mass normalized susceptibility.*

3.4.4 Stepwise demagnetization and paleomagnetic directions

All samples were stepwise demagnetized using either 10 steps with a peak alternating field up to 75 mT or 11–15 steps using thermal demagnetization up to 680°C. Remanent magnetization measurements were performed in magnetically shielded rooms using 2G Enterprises Inc., three-axis superconducting quantum interference device magnetometers, either manually using the Cryomag program (Wack, 2010) or with the SushiBar automated system (Wack and Gilder, 2012). Remanent magnetization directions were determined with principal component analysis (Kirschvink, 1980); Fisher statistics (Fisher, 1953) were applied to the site mean and overall mean directions.

Demagnetization characteristics of the impact melts (figures 3.5a–3.5l) are similar to those of the basement rocks (figures 3.5m–3.5p). Both thermal and alternating field demagnetization unblock magnetization components that decay univectorially to the origin after the first few demagnetization steps. Despite the presence of a single magnetization direction, normalized thermal demagnetization decay plots usually identify multiple inflections at temperatures consistent with the in-field thermoremanent data (figure 3.2), e.g., indicative of titanomagnetite and titanohematite. Alternating field demagnetization to 75 mT removes nearly all of the original moment in some samples (figure 3.5k), while for others it is less effective (30% in figure 3.5i, 70% in figure 3.5e). Magnetization directions for the latter case still trend toward the origin, which shows that the higher coercivity component possesses the same direction as that with lower coercivity.

An important aspect of the demagnetization data is that a single magnetization direction of normal polarity was recorded by all magnetic phases in each sample, meaning that the blocking of the remanence was coeval for all magnetic recorders in a given rock. This observation holds true even when accounting for directional differences among samples throughout the crater, which vary enough to be visible (if present) on the orthogonal plots. The fact that we observe no such difference implies that the creation of titanohematite (oxidation) occurred above titanomagnetite Curie tempera-

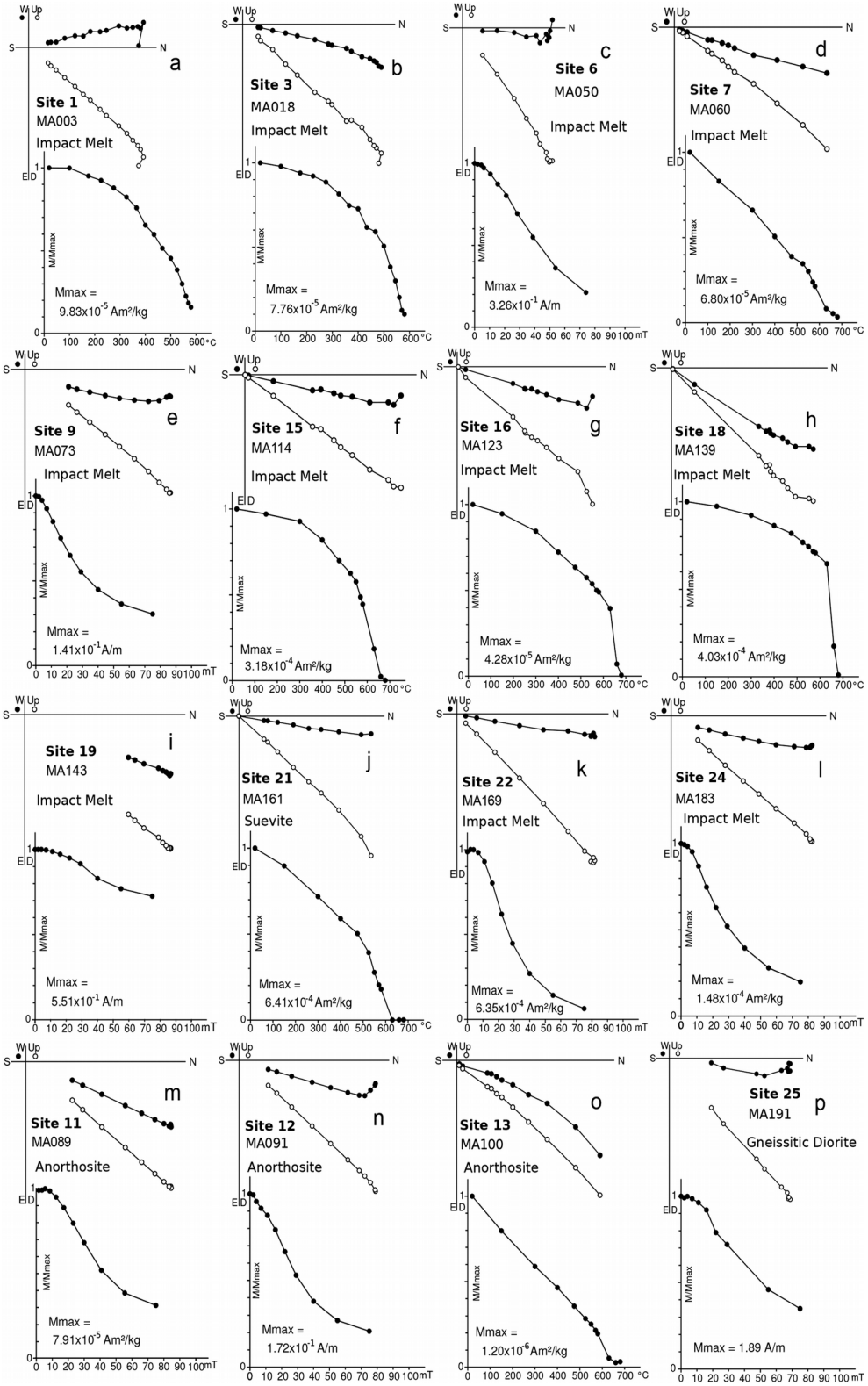

Figure 3.5: Orthogonal projections of stepwise demagnetization and normalized magnetization decay plots for samples collected on the surface.

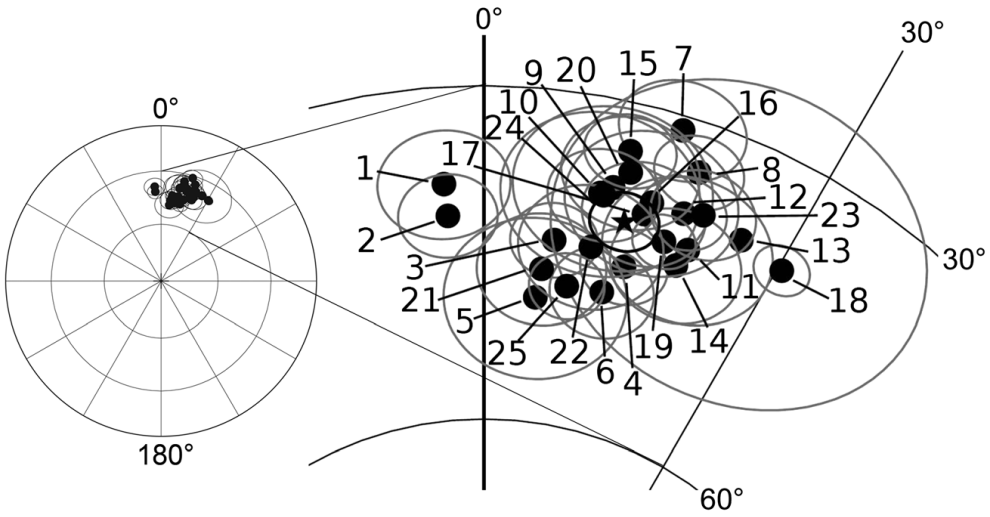

Figure 3.6: Stereographic projection of the site mean directions with α_{95} in gray (data from Table 3.1). The star with black α_{95} denotes the mean of the site means.

tures and that no subsequent alteration by weathering or hydrothermal activity influenced the ferrimagnets. Hence, the titanohematite likely originated from high-temperature oxidation that occurred during degassing and not from convection or diffusion that brought oxygen down into the melt from the surface.

Sample directions within sites are generally well grouped, with the best estimates of the precision parameter (k) >100 in 21 of 25 sites (table 3.1). Only site 13 (anorthosite from Maskelynite Peak) has an α_{95} (the radius of the cone about which the true mean lies with 95% confidence limits) exceeding 10°, although its mean is based on only three samples with relatively weak magnetizations (table 3.1). Site mean directions span 35° in declination and 18° in inclination resembling a range typical of that observed over the last few millennia (figure 3.6) (Bucur, 1994; Hervé et al., 2013). Sites 1 and 2 have the most westerly declinations, yet they were sampled nearby site 3 whose mean direction is distinct from them at 95% limits. We observed no fault between these three sites, whose elevations (600–650 m; table 3.1) are the highest of any impact melt sampled in this study. Sites 17–19 were also sampled in close proximity, yet the direction of site 18 lies well away from the other two, at the easternmost extremity of all site mean directions. Interestingly, site 18 is an impact melt dike, so its magmatic history could be different from the nearby sites if it intruded and cooled at a later time.

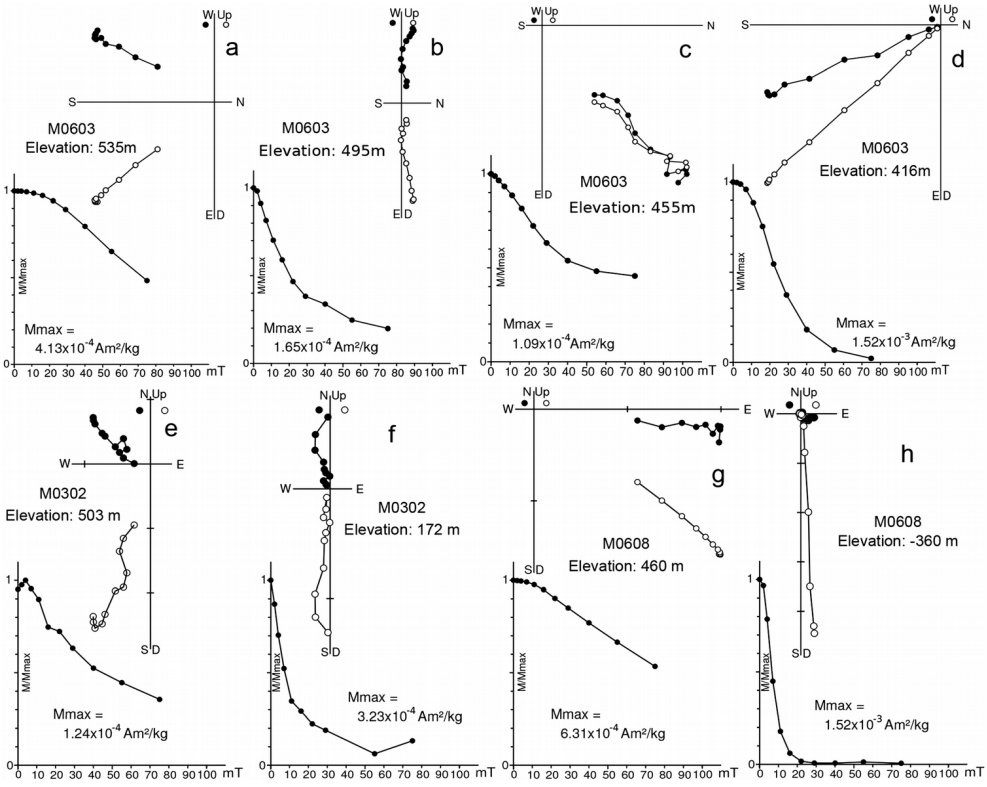

Figure 3.7: Orthogonal projections of stepwise demagnetization and normalized magnetization decay plots for samples from the deep drill cores.

Of importance is that the site mean directions from the basement rocks lie well within the distribution of the impact melts. The average direction of the impact melts and of the basement rocks is indistinguishable at 95% confidence limits. This suggests that the basement rocks acquired their remanence directions in the Triassic, likely from thermal overprinting. The overall mean direction of our 25 sites (declination [D] = 14.2°, inclination [I] = 41.1°, k = 125, α_{95} = 2.7°) is indistinguishable within 95% confidence limits from that of Larochelle and Currie (1967) (D = 12.0°, I = 41.2°, k = 91, α_{95} = 4.8°, N = 11 sites) based on directions derived from a single demagnetization step at 20 mT (no principal component analysis) and excluding one site (their site 11). The overall average paleomagnetic pole from our study is longitude = 84.7°E, latitude = 60.2°N, and A_{95} = 2.8°.

Figure 3.7 shows stepwise alternating field demagnetization results of the impact melts from the deep drill cores, which were drilled vertically, except for M0302 that was drilled 60° from horizontal. The declination component is arbitrary. The room

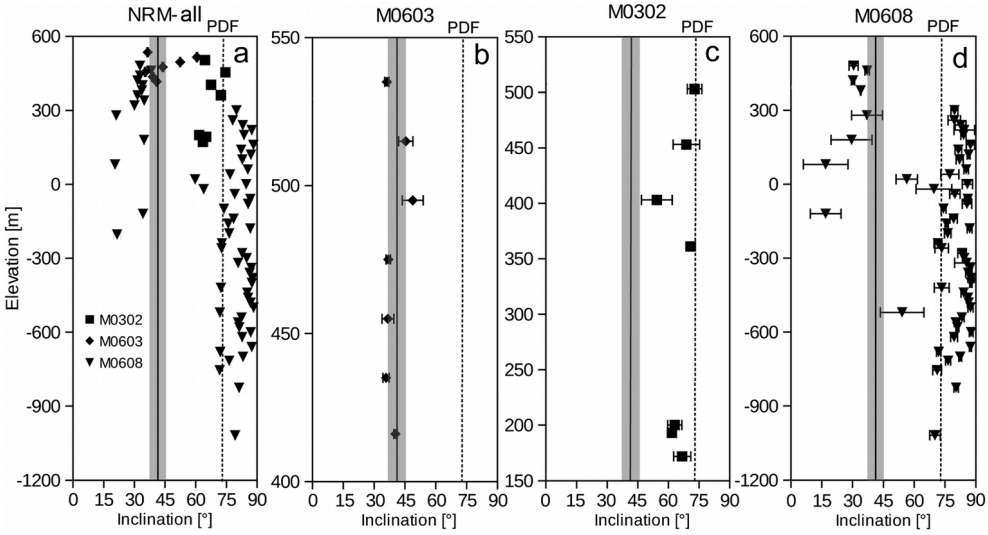

Figure 3.8: Paleomagnetic inclinations of drill core samples as a function of elevation relative to sea level. Uncertainties are the angular deviations associated with the line fitting procedure used to determine the magnetization directions. The black line at 41.1° represents the overall average inclination with 2σ uncertainty limits in gray (Table 3.1). The dashed line is the present-day field (PDF) inclination (73.8°); the expected axial centric dipole inclination is 68.2°. (a) Inclinations of the natural remanent magnetization (NRM), which is measured at room temperature. (b–d) Inclinations derived from principal component analysis of the demagnetization spectra.

temperature (natural) remanent magnetization inclinations separate into two general bands: relatively shallow (20° to 45°) and relatively steep (60° to 90°) (figure 3.8a). Demagnetization trajectories in most samples from core M0603 decay toward the origin and yield inclinations based on line-fit analysis between 35.8° and 48.8° with an average of 40.0 ± 5.4° (figures 3.7a–3.7d and 3.8b), within 95% confidence limits of 40.8 ± 2.2° calculated from inclination-only statistics on the site mean data (table 3.1). Neither a systematic change in inclination nor any significant deviation in inclination occurred within the time represented by the 119 m of impact melt that cooled through the titanomagnetite blocking temperature.

Demagnetization trajectories from M0302 and M0608 are more complex than in M0603 (figures 3.7e–3.7h). Most samples from M0302 and M0608 possess inclinations 60° or greater (figures 3.8c–3.8d), which we interpret as drilling-induced remagnetizations, since they lie near the expected present-day field inclination (73.8°) at Manicouagan, or parallel to the core's axis (90°). Some scatter in the inclination data in M0302 could be related to the nonvertical drill direction. Although some sam-

ples have shallower inclinations, including a trend toward shallow (15°) inclinations in M0608 with depth, we are loath to interpret them in a geomagnetic sense given the propensity of effects related to drilling. Hence, samples collected at the surface, as well as those from M0603, display a pattern typical of secular variation. These deposits span a total thickness from 653 m (site 1) to 172 m (lowest sample in core M0603), meaning that no significant aberration in geomagnetic field direction occurred in the time it took to cool 481 m of impact melt through the blocking temperatures of the ferrimagnets.

3.4.5 Paleointensity

Absolute paleointensity experiments were performed according to the multispecimen, parallel differential, partial thermal remanent magnetization (pTRM) protocol of Dekkers and Böhnel (2006) on 186, 5 mm diameter cylindrical specimens taken from outcrops and from core M0603 that escaped drill-induced overprinting. The multispecimen method was selected in preference to the classic Thellier-Thellier-type experiments given the complex magnetic mineralogies and propensity of multidomain-sized grains in the Manicouagan samples. Moreover, the magnetization of the samples rarely alters when heating in air at high (>500°C) temperatures (figure 3.2). We only used specimens if the angle between their inclination measured at room temperature deviated less than 60° from the core's z axis, which was the applied field direction in the laboratory. Sample magnetizations were measured after demagnetizing in two steps at 100°C and 500°C in a null field. After null field heating to 500°C, we again heated them to 500°C and cooled them down to room temperature in the presence of a magnetic field (pTRM step), after which the samples were thermally cycled to 100°C in a null field before their magnetizations were measured. A heating threshold of 500°C was chosen because it was low enough to avoid alteration and at least 20% of the natural remanent magnetization decayed by 500°C in stepwise thermally demagnetized samples (figure 3.5). The pTRM step was made in six discrete

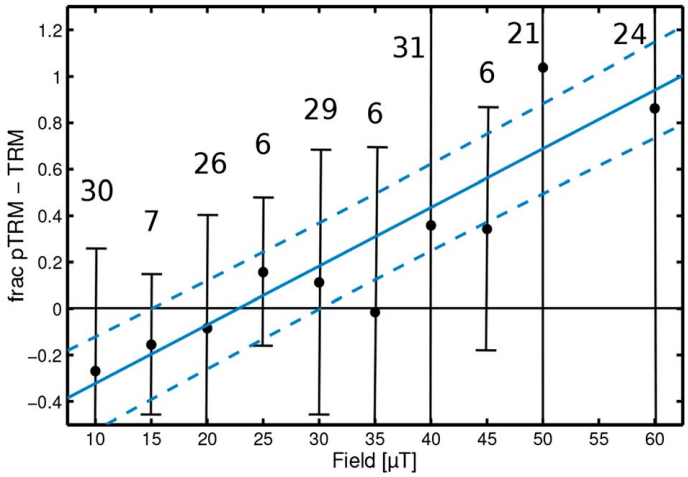

Figure 3.9: Paleointensity measured with the multispecimen parallel differential pTRM method (Dekkers and Böhnel, 2006). Black circles are the median values; the number of samples used at each field is given together with the single standard deviation. The solid blue and dashed lines represent a linear fit and one standard deviation of the data. The zero-crossing point is at 22.8 ± 7.7 μT.

fields from 10 to 60 μT for the surface samples and in eight discrete fields from 10 to 45 μT for the drill core samples.

Figure 3.9 shows the median normalized (pTRM-TRM)/pTRM values and standard deviations obtained at each field increment after subtracting the magnetization acquired below 100°C to avoid minor overprints. The solid blue line represents the linear fit of the data with the 1σ confidence envelope (dashed blue line). The zero-crossing point of the fit corresponds to the paleointensity (22.8 ± 7.7 μT). Treating the surface and the M0603 core samples separately yields paleointensities of 21.0 ± 11.8 μT and 25.4 ± 14.4 μT, respectively.

3.4.6 Anisotropy of magnetic remanence

The anisotropy of anhysteretic remanent magnetization was measured on 191 samples with a decaying alternating field between 20 and 0 mT and a bias field of 50 μT using the automated SushiBar system with a 12 position protocol (Wack and Gilder, 2012). Samples possessing inherited clasts were excluded, which explains the absence of data from sites 4 and 5. Table A2 lists the mean eigenvalues, the principal axis directions, the corrected anisotropy degree (P') (Jelinek, 1981), and the shape

parameter (T) (Jelinek, 1981) for each site. The impact melts have an average anisotropy degree of 13%, while that for the basement rocks is 20%. Most fabrics are triaxial (T around 0).

Figure 3.10a shows stereonet plots of the bootstrapped principal axis directions at the different impact melt sites in the crater. Data from sites collected in close proximity were pooled together. At each location, we calculated the radial angle with respect to the crater's center and plotted it against the declination of the major anisotropy axis (M1) (figure 3.10b). Two solutions are possible for the M1 axis declinations. Figure 3.10b displays the option that lies in a band of ±90° with respect to the radial angle, where it is seen that six of seven points deviate less than ±45° from the 1:1 line. In the case of a completely random relationship between radial angle and M1 declination, the probability for each datum to lie no more than 45° from the 1:1 line is 1/2. Thus, the probability of having six of seven points within ±45° is 5% for a purely random process. If we count site 15, which lies closest to the crater's center of all the sites, and whose uncertainty does not exclude the case of lying outside the ±45° band, then the probability for randomness becomes 16%.

The idea behind making figure 3.10 originated during fieldwork near site 24 where a clast-laden impact melt exhibits a well-developed, ductile flow fabric whose lineation trends radially from the crater's center (figure 3.1e). Although no fabric is readily observable by eye in most impact melt locations, figure 3.10b implies that there is a general correlation between the trend in the flow lineation versus location in the crater; e.g., the fabrics trend radially away from/toward the crater's center. This may have been caused during crater formation, when the impact melts moved outward (centrifugally) from their site of origin, or during (centripetal) back flow of the impact melt toward the crater's center (Dence et al., 1977). Macroscopic deformation fabrics near site 24 suggest flow was outward.

Such fabrics are normally impossible to resolve in inch (2.5 cm) cores because inherited clasts entrained in clast-bearing impact melt or melt-bearing breccias have their own, preimpact fabrics that obscure any fabric related to flow. The selected Manicouagan impact melts are largely devoid of inherited clasts, leading to a more robust

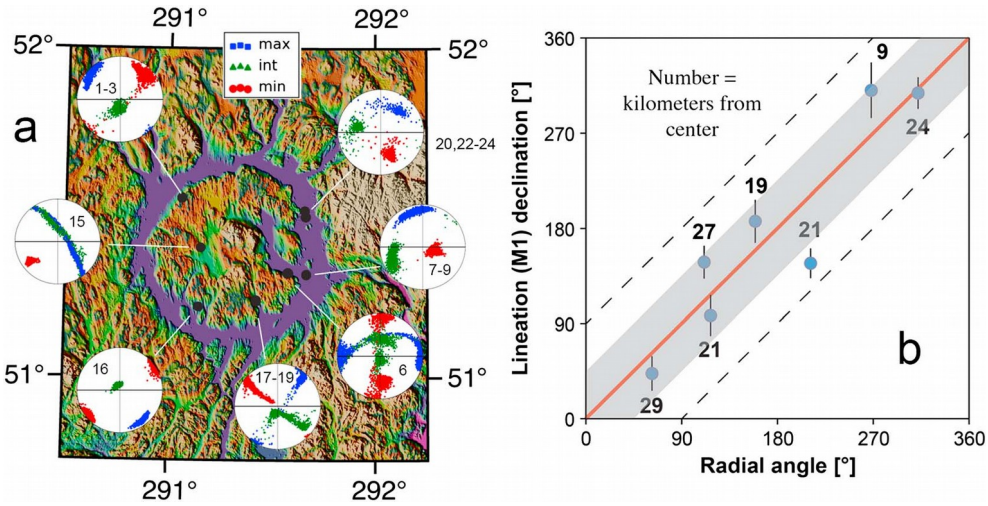

Figure 3.10: (a) Topographic map of the Manicouagan crater with the bootstrapped anisotropy of remanent magnetization principal axis directions for each group of impact melt sites (black circles). (b) Declination of the major axis (M_1) of anisotropy of magnetic remanence (table A2) versus radial angle from the crater's center. The 1:1 line is shown in red, the ±45° swath about the 1:1 line is in gray, and the dashed line delimits ±90° swath about the 1:1 line.

interpretation of the anisotropy data in terms of a primary flow fabric. One could expect that the fabric would be better defined closer to the crater margins where the shear component due to oversteepened walls would be greater, which is why figure 3.10b lists distance from the center in kilometers. However, a potential correlation is obscured since most sites were collected near the annular lake between 20 and 30 km, nor can one discount radially directed flow during uplift of the central peak. Given the wide range in fabric type (oblate, triaxial, and prolate), we do not expect all sites to correlate well; further dedicated work on this topic seems warranted.

3.5 Interpretations

3.5.1 Crater formation processes

Hydrothermal processes in impact craters have received increasing attention due to their potential importance for the origin of life on Earth and other planets (e.g., Osinski et al., 2001; Abramov and Kring, 2005). However, the spatial distribution of the iron oxides at Manicouagan is better explained by a model of degassing and oxygen

diffusion in the upper few hundred meters of the impact melt, rather than an advecting system associated with deeper-seated hydrothermal activity. If a hydrothermal plumbing system once existed within the uppermost part of the crater stratigraphy, any trace of it has been removed by erosion.

The magnetic anisotropy data provide a unique opportunity to track impact melt flow kinematics present during the earliest stages of impact crater development. Melosh and Ivanov (1999) calculated that the transient crater collapses within 100 s after impact. Thus, outward flow or return of the melt as it flowed back into the crater must have occurred relatively soon after impact, and the melt viscosity must have been high enough to produce a systematic alignment of mineral grains. Titanomagnetite and titanohematite crystallize from >1000°C to as low as 600–700°C depending on magma chemistry (Buddington and Lindsley, 1964; Hargraves and Petersen, 1971; Lipman, 1971), so if the fabric truly reflects complex crater formation processes, the molten material must have fallen below its liquidus and viscosity increased within minutes after impact. Clearly, a considerable time lag exists between crater formation and when the magnetic remanence was acquired (section 3.5.3). It would seem that shear should be higher near the contact with the basement floor, which is hard to ascertain. For complex impact craters, a central uplift grows as the floor rebounds (e.g., Grieve et al., 1981). Because the final distribution of the impact melt appears to be controlled by faults surrounding the central uplift (Mont de Babel) (Spray et al., 2010), it could be that a growing central uplift caused the impact melt to flow radially away from it. Hence, the radial distribution of the maximum anisotropy axes could be due to outward or back flow into the collapsing transient crater and/or flow away from the emerging central uplift.

3.5.2 The central magnetic anomaly

A positive magnetic anomaly with an amplitude of 2000 nT lies just southwest of the central uplift (figure 3.1b). Whereas Coles and Clark (1978) attributed the distinct magnetic anomalies outside the crater to iron ore deposits, they could not correlate the strong central magnetic anomaly with the local geology. High horizontal mag-

netic field gradients led them to propose that the anomaly's source must be relatively shallow. Their model used a paleomagnetic direction of D = 10° and I = 40° (Larochelle and Currie, 1967; Robertson, 1967) with an annular-shaped source body, 8 × 12 km, extending 2 km below the surface with a magnetization of 11 A/m. Given our new findings, only the deeper levels of the impact melt with the more enriched titanomagnetite can satisfy such large magnetization values.

Scott et al. (1996) analyzed a drill core that penetrated basement rocks near the eastern part of the anomaly to a depth of 472 m (S in figure 3.1b). Relatively high magnetic susceptibility (10^{-3} to 10^{-1} SI) and high remanent magnetizations (0.1 to 100 A/m) led them to ascribe the magnetic anomaly to basement rocks that became enriched in magnetite due to shock decomposition of garnet and pyroxene, followed by hydrothermal alteration that favored iron oxidation. However, if hydrothermal activity and shock related to impact did create new magnetite, we would expect the paleomagnetic inclinations to be consistent with that of the impact (~40°), yet the inclinations from their core are <30°, which leads us to suspect the presence of a drilling-induced overprint. On the other hand, mafic gneisses within the central anomaly region have susceptibility values equal to or greater than the deep differentiated impact melts (L. Thompson, unpublished data), so the mafic gneisses likely play a significant role in producing the positive anomaly. Although the deeper impact melts contribute to the central anomaly's structure and amplitude, their influence appears much less than that of the underlying mafic gneisses.

3.5.3 Effect of impact on the geodynamo

Stepwise demagnetization reveals that all rocks from the Manicouagan impact structure possess a single normal magnetization component whose overall mean likely averages out geomagnetic secular variation. Converting the overall mean direction into a virtual geomagnetic pole and plotting it together with the North American plate apparent polar wander paths of Besse and Courtillot (2002) and Torsvik et al. (2001) shows remarkable coincidence with both (figure 3.11a). The Manicouagan pole lies near the 205 Ma pole from the Torsvik et al. (2001) path and on the 210 to 220 Ma

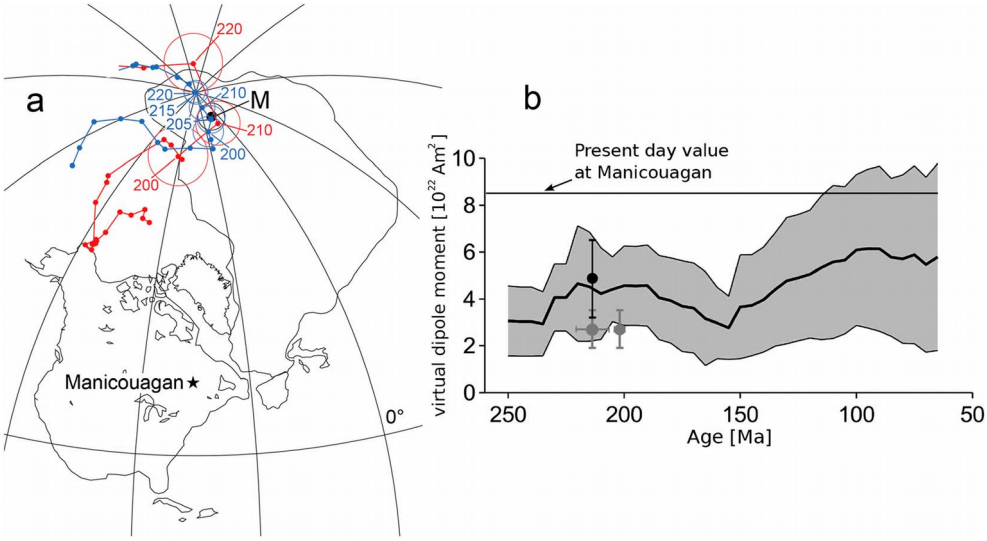

Figure 3.11: (a) Paleogeographic reconstruction in a 214 Ma reference frame with respect to North America (Euler parameters from Torsvik et al. (2001)). Apparent polar wander paths of North America are shown in blue (Torsvik et al., 2001) and red (Besse and Courtillot, 2002); numbers are ages in megayears. The paleomagnetic pole for Manicouagan (M, this study) is in black. (b) Evolution of the virtual dipole moment during the Mesozoic using a running average (thick black line) with a window size of 20 Ma; the gray region represents the single standard deviation (PINT database of Biggin et al. (2010)). The black circle with black 1σ uncertainty envelope denotes the virtual dipole moment from Manicouagan, and gray circle with gray uncertainty envelope denotes the virtual dipole moment from the Rochechouart crater for 214 ± 8 Ma (Kelley and Spray, 1997) and 201 ± 2 Ma (Schmieder et al., 2010).

segment of the Besse and Courtillot (2002) path. The latter is in better agreement with the radiometric ages of the crater (e.g., 214 ± 1Ma (Hodych and Dunning, 1992)).

Using an inclination of 41° to convert the 22.8 ± 7.7 μT paleointensity into a virtual dipole moment yields $4.9 \pm 1.6 \times 10^{22}$ Am^2. Compared to the global paleointensity database of Biggin et al. (2010) (figure 3.11b), the Manicouagan paleointensity result falls close to the average trend – again suggesting that secular variation at Manicouagan has been averaged out in our data set. In contrast, the virtual dipole moment obtained from the Upper Triassic Rochechouart (France) crater likely did not include enough time averaging (Eitel et al., 2014) and lies away from the average global trend (figure 3.11b). Nonaveraging of secular variation of the Rochechouart data makes it difficult to use paleomagnetism (direction and intensity) to test the hypothesis for a fragmented, or Shoemaker-Levy 9-type, impact to explain the origin of both

craters (Spray et al., 1998), although different magnetic polarities recorded in their impact melts suggest different formation times (Kent, 1998; Eitel et al., 2014).

Assuming an average thickness of 200 m for the impact melt at Manicouagan, Onorato et al. (1978) calculated that it took 5300 years to cool from 1227°C to 627°C. Knowing now that the impact melt can reach up to 1500 m in thickness (Spray and Thompson, 2008), one can also consider the cooling history of a 5 km wide by 1 km thick felsic magma chamber (Bea, 2010) as an analog for the thickest impact units near the center. Given an initial temperature of 1000°C, full crystallinity, as well as passage through the blocking temperature of hematite or magnetite, would not be reached even after 15,000 years in the center.

That only a single, normal magnetic polarity exists in all samples is not incompatible with the durations of the normal polarity chrons around 214 Ma (Late Triassic and Norian) that average ~1 million years (E13n and E14n in Kent and Olsen (1999) and Alaunian 2 in Gallet et al. (2007)). Following the heat conduction equations in Turcotte and Schubert (1982), and assuming that 100 m of impact melt has been eroded above the topographically highest sampling site, suggests that the uppermost site would take 382 years after impact to cool to 700°C, and 860 years to 500°C, while the lowest site would cool to 700°C 13,750 years after impact and to 500°C after 31,000 years. Given the large uncertainty surrounding the initial conditions and the exact cooling mechanism, we only wish to emphasize that the sampled stratigraphy spans from several hundred to several thousand or even tens of thousands of years following the impact. Anything above 3000–5000 years is within normal overturn times in the outer core, i.e., the time needed for a geomagnetic reversal (Bogue and Merrill, 1992; Leonhardt and Fabian, 2007; Valet et al., 2012), so we should have observed an effect had the Manicouagan impact perturbed the dynamo process.

We conclude that the seismic energy released from the Manicouagan impact was insufficient to disturb the dynamo process (such as through oscillation of the inner core) in a way that resulted in observable changes in field direction or intensity on the Earth's surface. Given the relatively large size of the Manicouagan crater together with the amount of time averaging allowed by the thick impact melt, it will be diffi-

cult to find a better target in which the impact-geodynamo hypothesis can be tested on Earth. It should be borne in mind, however, that while Manicouagan is relatively large in the context of Earth's limited impact crater inventory, it remains small by solar system standards (e.g., Taylor, 2001). For example, the South Pole Aitken impact basin on the Moon is 2400 km in diameter, Hellas on Mars is 2300 km diameter, and Caloris on Mercury is 1550 km diameter. Larger impacts could have shock-heated the Martian core leading to the eventual demise of its dynamo (Arkani-Hamed and Olson, 2010) or changed the rotation rate of the Moon thereby generating a weak and short-lived lunar dynamo (Le Bars et al., 2011). None of Earth's known surviving impact structures has a rim-to-rim diameter >300 km.

3.6 Conclusions

A comprehensive paleomagnetic and rock magnetic study of the Manicouagan impact melt sheet and uplifted basement rocks, combined with mineralogical, petrological, drilling, and field data, has yielded important constraints regarding the structure's formation:

1. There is a lack of a significant hydrothermal activity within the impact melt sheet. This is compatible with titanohematite developing at >570°C during oxi-exsolution as part of the melt crystallization process and implies that the impact event took place within a relatively dry setting on subaerial continental crust.
2. Magnetic anisotropy data, combined with field evidence, suggest that a record has, in places, been retained of the dynamic flow of impact melt during transient crater collapse and central uplift formation. It is difficult to constrain the sense of movement, but the direction is generally radial. The flow sense could be centrifugal (outward) or centripetal (inward). There is an indication that outward flow is favored, which, if correct, may be a response to the emergence of the central uplift during modification stage tectonics. Large-scale convection likely plays a role several hundred meters below the surface in the thickest portion of the melt sheet.

3. Magnetic susceptibility data indicate that fractionation and titanomagnetite enrichment occurred in the lower portion of impact melt that formed in a trough structure that accumulated over 1 km of impact melt, which may be a fault-bounded graben, as suggested by Spray and Thompson (2008). The central magnetic anomaly high is partially produced from the titanomagnetite-enriched deeper levels in the thick impact melt; however, meta-gabbroic rocks likely account for the bulk of the anomaly.
4. The central, thicker impact melt unit does not record any change in magnetic field direction or intensity. This indicates that the Manicouagan impact was not large enough to affect Earth's dynamo, and in combination with our previous work (Koch et al., 2012; Eitel et al., 2014; Hervé et al., 2015), any link between meteorite impacts and geodynamo disturbances should be considered improbable, at least during the Phanerozoic when impact frequency and meteorite sizes were lower than during the earlier stages of Earth's evolution (French, 1998). However, it should be kept in mind that the Manicouagan event is relatively small at the solar system scale, e.g., the South Pole Aitken crater on the Moon has a diameter of 2400 km versus Manicouagan's 85 km.

3.7 Acknowledgments

Funding for field and laboratory work was provided by the Deutsche Forschungsgemeinschaft to S.A.G. (project GI712/6-1) under the auspices of SPP1488, Planetary Magnetism. Field operations were also supported through the University of New Brunswick's Manicouagan Impact Research Program, which is funded by grants awarded to J.G.S. from the Canadian Space Agency, the Canada Research Chairs program, and the Natural Sciences and Engineering Research Council of Canada. We thank Nicolas Swanson-Hysell, Mike Dence, and an anonymous reviewer for their helpful suggestions that improved this work. Editorial handling by André Revil and an anonymous Associate Editor are appreciated. Any data herein can be obtained by contacting the corresponding author.

4 Magnetic signatures of terrestrial meteorite impact craters: A summary

The following chapter (Gilder, Pohl and Eitel, 2018) was published under the title "Magnetic Signatures of Terrestrial Meteorite Impact Craters: A Summary" as part of the book *Magnetic Fields in the Solar System – Planets, Moons and Solar Wind Interactions*.

4.1 Abstract

This chapter summarizes the magnetic characteristics of meteorite impact craters. Magnetic mineralogies of both impact melts and target rocks are described, as are the paleomagnetic signals they retain and the magnetic field anomalies they produce. Particular emphasis is given to five craters studied under the umbrella of the Deutsche Forschungsgemeinschaft's Schwerpunktprogramm, Planetary Magnetism: Manicouagan (Canada), Mistastin (Canada), Ries (Germany), Rochechouart (France), and Vredefort (South Africa), with a synthesis from other craters worldwide. A special problem addressed here is whether shock waves generated during impact influence the geodynamo. We conclude that the seismic energy released during the formation of craters up to 90 km in diameter is insufficient to disturb the dynamo process in a way that would provoke observable changes in field direction or intensity at the Earth's surface. We show that shock can permanently modify magnetic properties of the target rocks; however, it is difficult to assess the relative influence between thermal and pressure effects on their remanent magnetizations. Distinguishing between shock and thermal overprinting and then unraveling these signals from the original remanence remain important problems that bear on the interpretation of

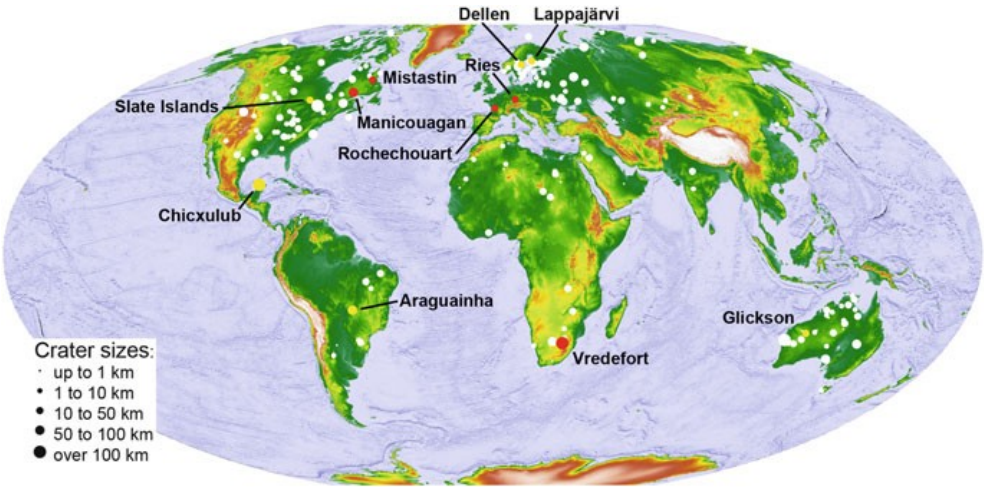

Figure 4.1: Recognized terrestrial meteorite impact craters. Craters studied by us discussed in this chapter are indicated in red; craters whose data are used in some figures are in yellow.

magnetic anomalies in impact craters as well as our understanding of heat production from collision. Paleomagnetic directions from impact melts and suevites are well clustered at each crater, which suggests that building of the structures was completed before the ferrimagnetic minerals cooled through their Curie temperatures.

4.2 Brief description of an impact event with relevance to magnetism

Meteorite impact craters are ubiquitous throughout our solar system and mark important events in planetary evolution (Shoemaker, 1977; French, 1998). To date around 190 impact craters have been identified on the surface of Earth (French 1998; Earth Impact Database: www.unb.ca/passc/ImpactDatabase/) (figure 4.1). When a bolide hits the Earth with enough energy, some of the terrestrial material may be vaporized. A larger part, up to several times the volume of the impactor, will be melted (Pierazzo et al., 1997; Pierazzo and Melosh, 2000; Barr and Citron, 2011; Quintana et al., 2015). The melt can form massive impact melt sheets within the structure, smaller isolated melt bodies within and around the crater, and/or minor melt pockets within breccias (suevites) and dikes inside or outside the structure. Friction between rock masses during crater formation can result in micromelts (pseudotachylite). A small

volume of melt is thrown airborne where it is rapidly quenched into glass, called tektite, that can be transported up to hundreds of kilometers away from the crater.

Impact melt thicknesses are low in small impact craters and, on Earth, thicker melt sheets are often eroded in larger craters such that melt thickness greater than 100 m is rare. The close resemblance in chemistry and petrology between impact melts and volcanic rocks was one of the arguments against an external origin for the craters (e.g., Currie and Larochelle, 1969 for Mistastin) – a debate that persisted to the early 1990s for the Vredefort crater (Antoine et al., 1990). This resemblance is also seen in magnetic mineralogy, with both containing iron oxides predominantly within the magnetite-ulvospinel solid solution series. Moreover, the relatively rapid cooling rates produce grain sizes toward the single to pseudo-single domain range associated with stable and strong remanent magnetizations that are favorable for paleomagnetic studies. Such ideal magnetic carriers record the magnetic field when they cool through their blocking (Curie) temperatures, thereby enabling paleomagnetists to study geomagnetic effects like secular variation or deformation related to crater formation.

Impact craters produce distinctive magnetic and gravity anomalies (e.g., Pilkington and Grieve, 1992; Plado et al., 1999; Ugalde et al., 2005). While the interpretation of gravity anomalies is rarely contentious, the opposite is true for magnetic anomalies. The complexity of the geometry and polarity of the sources make magnetic anomalies more difficult to model due to the confluence of whether a crater contains impact melt, the volume of melt, and the nature of the basement rock. As permanent magnetizations tend to dominate aeromagnetic expressions, the polarity recorded in the impact melts and suevites, if present, typically dictates the sign of the anomalies. However, in several cases it is difficult to unravel whether the signal from the target rocks is primary, a thermal overprint, or influenced by shock. For the latter, there is confusion whether shock demagnetizes the target material or remagnetizes it parallel to the ambient field direction. Other ambiguities are whether hydrothermal systems create new magnetic minerals or provide heat to overprint existing remanence direc-

tions, and how long the hydrothermal process lasts, all which bear on the timing when the lock-in of magnetic remanence occurs after impact.

In this contribution, we discuss the magnetic carriers found in melt-bearing rocks in various craters, as well as the influence of shock on the target rocks. We give some examples of the intriguing magnetic anomalies produced by the impact structures. Paleomagnetic directions from several craters are presented to draw conclusions on the formation rate and subsequent tectonic modification of the structures. Finally, the energy transferred to the Earth during impact can be so high that several workers postulated whether impacts can perturb the geodynamo process (e.g., Glass and Heezen, 1967; Durrani and Khan, 1971). This topic and the others mentioned above are discussed here in light of our findings at five impact craters, Manicouagan (Canada; Eitel et al., 2016), Mistastin (Canada; Hervé et al., 2015), Ries (Germany; Koch et al., 2012), Rochechouart (France; Eitel et al., 2014), and Vredefort (South Africa; Carporzen et al., 2012), and by comparing with published data from several other craters.

4.3 Link between crater structure and local aeromagnetic signatures

The ca. 15 Ma Ries (Germany) impact structure serves as a good example of a well-preserved crater, whose subsurface is well characterized through drilling and seismic exploration, and it has abundant magnetic data (figure 4.2) (e.g., Pohl et al., 1977; Pohl, 1977). The suevite deposits attain up to 400 m in thickness within the inner ring, while several, thinner, isolated pockets crop out near the inner ring and beyond. The impact happened while the Earth's magnetic field was in the reversed polarity state, opposite of today's normal polarity field, so that the combination led to lower than average (negative) magnetic anomalies. The thicker and more laterally extensive the melts, the longer the wavelength of the negative anomalies. Isolated patches of suevite yield complex, short-wavelength anomalies as sketched above the cross section in figure 4.2a. The short-wavelength positive anomalies in the SW part of the

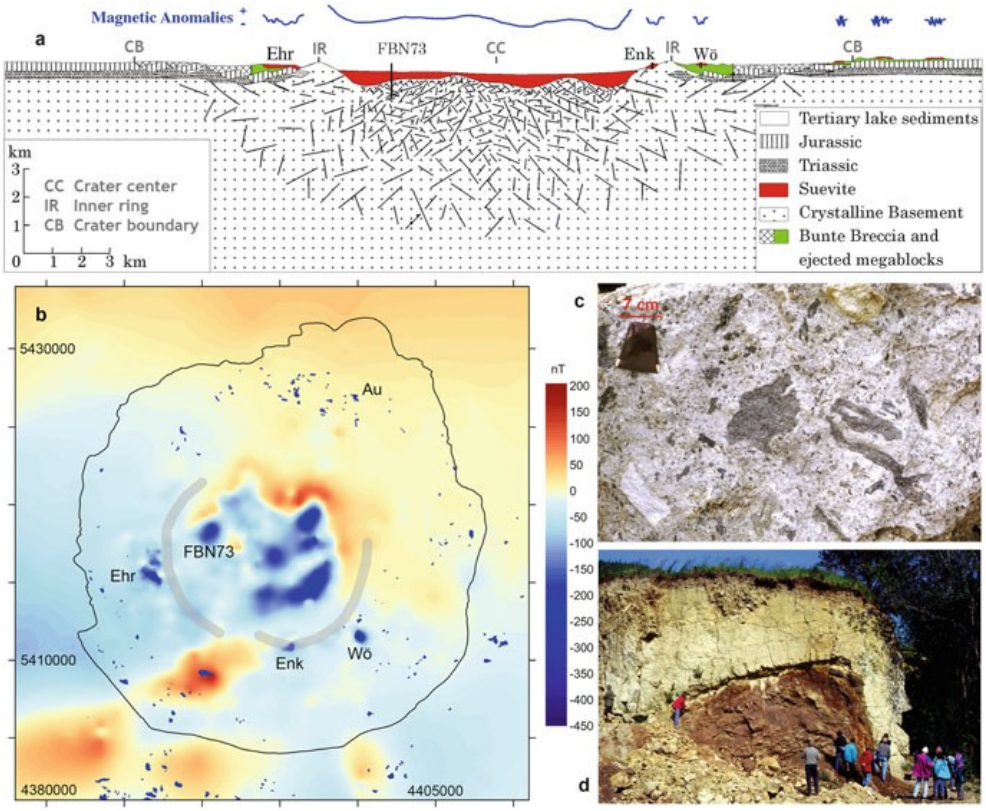

Figure 4.2: Schematic geologic cross section of the Ries (Germany) impact structure (a). Impact-created lithologies are colored. Impact breccia and melt were emplaced when the field was reversed, which produce negative magnetic field anomalies in today's normal polarity field. Thick deposits inside the inner ring (indicated in grey in the magnetic anomaly map [b]) produce long-wavelength anomalies while isolated patches of suevite and impact melt produce erratic, short-wavelength anomalies as sketched above the cross section. Drill holes FBN73, Wö (Wörnitzostheim) and Enk (Enkingen) reached 1200 m, 180 m, and 100 m depth, respectively. (b) Magnetic anomaly map of the Ries impact structure. Small dark blue spots represent suevite and impact melt outcrops. Thin black line demarcates the crater rim; Ehr stands for Ehringen. (c) Photo of suevite from Öttingen containing grey impact melt and crystalline rock clasts in a fine-grained matrix. Key holder in upper left is 7 cm in length. (d) Photo from the Aumühle (Au) quarry showing suevite (yellow-grey) lying on top of the Bunte Breccia ejecta (red-brown).

aeromagnetic map are generated by the underlying basement rocks, unrelated to the impact (Pohl et al., 1977).

Magnetic anomaly maps of impact craters are quite diverse, yet most reveal the circular nature of the structures (figure 4.3). The 19 km diameter Dellen (Sweden) structure contains a melt sheet 9 km in diameter, up to 500 m thick, with normal magnetic polarity (Bylund, 1974) that produces fairly small-wavelength positive anomalies up to a few 100 nT (Henkel, 1992; Geological Survey of Sweden,

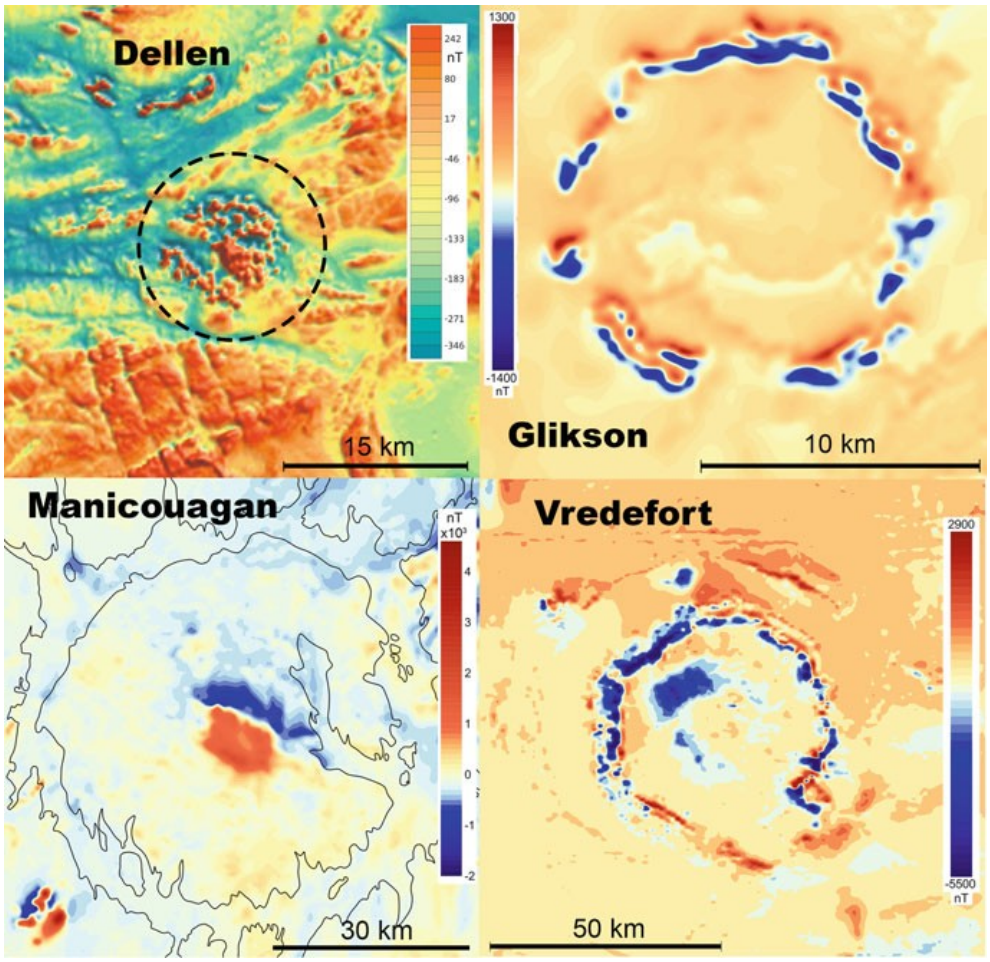

Figure 4.3: Magnetic anomaly maps of the Dellen (Sweden), Glikson (Australia), Manicouagan (Canada) and Vredefort (South Africa) craters. The image for Dellen is courtesy of the Geological Survey of Sweden, www.sgu.se: 61.8°N, 16.8°E, diameter ca. 15 km, age ca. 89.0 Ma, anomaly range +250 to -1750 nT, erosion level 5 (crater-fill breccias/melt rocks partly preserved). Data for Glikson are courtesy of Geoscience Australia: 24.0°S, 121.6°E, diameter ca. 19 km, age <508 Ma, anomaly range +1280 to -1330 nT, erosion level 5. Data for Manicouagan are courtesy of the Natural Resources of Canada, Geoscience Data Repository for Geophysical Data, 2014 (http://gdr.agg.nrcan.gc.ca/gdrdap/dap/search-eng.php), 51.4°N, 68.7°W, diameter ca. 90 km, age 214 Ma, anomaly range +4200 to -1900 nT, erosion level 4 (rim largely eroded, crater-fill breccias/melt rocks preserved). Vredefort (data from the Geological Survey of South Africa – see Corner et al. (1990) and Antoine et al. (1990)), 27.0°S, 27.5°E, diameter ca. 250 km, age 2023 Ma, anomaly range +3000 to -5500 nT, erosion level 6 (crater-fill breccias/melt rocks eroded, isolated breccia dikes). Erosion levels from Osinski and Ferriere (2016).

www.sgu.se). The Glikson structure possesses a distinct, 14 km diameter magnetic ring anomaly that was interpreted by Macdonald et al. (2005) to result from the truncation and folding of mafic sills into a circular-symmetric syncline. The exposed

rocks in the Glikson structure consist entirely of sandstone (Shoemaker and Shoemaker, 1997).

The 215 Ma Manicouagan (Canada) crater, whose rim-to-rim diameter of 90 km ranks it as one of the ten largest impact craters on Earth, possesses an exceptionally thick impact melt sheet, with >1 km of clast-free, differentiated impact melt and a further 400 m of clast-laden impact melt at the center (Spray and Thompson, 2008). The melt rock is so thick in the center that it underwent differentiation, where titanomagnetite enrichment occurred in the lower portion of the melt (Eitel et al., 2016). The central magnetic anomaly high is partially produced from the titanomagnetite-enriched deeper levels in the thick impact melt; however, meta-gabbroic rocks within the central anomaly region have susceptibility values equal to or greater than the deep differentiated impact melts (L. Thompson, unpublished data), so they likely contribute to the anomaly's presence; further work is required to solve the origin of the magnetic anomalies from Manicouagan. One obstacle is that the rocks from the drill cores that access the deeper levels of the structure have drilling-induced overprints that both reoriented the original directions and changed the magnetization intensities (Eitel et al., 2016); these potential affects are often not considered when interpreting the magnetizations of rocks drilled in other craters.

The 2 Ga Vredefort structure is likely the largest crater on Earth (>250 km original diameter). Up to 8 km of erosion since its formation has exposed a complete cross section of Archean crust: going from upper mantle facies (harzburgite) in the center, grading to highly depleted granulite typical of the lower crust, a ductilely deformed metamorphic suite, undeformed granites, and then folded Witwatersrand basin sediments whose fold axes parallel the circular structure of the crater. Corner et al. (1990) proposed that the upturned ferruginous shales of the West Rand Group give rise to the prominent negative anomalies marking the perimeter of the Vredefort dome (figure 4.3). A "horseshoe-shaped" region of strong (<-1000 nT) negative anomalies lies near the amphibolite to granulite metamorphic facies transition, analogous to the Conrad discontinuity (Corner et al., 1990; Muundjua et al., 2007), where impact-related thermal and shock metamorphism are significantly higher than in

other parts of the structure (Hart et al., 1991). Muundjua et al. (2007) suggested that focusing and defocusing of shock waves at this rheologic interface during impact enhanced the magnetic signature at this boundary from a combination of both thermal and shock effects.

Key to these interpretations is that shock from the impact created single-domain magnetite within the planar deformation features in quartz (Cloete et al., 1999). That two generations of magnetite existed in Vredefort basement rocks was substantiated by Carporzen et al. (2006), who found two distinct Verwey transitions that were clearly linked to >2.7 Ga multidomain magnetite and to single-domain magnetite that was thought to be created during the impact event at 2 Ga. However, this latter interpretation was proved false by Carporzen et al. (2012), who drilled two 10 m deep cores in the negative anomaly region. They found that the single-domain magnetite that carried the lower of the two Verwey transition temperatures disappeared about a half meter below the surface. Coupled with a wide range of magnetic experiments, Carporzen et al. (2012) concluded that the majority of the single-domain magnetite was created by lightning strikes. Salminen et al. (2013) arrived at a similar conclusion from laboratory experiments that produced artificial lightning strikes on Vredefort rocks. Hence, the most likely explanation for the negative “horseshoe” anomaly comes from thermal overprinting during impact when the field was in a reversed polarity state (Hargraves, 1970; Jackson, 1982; Carporzen et al., 2005). Rocks closer to the center of the crater are relatively magnetite poor (Hart et al., 1995; Carporzen, 2006), which explains the lack of negative anomalies there.

Several other notable examples of magnetic anomalies exist. For example, concentric circular anomalies with amplitudes ranging from 50 to 4 nT are described for the Foelsche, Yallalie, and Wolfe Creek caters (Australia; Hawke, 2003, 2004). Hawke (2003) interpreted the anomaly pattern at Yallalie to be due to remanently magnetized impact melt or post-impact hydrothermal activity. Indeed, hydrothermal activity is occasionally evoked as the cause of magnetic anomalies, such as at Chicxulub (Mexico; Pilkington and Hildebrand, 2000) and Haughton (Canada; Quesnel et al., 2013). The Haughton anomaly map contains a particularly spectacular positive spike of ca.

700 nT in the center (Pohl et al., 1985; Glass et al., 2002, 2005). Pohl et al. (1985, 1988) ascribed the anomaly to magnetite-bearing, shocked crystalline basement with vertically downward inclinations. Quesnel et al. (2013) found that pyrrhotite-bearing melt rocks also possessed downward-directed inclinations; their magnetic models suggest that the source of the central anomaly is a magnetized body with a 1 km deep root that was created by post-impact hydrothermal alteration of the basement.

Scott et al. (1997) reviewed the magnetic anomalies of four Canadian craters: West Hawk, Deep Bay, and Clearwater (East and West). All four impact structures exhibit reduced magnetizations that extend beyond their morphologically defined limits. Scott et al. (1997) concluded that the target rocks beneath the crater floors must reflect an impact-induced reduction in NRM intensity and susceptibility to account for discrepancies between observed and modeled data. While shock has clearly been shown to modify the magnetic properties of ferromagnetic minerals, experimental results indicate that shock can either magnetize a rock parallel to the ambient field or demagnetize a rock in a manner analogous to alternating field demagnetization (Dunlop et al., 1969; Hargraves and Perkins, 1969; Cisowski and Fuller, 1978; Pohl et al., 1975; Gattacceca et al., 2007). For example, an alternative explanation for the negative anomalies in the West Clearwater structure is that impact melt and basement rocks have reverse polarities, consistent with their deposition during the Kiaman reversed superchron (Zylberman et al., 2015), thus giving rise to negative magnetic anomalies. Shock effects on magnetization are discussed further below.

A final point concerns the role of faulting and the circular expression of magnetic anomalies. Chicxulub (Mexico) serves as a good example where a system of regional vertical faults surrounding the central portion of the crater explain the magnetic high and lows of the aeromagnetic anomalies over the southern sector of the crater (Rebolledo-Vieyra et al., 2010). Circular fault systems, predicted in structural models of formation and evolution of complex multi-ring craters, are well documented in Manicouagan where intensive drilling for mineral exploration indicates that the distribution of the impact melt is controlled by vertical faults with 100s to 1000s of meters of offset surrounding the central uplift (Spray and Thompson, 2008; Spray et al., 2010).

Ring faults likely facilitated the transport of fluids that led to the creation of massive sulfide ore deposits at Sudbury, where anisotropy of magnetic susceptibility reveals strongly developed lineations in the fault zones (Hirt et al., 1993; Scott and Spray, 1999).

4.4 Magnetic mineralogy

4.4.1 Melt rocks

Titanomagnetite ($Fe_{3-x}Ti_xO_4$), mostly with low Ti concentration (Ti < ca. 5% with corresponding Curie temperatures from 525 to 580°C), is the dominant magnetic mineral found in melt rocks, followed by pyrrhotite ($Fe_{1-x}S$) and then titanohematite ($Fe_{2-x}Ti_xO_3$). Fregerslev and Carstens (1976) and Kukkonen et al. (1992) (Lappajärvi) and El Goresy (1968) (Ries) report the presence of FeNi spherules or nickel-bearing native iron. Although definitive magnetic evidence such as Curie temperatures >680°C is not provided, the presence of FeNi inclusions in impact glasses seems well established (El Goresy et al., 1968). Badjukov et al. (1989) report metallic Fe (>2% Ni) in suevite in the Kara (Russia) crater, while Öhman et al. (2003) report Curie temperatures of fresh impact glasses from Kara solely within the magnetite range. Perhaps the greatest obstacle in drawing conclusions on magnetic mineralogy stems from the relatively low number of observations compared to the enormous volume and heterogeneity of available material.

Little attention has been paid to the importance of the iron oxide composition on the temperature, oxygen activity, and cooling time of the melts produced by impacts. For example, Eitel et al. (2014) found that the impact melt-bearing rocks in the Rochechouart crater contain distinctly different titanohematite compositions at three different places – ranging from nearly pure hematite (Curie temperatures of 673 ± 9°C) in the Montoume quarry which contains the rocks with the highest melt degrees, followed by Curie temperatures of 656 ± 5°C and 630 ± 4°C at the Valette and Chassenon localities, respectively. The unique magnetic mineralogy at Valette produces

self-reversal behavior stemming from magnetic exchange interaction. Steiner (1996) also reported self-reversal-like behavior from the Manson (USA) and Chicxulub (Mexico) craters, although the evidence is fairly equivocal.

A noteworthy observation comes from the Chesapeake Bay (USA) structure where Mang et al. (2012) reported the existence of an anomalous ferrimagnetic pyrrhotite with Curie temperatures between 350 and 365°C, significantly higher than the known Curie temperature of 325°C for monoclinic pyrrhotite [Fe_7S_8]. Moreover, it lacks the 34 K Besnus transition characteristic of monoclinic pyrrhotite. This species has a metal-to-sulfur ratio of 0.81, which indicates a distinctly higher vacancy concentration than monoclinic pyrrhotite with a composition closer to smythite (Fe_9S_{11}). Mang et al. (2012) suggested that this phase was produced by shock metamorphism and carries a stable natural remanent magnetization. On the other hand, shock experiments on monoclinic pyrrhotite to 12 GPa found no change in the Curie or Besnus temperatures and no evidence for iron depletion (Louzada et al., 2010). Figure 7c in Mang et al. (2012) shows sub-micron-sized nickel-rich phases within a shocked pyrrhotite, which leads us to speculate whether the anomalously high Curie temperatures are rather due to Ni metal inclusions, since pure Ni has a Curie temperature of ca. 358°C (Wei et al. 2014). Confirming the existence of an anomalous ferrimagnetic pyrrhotite phase warrants further investigation.

Whether the ferromagnets in impact melt rocks are inherited or crystallized in the melt yields further information on the formation temperature of the system. Clear examples exist for shocked magnetite or pyrrhotite phases existing in impact melts and suevites (Chesapeake Bay: Mang et al., 2012; Bosumtwi: Kontny et al., 2007; Ries: Koch et al., 2012). Others contain euhedral grains with no shock features (Manicouagan: Eitel et al., 2016; Mistastin: Hervé et al., 2015). That shocked ferrimagnets in melt-poor suevites record the field direction acting at the time of impact suggests that they were heated above their Curie temperatures. On the other hand, if the temperatures did not exceed the Curie temperature, the rocks would tend to have low magnetization intensities with erratic demagnetization directions due to the randomized vectors of the inherited clasts. Such results would likely be considered spurious and

discarded. Alternatively, if a single inherited clast dominated the volume of the sample, it could contain a high magnetization intensity with stable demagnetization directions that would likely differ from the ambient field direction at the time of impact. Such samples might be disregarded as outliers.

Pilkington et al. (2004) documented the creation of iron hydroxide (limonite-goethite) in an impactite sequence from the Yax-1 drill hole in the Chicxulub crater. Concentrically zoned, botryoidal limonite-goethite is abundant as an interstitial phase in the matrix of reworked suevite. It occurs ubiquitously in the impactite sequence, mostly as open-space fillings in lithic basement fragments. These phases, as well as secondary magnetite, formed as a result of low-temperature (<150°C) alteration – they likely serve as the best examples of magnetic phases created by hydrothermal processes (see also Urrutia-Fucugauchi et al., 2004a). Botryoidal texture of hematite-rich impact bombs from the Araguainha structure led Jovane et al. (2011) to speculate that the hematite was produced by post-impact hydrothermal circulation. Hydrothermal alteration of the host rock was proposed to explain the origin of the magnetic anomalies at the Lake St. Martin crater (Coles and Clark, 1982). Yokoyama et al. (2015) proposed that fluid migration along faults altered the basement rock and created the circular magnetic anomaly pattern at the Vargeao structure. On the other hand, the spatial distribution of the iron oxides in the impact melts at Manicouagan is better explained by a model of degassing and oxygen diffusion in the upper few hundred meters of the impact melt, rather than an advecting system associated with hydrothermal activity (Eitel et al., 2016).

Pseudotachylite, a glass-bearing, pulverized rock, can be found in impact craters in quantities far exceeding pseudotachylite from non-impact-related faults. Relatively few studies have focused on the magnetic properties of pseudotachylite from impact structures. Elming and Bylund (1991) found that hematite carries the magnetization in two pseudotachylite sites from the Siljan (Sweden) crater and magnetite in another site. Pseudotachylite in the 45 km long, 10 to 500 m wide, South Range breccia belt in the Sudbury crater contains pyrrhotite (Scott and Spray, 1999). To our knowledge, only Nakamura and Iyeda (2005) have performed paleointensity experiments on

pseudotachylite. Their petrologic observations on samples from Sudbury reveal abundant fine-grained magnetite inclusions and coarse-grained multidomain magnetite and exsolved titanomagnetite.

Salminen et al. (2009) found that pseudotachylitic breccia from Vredefort contains two distinct magnetite phases: grains in the micrometer size range that are interpreted to carry remanence from the time of the impact and larger, altered (>50 μm) grains that carry a viscous remanence. Carporzen et al. (2006) identified single-Verwey transitions in eight pseudotachylite samples from four localities in Vredefort. The lower right image in Figure 4.4 shows an electron microprobe image of the magnetite from sample V0111A extracted a few 10s of cm from sample V0112 reported in Carporzen et al. (2006) that has a Verwey transition temperature of 94 K based on a field cooling experiment using a Quantum Design, magnetic property measurement system and 100 K from a Lake Shore Cryotronics alternating current susceptometer. Chemical analyses indicate that this mineral is Ti-free titanomagnetite, which suggests the relatively low Verwey transition temperatures stem from oxidation and not from cation (titanium) substitution. Because the pseudotachylite from this quarry yields paleomagnetic directions consistent with the impact at 2 Ga (Carporzen et al., 2005), the oxidation occurred during genesis. The formation temperature of the pseudotachylite must have exceeded the melting temperature of magnetite (1500–1600°C), and have been likely higher if the formation depth was 20 km. The fascinating texture could have developed during rapid decompression when magnetite micromelts agglomerated to form larger crystallites.

4.4.2 Target rocks

How meteorite impacts modify the magnetic signals of the target rocks is as complex as the diverse petrology existing in the myriad of craters. Images of fractured grains are published for Bosumtwi (Kontny et al., 2007), Keurusselkä (Raiskila et al., 2011), and Sudbury (Giroux and Benn, 2005). Figure 4.4 shows a few curious examples (V0006A and V0015A) from the granulite facies rocks in Vredefort collected in

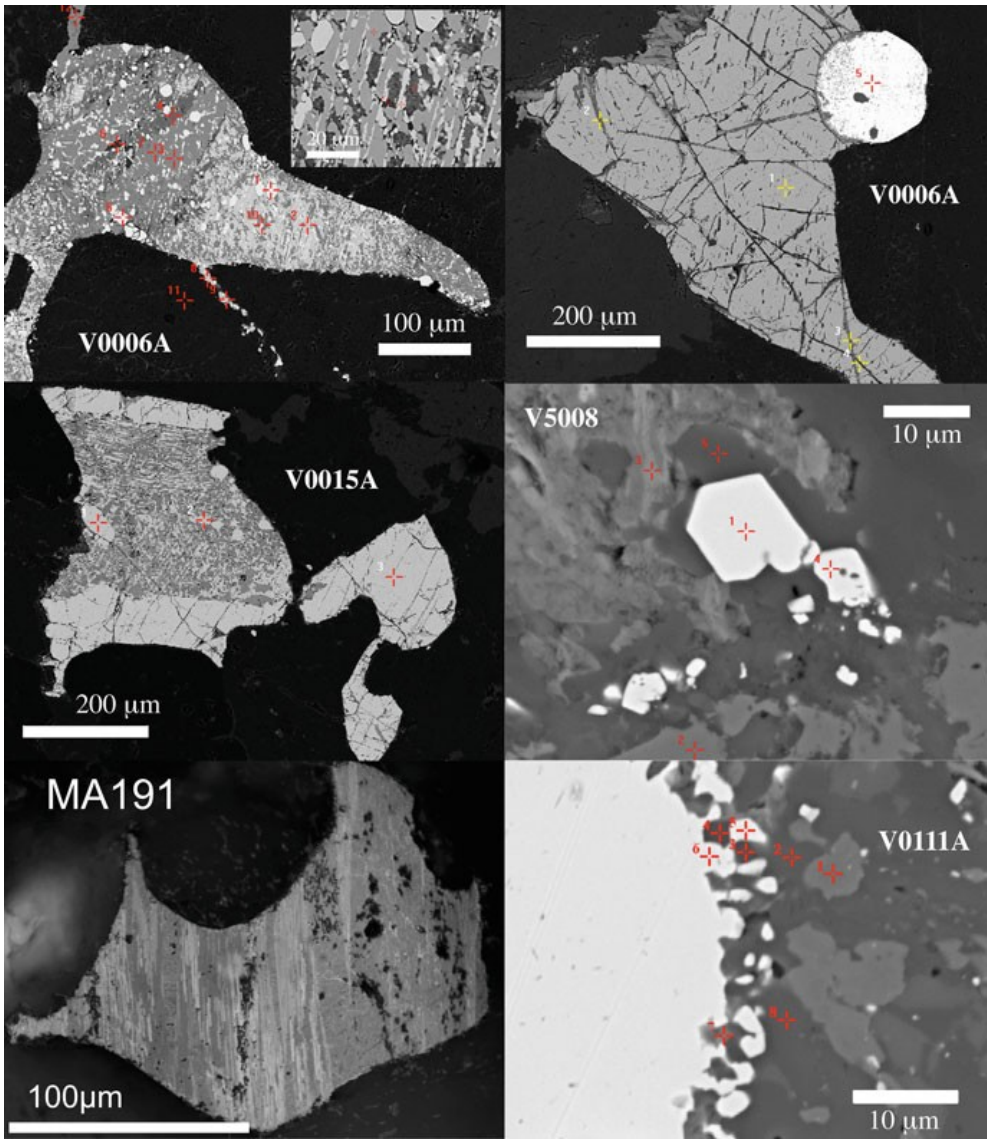

Figure 4.4: Electron microprobe images of rocks from the Vredefort (V) and Manicouagan (MA) craters. The image on the upper right is Ti-poor magnetite showing fractures interpreted to be shock induced. The round bright mineral is monazite (rare earth element-bearing phosphate). The image on the upper left is highly exsolved titanomagnetite that comes from the same 1-in. core as that on the upper right. Bright (dark) grains are Ti-poor (rich) titanomagnetite. Middle left image of sample V0015A contains a combination of the two examples from V0006A. Margins are Ti-poor, fractured magnetite, while the interior is highly exsolved titanomagnetite with no cracks. V5008 contains euhedral Ti-poor magnetite with no evidence for shock. V0111A comes from a pseudotachylite in the Otavi quarry in Vredefort. The bright mineral is Ti-poor magnetite. MA191 shows an exsolved iron-titanium oxide from a gneissic diorite (Eitel et al. 2016).

the "horseshoe" region containing the most negative magnetic anomalies inside the crater (figure 4.4). The image on the upper right is Ti-poor magnetite showing evi-

dence for shock. Darker material in the cracks is likely sphene (Ca, Ti silicate). The image on the upper left comes from the same 1-in. core as that on the right. This grain consists of highly exsolved iron-titanium oxide whose morphology is highly rounded. The bright regions are Ti-poor magnetite while the darker material is Ti-rich magnetite. Some titanomagnetite from the main body appears to have been injected into surrounding minerals.

Sample V0015 (middle left image in figure 4.4) was collected a few meters from V0006. This sample shows a combination of the two examples above whose margins are composed of Ti-poor, shocked magnetite, while the interior is highly exsolved titanomagnetite with no cracks. Sample V5008 comes from a granite quarry in the northwest part of the Vredefort crater, about 1.5 km from the contact with the sediments, outside the region with distinctive negative anomalies. It contains euhedral Ti-poor magnetite with no evidence for shock. In comparison, the lower right image (MA191) from Manicouagan shows an exsolved iron-titanium oxide from a gneissic diorite (Figure 3 in Eitel et al., 2016). Its non-euhedral morphology mimics that of the exsolved titanomagnetite from Vredefort, except that MA191 shows only one preferred exsolution plane, whereas V0006A has multiple planes. We think that the shock texture in V0006A stems from the 2 Ga meteorite impact whereas the multiplanar exsolution texture might be due to partial melting from lightning strikes. More work is needed to understand the shock textures and morphologies of iron oxides from target rocks.

4.4.3 Shock remanent magnetization

Static and dynamic pressures have the potential to drastically change the magnetic properties of the ferromagnetic minerals in rocks (Hargraves and Perkins, 1969; Pohl et al., 1975; Cisowski and Fuller, 1978; Gattacceca et al., 2010; Louzada et al., 2010; Tikoo et al., 2015; Bezaeva et al., 2016). A natural remanent magnetization (NRM) acquired in the Earth magnetic field can be appreciably reduced by weak shock waves as low as 1 GPa. On the other hand shock waves can generate new remanent

magnetizations in an ambient field on par with the strength of that of the Earth (~50 μT) and thus overprint the preexisting NRM. Experiments show that these shock remanent magnetizations (SRMs) primarily affect the grains with relatively low coercive forces that can be removed by alternating field demagnetization. Thermal effects can be neglected for pressures less than a few GPa. Higher pressures lead to irreversible changes of the mineralogical and magnetic properties, such as susceptibility or coercive force, and thermal effects can no longer be neglected, which leads to an ambiguity whether the remanence in target rocks is due to an SRM (shock remagnetization in the absence of a thermal overprint) or whether they are complete or partial thermal overprints that potentially erased an SRM. Distinguishing an SRM from a thermal (TRM) or chemical (CRM) remanent magnetization is a complex problem (Halls, 1979).

Among the earliest investigations for shock remanent magnetization (SRM) was a study at the Barringer (USA) impact structure. There, Hargraves and Perkins (1969) found no evidence for modification of the magnetic remanence at four, hematite-bearing red bed sites around the rim of the crater when compared to the changes measured from shock created by underground nuclear explosions on magnetite+hematite-bearing tuff or compared to laboratory ballistic shock experiments on magnetite-bearing basalt. Further work by Cisowski and Fuller (1978) suggested that dolomite and sandstone in the crater underwent changes in remanence and hysteresis properties with increasing degrees of shock metamorphism. Remanent directions in deformed Ordovician sediments at the Kentland structure (USA) are solely of normal polarity and fail the fold test, which led Jackson and Van der Voo (1986) to conclude that the magnetization directions do not stem from a shock remanence since the directions post-date deformation, but they could be related to heat generated from the impact. Deformed carbonate rocks at the Weaubleau (USA) structure possess post-folding magnetizations that cannot be an SRM, but are possibly related to fluids generated from the impact event that created a chemical remanent magnetization (Dulin and Elmore, 2008). Agarwal et al. (2015) found no evidence for shock-related reorientation of the magnetic principal axes in the magnetite-bearing basement rocks 4–

8 km from the center of the Lockne (Sweden) crater where shock pressures were relatively low (<0.5 and >0.2 GPa). In a borehole 4 km from Lockne's center, Melero-Asensio et al. (2015) found that the magnetic properties of rocks affected by the impact show a slight weakening in the coercivity of magnetic minerals in comparison with rocks not affected by the impact.

Evidence for shock remanent magnetization at the Lonar (India) crater is hotly contested. Rao and Bhalla (1984) claimed that systematic variations in magnetization intensity and susceptibility could be detected over a radial distance of 150 m in the target basalt flows. Cisowski and Fuller (1978) suggested that shock influenced the remanence and the coercivity of the basalts. Nishioka and Funaki (2008) imparted ballistic shock on Lonar basalts – the magnetic remanence and susceptibility were reduced and the principal axes of magnetic anisotropy ellipsoid became reoriented and distorted. Consistent with these experimental results, Misra et al. (2010) found a lowering of the degree of anisotropy compared to unshocked rocks as well as widely scattered principal axes of the magnetic anisotropy ellipsoid directions from basalts collected around the rim. However, Misra et al. (2010) and a subsequent study by Arif et al. (2012) failed to apply a tilt correction for folding around the rim. Louzada et al. (2008) did apply a tilt correction and found that viscous (and/or chemical) remanent magnetization acquired in the ca. 50 kyr subsequent to crater formation obscured any evidence of shock remanent magnetization, which calls into question the interpretations of the anisotropy data. Moreover, Agarwal et al. (2016) found no significant differences in the magnetic fabrics of the Lonar basalts in the deformed rim or farther away.

Halls (1979) argued that the magnetic directions of a magnetization component isolated in the low-coercivity part of the alternating field unblocking spectrum of target rocks from the Slate Islands crater were reoriented by the passage of a shock wave within 2–3 s following meteorite impact. The main evidence for the overprint being acquired as a shock remanent magnetization was that the low-coercivity magnetization component clustered more tightly after making a structural correction based on shatter cone directions. The magnetization of the matrix of clastic breccia dikes that

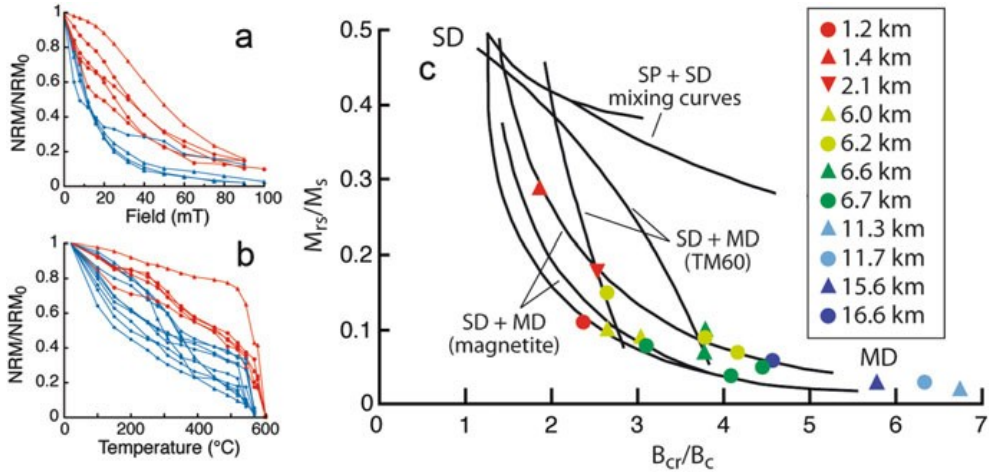

Figure 4.5: Rock magnetic data from anorthositic basement rocks from the Mistastin impact structure (from Hervé et al., 2015). (a) and (b) Normalized alternating field and thermal magnetization intensity curves comparing samples in red that were thermally remagnetized by 36 Ma impact melts with those in blue that were not thermally remagnetized. (c) Day plot (Day et al., 1977) of the remanence ratio (remanent saturation magnetization [M_{rs}]/saturation magnetization [M_s]) versus the coercivity ratio (coercivity of remanence [B_{cr}]/bulk coercive force [B_c]) with single-domain (SD)-multidomain (MD) and superparamagnetic (SP)-SD mixing curves for pure magnetite and titanomagnetite from Dunlop (2002). Samples are color coded as a function of radial distance from the crater's center.

formed during the impact event had a similar direction, which led Halls (1979) to interpret it to have formed as a thermal remanent magnetization due to frictional heating during their emplacement. A subsequent study by Fairchild et al. (2016) on Slate Islands breccia dikes confirmed this thermal remanent magnetization interpretation by demonstrating that clasts within the dikes were overprinted as well. This work found a tight grouping of paleomagnetic directions in breccia dikes throughout the Slate Islands structure in the absence of a tectonic correction, which implies that the dikes cooled and locked in magnetic remanence over a time interval in which the impact structure was not deforming. These results indicate that the crater reached a stable geometry within 6 min of the impact based on thermal modeling of the thinnest dikes. The overprint component in the target rocks away from the dikes unblocks mostly between 275 and 325°C, which may indicate that the overprint is thermal in origin (Tikoo et al., 2015; Fairchild et al., 2016), in contrast with the SRM interpretation of Halls (1979).

At Mistastin, thermally remagnetized anorthositic basement rocks near the contact with impact melts have higher remanent magnetizations and higher coercivities than non-thermally remagnetized anorthositic basement rocks (Hervé et al., 2015) (compare red and blue curves in figure 4.5a, b). Hence, the thermally remagnetized samples with the heightened coercivities could be mistaken as a shock product. This highlights the ambiguity whether an SRM is due to remagnetization solely by passage of shock waves through the target rock, or whether heat from the impact thermally overprinted the target rock (Bezaeva et al., 2016), which also increased the coercivity and unblocking spectra as is the case for Mistastin. The Day plot (figure 4.5c; Day et al., 1977) yields information on the domain state from magnetic hysteresis parameters. Mistastin basement rocks exhibit a progression from multidomain towards increasingly single-domain-like behavior approaching the crater's center (Hervé et al., 2015). We think this pattern arises from the strain due to shock and not thermal effects from shock, consistent with laboratory experiments (Carporzen and Gilder, 2010; Reznik et al., 2016), although the samples from the central uplift (Horseshoe Island) might also be thermally influenced.

4.5 Paleomagnetism

4.5.1 Crater Formation Processes

Paleomagnetic studies in impact craters can shed light on crater formation processes. The transient crater becomes filled with impact melts and breccias, and then rebound occurs, which might cause displacement of the crater fill material. Larger craters have central uplifts and even larger craters have multiple rings. Questions arise as to how fast these processes occur and how the structural features form kinematically. Paleomagnetism can help answer these questions by examining the dispersion in directions from rocks sampled around the crater (figure 4.6), noting that one needs to unravel the effect of geomagnetic secular variation, which creates directional dispersion through dipole wobble, from directional reorientation due to kinematic readjustment. One must keep in mind that the "paleomagnetic clock" starts ticking only after

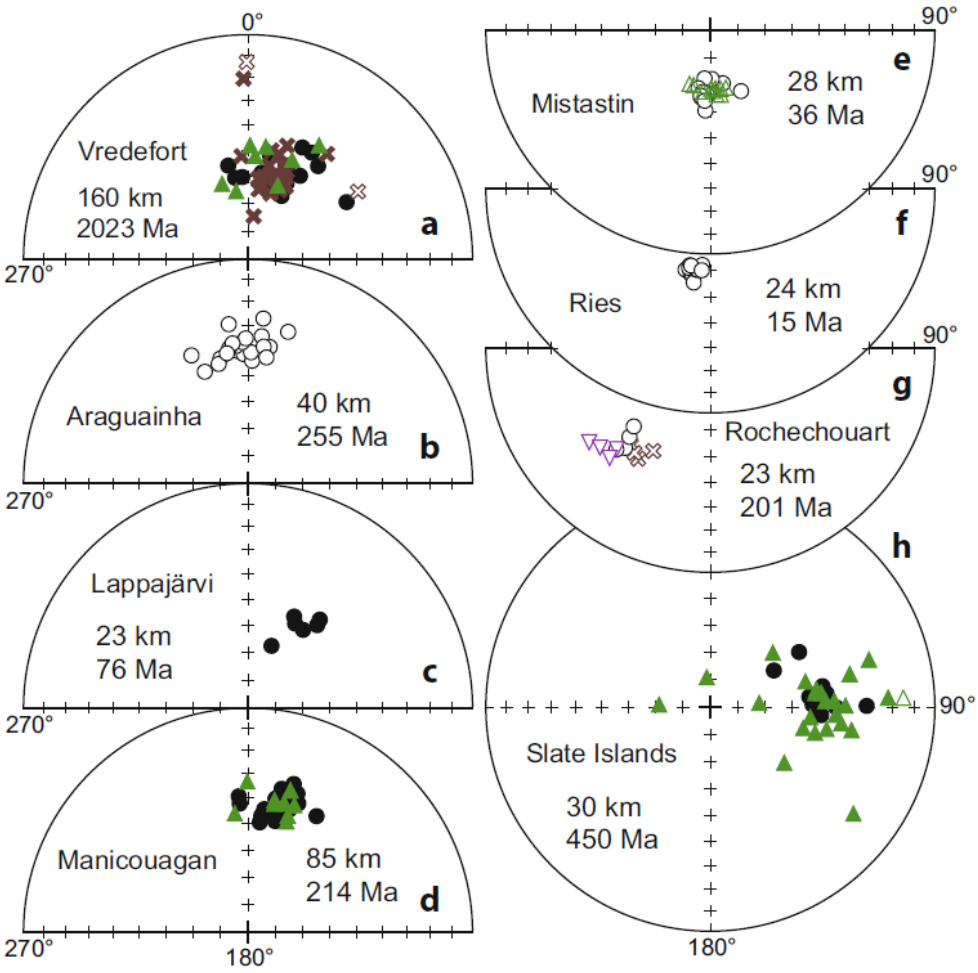

Figure 4.6: Site mean paleomagnetic directions from impact melt-bearing rocks from eight craters. Age and diameter data from http://www.passc.net/EarthImpactDatabase/index.html. Open symbols: upper hemisphere, solid symbols: lower hemisphere. (a) Vredefort: circles from Salminen et al. (2009), triangles from Hargraves (1970), crosses from Carporzen et al. (2005); (b) Araguainha: Yokoyama et al. (2014); (c) Lappajärvi: Pesonen et al. (1992); (d) Manicouagan: circles from Eitel et al. (2016), triangles from Larochelle and Currie (1967); (e) Mistastin: circles from Hervé et al. (2015), triangles from Currie and Larochelle (1969); (f) Ries: Pohl (1965); (g) Rochechouart: circles from Eitel et al. (2014), triangles from Pohl and Soffel (1971), crosses from Carporzen and Gilder (2006) (two data points inverted to reversed polarity); (h) Slate Islands: circles from Fairchild et al. (2016), triangles from Halls (1979).

the ferromagnets in the studied rocks cool through their Curie temperatures. The clock in craters <30 km in diameter with melt thicknesses generally <100 m (e.g., Ries or Rochechouart) likely begins within days to 10s or 100s of years of formation; however, it can be as long as a few 10^4 years in larger craters like Manicouagan where impact melts reach several 100s of meters thick. To a first order, figure 4.6

shows that structural modifications related to crater formation completely ceased over these time scales. The general impression is that the smaller the crater, the less the dispersion, which makes sense recalling that smaller craters likely have thinner impact melts that cool quicker, so they record less time and smaller secular variation amplitudes.

4.5.2 Do Meteorite Impacts Influence the Geodynamo?

Because the energy released during an impact can exceed that of the strongest terrestrial earthquakes by several orders of magnitude, several workers have questioned whether impact events can perturb the magnetohydrodynamic regime in planetary interiors and influence the magnetic field generation process. Testing this has been our overriding motivation over the last several years. Here we summarize our findings and give additional evidence from other craters.

Glass and Heezen (1967) were among the first to link changes in the geomagnetic field to a meteorite impact event by claiming that the Australasian microtektite field was deposited during the period coinciding with the last known reversal (Brunhes-Matuyama). Durrani and Khan (1971) then suggested that the slightly older Ivory Coast microtektite field was deposited just above the base of a brief magnetic chron known as the Jaramillo event. Further drilling in the Atlantic Ocean led Glass and Zwart (1979) to conclude that the Ivory Coast microtektite field was four times larger than previously thought. They correlated the tektite layer with the beginning of the Jaramillo event.

The association of meteorite impacts with geomagnetic field reversals led several workers to explore how an impact event could perturb the geodynamo (e.g., Schwarzschild, 1987). Muller and Morris (1986) postulated that the link between impacts and geomagnetic perturbation occurred through climate change. They calculated that if sea-level fluctuations were large (>10 m) and rapid (a few 100 years) enough before adjustments in the moment of inertia could take place, then shear would occur between the Earth's mantle and solid core, which would deform convec-

tion cells in the liquid outer core, thereby influencing the magnetic field. Their scenario predicted that the dipole component of the geodynamo would diminish with a concomitant increase in higher order components, which are characteristics of field reversals and transitions. Pal and Creer (1986) performed a statistical analysis of field reversals and found a correlation with episodes of bombardment. Like Muller and Morris (1986), and later Burek and Wänke (1988), Pal and Creer (1986) postulated that meteorite impacts would create turbulence in the outer core leading to lower field strength and a departure from axial symmetry, consistent with reversal models.

Won and Kuo (1973) worked out the conditions for which the solid inner core begins oscillating from translational motion due to an earthquake. They found that a magnitude 8.8 earthquake (10^{18} J of energy released) would provoke an inner core oscillation with an amplitude of 58 cm. The amount of inner core oscillation required to modify the magnetohydrodynamic regime in the outer core is unknown, although Roberts et al. (2009) and Arkani-Hamed and Olson (2010) proposed that bombardment by very large meteorites producing craters >2500 km in diameter could stop the Martian dynamo.

Loper and McCartney (1990) computed that dynamical coupling between the core and mantle is too strong to allow large angular displacements to occur and thus refuted an extraterrestrial origin for field reversals. Rice and Creer (1989) calculated that shock spallation, either at the core-mantle or inner-outer core boundaries, would not provide enough energy to significantly disturb the geomagnetic field. More detailed work on the Australasian and Ivory Coast microtektite fields, including a more detailed examination of sedimentation rates, provided evidence that deposition of the tektite fields was shifted by 8–15 kyr from the nearest geomagnetic event (Burns, 1990; DeMenocal et al., 1990; Schneider and Kent, 1990; Schneider et al., 1992; Glass et al., 1991). Hartl and Tauxe (1996) subsequently found a global decrease in paleointensity approximately 15 kyr prior to the Brunhes-Matuyama reversal, suggesting that it may have commenced earlier than previously thought – precisely at the time when the Australasian microtektites were deposited. Two suevite sites associ-

ated with the Bosumtwi crater that produced the Ivory Coast microtektite field yielded normal polarity directions consistent with emplacement during the Jaramillo chron (Plado 2000). Polarity designations of directions from unoriented drill cores (Elbra et al. 2007) cannot be assigned with confidence; given the crater's proximity to the geographic equator, latitudinal variations in the position of the geomagnetic equator obscure polarity designation based on inclination-only data.

Tektite production represents only a small fraction of the material created during a meteorite impact, whereas a much larger volume of the target rocks is heated, often melted, and deposited near the crater. For this reason, a more straightforward test for a relationship between meteorite impacts and geomagnetic field changes can be performed by examining the thermal remanent magnetization of the melt rocks and impact breccias (suevites) acquired during cooling through the Curie temperatures of the magnetic minerals after the impact. We thus initiated a paleomagnetic study of rocks within meteorite craters whose ferromagnetic minerals cooled through their Curie temperatures after impact. The objective was to sample impact lithologies as a function of cooling time, e.g., from the margins toward the interior of impact melt sheets, to identify potential changes in magnetic field direction and/or intensity.

We carried out such work in the Ries (Germany: Koch et al., 2012), Rochechouart (France: Eitel et al., 2014), Mistastin (Canada: Hervé et al., 2015), and Manicouagan (Canada: Eitel et al., 2016) craters. In the first three, we found no evidence for aberrant directions or for paleointensity values outside the range of expected values. That anomalous field behavior was not observed in any of them could result from insufficient amounts of energy released during these impact events, or because the rocks cooled too fast after impact and "missed" the event. The amount of time captured by the magnetic record in these craters did not exceed 400 years. At the Manicouagan structure, we sampled stratigraphic thicknesses corresponding to several hundred to several thousand or even tens of thousands of years of cooling time following the impact. These time scales exceed normal overturn times (3000–5000 years) in the outer core, i.e., the time needed for a geomagnetic reversal (Bogue and Merrill, 1992; Leonhardt and Fabian, 2007; Valet et al., 2012), so we should have observed an ef-

fect had the Manicouagan impact perturbed the dynamo process. Our overall conclusion is that the seismic energy released from terrestrial impacts that create craters <90 km in diameter is insufficient to disturb the dynamo process (such as through oscillation of the inner core) in a way that results in observable changes in geomagnetic field direction or intensity on the Earth's surface.

The 180 km diameter Chicxulub crater should be a candidate for further research. In the Yucatan-6 exploratory well, about 60 km from the crater's center, paleomagnetic research on impact melts and breccias yielded inclinations of -40° to -45°, indicating a reverse polarity field during impact around the Cretaceous-Tertiary boundary (Urrutia-Fucugauchi et al., 1994). These inclinations lie within the range of expected values predicted by the apparent polar wander path for North America, which suggest that the rocks were not overprinted during drilling and extraction. Subsequent paleomagnetic work by Rebolledo-Vieyra and Urrutia-Fucugauchi (2004) on a different borehole (Yax-1) confirmed that impact breccias have reverse polarities and that carbonates deposited up to 56 cm over the impact breccias also contain reverse polarity. Above this, four samples from 20 cm of carbonate have normal polarity, which leads us to wonder whether the polarity flip could represent a link between impact and reversal. However, there is room for doubt as the data in Figure 3 of Rebolledo-Vieyra and Urrutia-Fucugauchi (2004) indicate that demagnetization was sometimes incomplete and that some samples with downward-pointing inclinations could be drilling-induced overprints. Urrutia-Fucugauchi et al. (2004a) presented a much more complicated stratigraphic profile of inclinations from the same core. They interpreted the reverse magnetization as the primary component in the breccias, with the rest of the remanences being acquired during an extended interval where secondary partial or total remagnetization occurred. The latter seems well substantiated by magnetic mineralogy studies by Pilkington et al. (2004). Further paleomagnetic work on the impactite sequence in Yax-1 yielded an even more complicated pattern of inclination variation with depth (Velasco-Villareal et al., 2011). Future drilling should shed more light on this intriguing problem.

4.6 Conclusions

Meteorite impact structures are among the most dominant topographic expressions in the Solar System. They commonly possess distinct magnetic anomalies. Magnetic expressions of impact craters have been used on Mars to date the history of its dynamo (Hood et al., 2003; Lillis et al., 2013). Shock waves from impact were proposed to influence the geodynamo and even to stop the Martian dynamo (Roberts et al., 2009; Arkani-Hamed and Olson, 2010). Our data indicate that the impact events producing the Manicouagan, Ries, Rochechouart, and Mistastin structures had no observable affect on Earth's dynamo (Koch et al., 2012; Eitel et al., 2014; Hervé et al., 2015; Eitel et al., 2016); hence geodynamo disturbances from impacts should be considered improbable during the Phanerozoic when impact frequency and meteorite sizes were lower than in the Precambrian (French, 1998). Other places in the Solar System host craters much larger than on Earth, such as the South Pole Aitken crater on the Moon (2400 km) or Hellas Planitia on Mars (2300 km), so the influence could be significantly different in those cases.

Paleomagnetic directions in the impact melts and suevites from all studied craters show limited dispersion regardless of size. This suggests that tectonic adjustments, including the formation of central peaks, should be faster than it took the impactites to cool to ca. 600°, which is true even for very thin bodies that cooled within 10–100 days of impact. Further work is needed to unravel how shock pressures and thermal effects related to shock influence the magnetic remanence and rock magnetic characteristics of the target rocks. A dichotomy exists in that strain has a disproportionate influence on grains with low unblocking temperatures, yet produces systematically more single-domain-like grains whose unblocking spectra should be shifted higher as observed from thermal effects in Mistastin (figure 4.6). While shock experiments in Earth-like fields show that the magnetization vector can reorient parallel to the ambient field (e.g., Pohl et al., 1975; Gattacceca et al., 2008), static compression experiments do not, despite comparable changes in rock magnetic parameters (e.g., Hamano, 1983; Valeev and Absalyamov, 2000; Gilder et al., 2006).

4.7 Acknowledgments

We thank the many collaborators and friends that contributed to this work: Ian Garrick-Bethell, Jennifer Buz, Laurent Carporzen, Armand Galdeano, Joshua Gilder, Rodger, Craig and Jarred Hart, Gwenaël Hervé, Joseph Hodych, Joe Kirschvink, Stephan Koch, Thomas Kunzmann, Maxime Le Goff, Eduardo Lima, Claude Marchat, Cassandra Marion, Manfriedt Muundjua, Francois Mazeaufroid, Gordon Osinski, Nikolai Petersen, Anne Pommier, John Spray, Paul Sylvester, Lucy Thompson, Claudia Trepmann, Ben Weiss, and Marie-France Yserd. This work was made possible through funding by Deutsche Forschungsgemeinschaft's Schwerpunktprogramm, Planetary Magnetism grant GI712/6-1. A thorough review by Nicolas Swanson-Hysell is greatly appreciated.

5 AF demagnetization and ARM acquisition at elevated temperatures in natural titanomagnetite bearing rocks

The following chapter (Eitel and Volk, in prep.) will be submitted under the title "AF demagnetization and ARM acquisition at elevated temperatures in natural titanomagnetite bearing rocks" to *Geophysical Journal International*.

5.1 Abstract

This article presents a series of rock magnetic experiments on natural low Ti titanomagnetites (Curie temperature between 534°C and 561°C) examining the effects of high temperature treatment on alternating field (AF) demagnetization and acquisition of an anhysteretic remanent magnetization (ARM). One of our sample sets comes from a borehole drilled through the impact melt sheet of the Manicouagan crater (Canada), the other from the Rocche Rosse lava flow on the island of Lipari (Italy). Hysteresis parameters indicate the magnetic carriers to be in the pseudo-single-domain range showing no evidence for oxidation. AF demagnetization experiments at 500°C have shown a significantly (by a factor between 1.4 and > 7.6) decreased median destructive field of the samples, while it is slightly increased by thermal treatment before applying the AF demagnetization, which is also expressed in a shift of the coercivity spectra towards lower and higher fields, respectively. The comparison of full ARM and partial thermal remanent magnetization (pTRM) at successively increased temperatures with a hybrid tARM reveals that combined additivity between the two kinds of remanences is fullled. Furthermore, a linear relationship was found between the peak magnetic field required to demagnetize a fraction of a full TRM of

a sample at a certain temperature and the one necessary to demagnetize the same fraction after heating to that temperature.

5.2 Introduction

Thellier type paleointensities are a robust method to estimate the strength of the magnetic field of ancient times. The method has a solid theoretical foundation in Néel theory (Néel, 1949). Thellier (1938) has introduced three laws for thermoremanent magnetization in single domain (SD) particles, which need to be fulfilled in order for the result to be valid:

1. reciprocity: a partial thermal remanent magnetization (pTRM) imparted in a certain temperature interval can be demagnetized by null field thermal cycling through the same temperature interval;
2. independence: pTRMs of two not overlapping temperature intervals do not influence each other;
3. additivity: the sum of the pTRMs of two not overlapping temperature intervals equals the pTRM acquired over the full temperature interval.

These laws have been tested for different minerals and particle sizes (e.g., Levi, 1979; Shcherbakova et al., 2000; Riisager and Riisager, 2001; Shcherbakov and Shcherbakova, 2001; Yu and Tauxe, 2005). Analoguously, reciprocity, additivity and independence of partial anhysteretic remanent magnetizations (pARM) were also tested (Yu et al., 2002a; 2002b; 2003). While the law of additivity of pARMs holds for all classes of material (Patton and Fitch, 1962), multidomain (MD) grains violate the laws of reciprocity and independence.

The nature of anhysteretic remanent magnetization (ARM) as well as the influence of various parameters on ARM intensity has been subject of a plenty of studies. Sugiura (1979) found a dependence of the ratios between ARM, TRM and SIRM (saturation isothermal remanent magnetization) on the magnetite concentration within a sample potentially leading to errors of a factor ≈ 6 when using the pseudo-Thellier method

(see Tauxe et al., 1995) – although not designed for that – for absolute paleointensity investigations on natural samples with typical concentrations of magnetite. An analysis of grain size dependence of ARM was performed and compared to multidomain theory (Stacey, 1963) by Gillingham and Stacey (1971). Egli and Lowrie (2002) performed a detailed theoretical study of ARM in dependence of parameters such as grain size and alternating field (AF) ramp rate. For magnetite grains up to 60 nm in diameter they found a dependence of ARM intensity on the grain size ($\propto d^2$), temperature ($\propto T^{-2/3}$) and a weak dependence on the ramping rate of the alternating field.

However, to our knowledge, so far the combined additivity of thermal and anhysteretic remanent magnetizations has never been studied. In this paper, we present a series of experiments imparting pTRMs (pTRM (T)) by in field heating and cooling of the samples to seven temperature steps, T_n, and imparting ARMs at the respective temperatures, while the heating-cooling process was performed in zero field (ARM(T)). These results are then compared to a combined thermal and anhysteretic remanent magnetization obtained by thermal cycling of the samples to the desired temperatures in the laboratory field and imparting an ARM, when the target temperature was held (tARM(T)).

Furthermore, we show the AF demagnetization behavior of a full TRM after thermal demagnetization to certain temperature steps, T_n, and compare it to AF demagnetization performed while samples are held at elevated temperature.

5.3 Sample description

Samples 525, 1125 and 1524 are natural samples from the Manicouagan impact crater (Québec, Canada). They are part of core M0608, described in Spray et al. (2010), drilled during a commercial mineral exploration program; the sample number represents the core depth in meters. This core was drilled through 1.5 km of clast-free and clast-laden impact melt. The rock magnetic properties of these samples were studied in Eitel et al. (2016). The only magnetic remanence carriers are Ti-poor titanomagnetites (Curie temperatures between 550°C and 561°C), with increasing

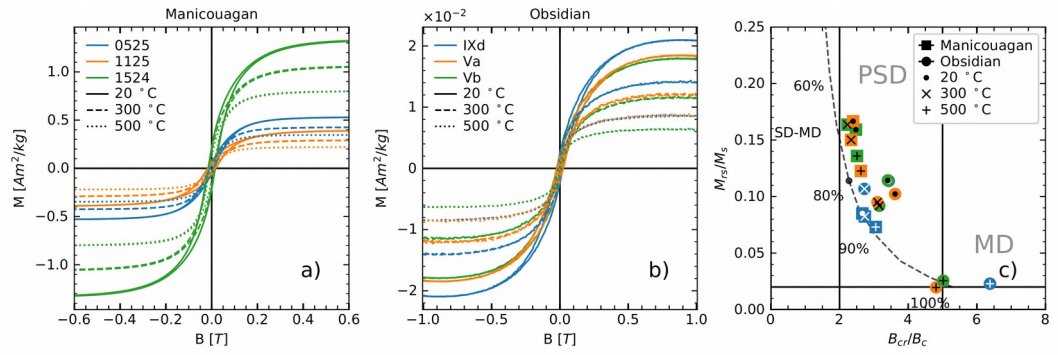

Figure 5.1: Hysteresis plots of the samples from a) Manicouagan; b) Rocche Rosse. c) Day plot (Day et al., 1977) showing all the samples are in pseudo single domain (PSD) state and the mixing line from Dunlop (2002). Square markers show samples from the Manicouagan sample set, round markers are obsidian samples. The colors correspond to the samples as defined in (a,b).

magnetite concentration towards the bottom; in the samples used here, (titano-)hematite is absent. The second set of samples was collected from the Rocche Rosse (Italy) obsidian flow. These obsidian samples are known for their high thermal stability (Leonhardt et al., 2006; Volk and Gilder, 2016). The dominating magnetic mineral is low-Ti titanomagnetite with an average Curie temperature of 538 ± 4°C (Volk and Gilder, 2016). No other magnetic mineral phases are present.

5.4 Results

5.4.1 Rock-magnetic properties

Hysteresis loops and backfield curves were measured with a LakeShore MicroMag 3900 Vibrating Sample Magnetometer (VSM). The hysteresis loops of the samples from the Manicouagan drill core (figure 5.1a; table 5.1) are all well saturated by 500 mT. Saturation magnetizations range from 0.4 Am^2/kg to 1.3 Am^2/kg, with the highest values at the bottom of the melt sheet. This effect which is confirmed by susceptibility data (Eitel et al., 2016) is interpreted to be caused by a higher titanomagnetite concentration in the lower part of the impact melt due to gravitational differentiation. In these samples, one could expect the magnetic carriers of the upper part to be smaller and thus more single domain (SD). On the other hand, the samples from

Table 5.1
Rock magnetic parameters for all samples determined from hysteresis loops and backfield curves at different temperatures.

Sample	T (°C)	Ms	Mrs	Bc	Bcr	Mrs/Ms	Bcr/Bc
0525	20	530.99	45.16	8.85	23.59	0.09	2.67
0525	300	426.50	35.15	6.93	18.59	0.08	2.74
0525	500	347.61	25.39	5.12	15.63	0.07	3.05
1125	20	391.93	65.31	17.65	42.28	0.17	2.39
1125	300	291.44	43.76	13.00	30.40	0.15	2.34
1125	500	220.48	27.04	8.07	21.15	0.12	2.62
1524	20	1329.99	211.79	15.48	38.33	0.16	2.48
1524	300	1057.25	173.00	12.96	28.90	0.16	2.23
1524	500	801.91	109.01	8.31	20.84	0.14	2.51
IXd	20	20.92	2.38	21.97	75.44	0.11	3.43
IXd	300	14.06	1.50	13.15	35.84	0.11	2.73
IXd	500	8.54	0.20	1.43	9.10	0.02	6.38
Va	20	18.42	1.88	22.48	81.36	0.10	3.62
Va	300	12.04	1.14	13.52	41.98	0.10	3.10
Va	500	8.61	0.17	1.94	9.35	0.02	4.81
Vb	20	17.90	2.05	22.80	77.70	0.11	3.41
Vb	300	11.48	1.05	13.06	41.20	0.09	3.16
Vb	500	6.34	0.16	1.54	7.71	0.03	5.02

Abbreviations are: T, temperature; Ms, saturation magnetization; Mrs, saturation remanence; Bc, coercive force; Bcr, coercivity of remanence. Moment given in (mAm^2/kg), coercivities given in (mT).

the lower part would be larger due to the longer cooling times and behave more multidomain (MD). In fact, the remanence ratios (M_{rs}/M_s) of the three samples are comparable. All samples plot within the pseudo single domain (PSD) range (figure 5.1c); just the M_{rs}/M_s of the intermediate sample is lower than that of the others.

The samples from Rocche Rosse (figure 5.1b) show a saturation magnetization around 2×10^{-2} Am^2/kg, one to two orders of magnitude less than the Manicouagan samples. Detailed rock magnetic experiments were described in Volk and Gilder (2016) and showed magnetic carriers in the pseudo single domain (PSD) range. All obsidian samples show similar hysteresis behavior and parameters, as can be seen in the Day (Day et al., 1977; Dunlop, 2002) plot in figure 5.1c. In general, an increased temperature shifts both the Manicouagan and the obsidian samples more towards the multidomain range.

5.4.2 AF-demagnetization

For stepwise alternating field (AF) demagnetization and anhysteretic remanent magnetization (ARM) acquisition, a custom made oven was built using a Pythagoras tube with the heating wires wound around back and forth in a double helix arrangement to avoid magnetic fields generated by the AC heating current. For the temperature isolation of the coil, the oven is surrounded by Promasil, a porous ceramics material of low thermal conductivity; cylindrical plugs close the front and the backside of the oven. The oven was inserted into a shielded 2G AF coil. Three glass tubes assure a gap between the oven and the coil to allow air circulation driven by a fan. The residual field inside the coil was measured with a 3-component fluxgate magnetometer and is in the order of ten nT. Prior to each AF demagnetization experiment, a full TRM was imparted to the samples in the direction of the core axis by cooling from 600°C with a 50 μT field applied in an ASC Scientic Thermal Demagnetizer, TD48. Measurements of the magnetic moment of the samples were performed using a JR6 spinner magnetometer. All experiments were performed in the magnetically shielded room at the Ludwig-Maximilians-Universität München.

For each sample, we AF-demagnetized a full TRM under the following conditions: (1) ordinary room temperature demagnetization (M_0 = M(0°C, 0°C)); (2) room temperature demagnetization of a 300°C thermally demagnetized remanence (M(0°C, 300°C)); (3) AF demagnetization while the sample temperature was held at 300°C (M(300°C, 300°C)); (4) room temperature demagnetization after heating to 500°C (M(0°C, 500°C)); (5) AF demagnetization while the sample temperature was held at 500°C (M(500°C, 500°C)). The direction of the AF-demagnetization was along the core axis, which corresponds to the TRM direction. In the following we denote the remanent magnetization remaining after AF treatment as $M(T_i, T_j)$, with T_i being the sample temperature during AF demagnetization and T_j the maximum temperature of the sample.

Figure 5.2 shows the thermal decay of the remanent magnetization for two representative samples M1125 and IXd after stepwise AF demagnetization at room tempera-

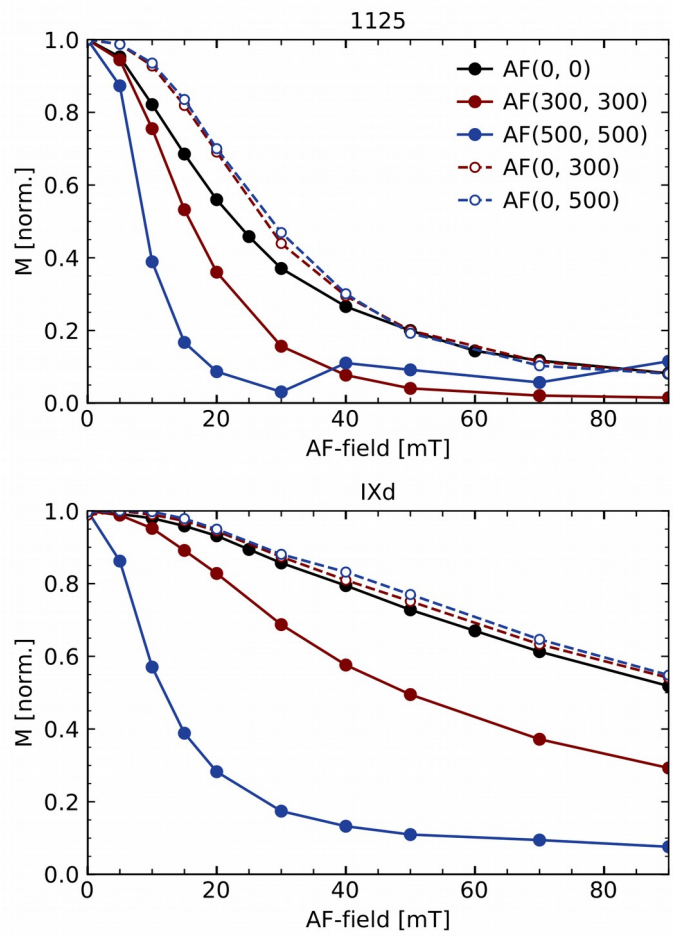

Figure 5.2: AF demagnetization at room temperature (black), after thermal demagnetization at 300°C or 500°C (open symbols, dashed lines) and at the indicated temperature (solid symbols).

ture (black line), and when the AF was applied during (solid lines) as well as after (dashed lines) heating to 300°C and 500°C. The normalized AF demagnetization curves at room temperature are similar with a slight increase in median destructive field (MDF) (table 5.2) after removing the magnetic moment of grains with an unblocking temperature lower than 300°C and 500°C. When AF demagnetization takes place while the samples are at elevated temperature, however, continuously weaker fields are able to demagnetize the sample.

The decay plots of sample IXd shown in figure 5.2b are similar for all three obsidian samples used in this study. Differences between specimens are more expressed in the Manicouagan samples. While samples 525 and 1125 (figure 5.2a) are comparable to

Table 5.2
Median destructive field (MDF) of the samples indicated in the first column for different temperatures.

MDF	T_0, T_0	T_0, 300°C	T_0, 500°C	300°C, 300°C	500°C, 500°C
0525	26.2 mT	29.1 mT	32.1 mT	15.9 mT	7.5 mT
1125	22.9 mT	27.6 mT	28.7 mT	15.9 mT	8.9 mT
1524	12.0 mT	14.7	17.8 mT	9.8 mT	8.4 mT
IXd	-	-	-	49.4 mT	11.9 mT
Va	-	-	-	55.3 mT	15.5 mT
Vb	-	-	-	55.1 mT	13.8 mT

MDF(T_0, T_0) is MDF of TRM without any additional heating, MDF(T_0,T_n) is MDF of TRM where AF is done at room temperature after thermally demagnetizing at T_n; for MDF(T_n,T_n), AF is applied at T_n.

each other, the MDF of sample 1524 that possesses a room temperature MDF (M_0) of 12.0 mT (about half of the two others) is reduced below 10 mT at 300°C. This can be attributed to the higher titanomagnetite concentration. The M(500°C, 500°C) demagnetization curve of sample 1524 assimilates to those of the two other samples from Manicouagan.

5.4.3 TRM, ARM and tARM acquisition

Figure 5.3 displays the results for pTRM(T) acquisition, ARM(T) acquisition and hybrid tARM(T) for samples M1125 and IXD, acquired in a 50 μT direct field along the sample axis. ARMs were acquired in a 90 mT peak AC-field superimposed with a 50 μT direct field. The two samples are representative for their respective sample groups and show largely different behavior. While the Manicouagan samples acquire a pTRM in the first heating step (100°C), the pTRM of the obsidian samples remains close to zero up to temperatures of 300°C and increases slowly up to 500°C. The samples acquire most of their pTRM (> 80%) in the narrow temperature window between 500 and 550°C.

The ARM acquisition of the samples from Manicouagan is relatively temperature independent up to a temperature of 400°C. At T > 400°C (450°C for sample 525), the ARM decreases and vanishes (not surprisingly) close to the Curie temperature of the samples (550°C to 561°C). The obsidian samples show similar behavior. The ac-

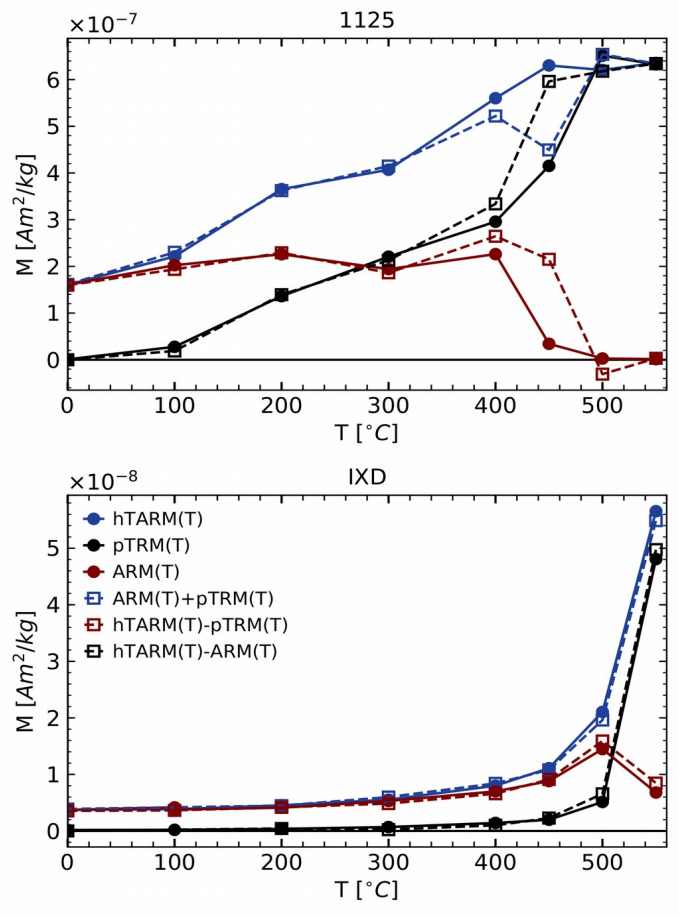

Figure 5.3: pTRM acquisition (black solid line), ARM acquisition (dark red solid line) and hybrid (blue solid line), for selected samples. Dashed lines show the additivity of the different acquisition modes.

quired ARM is constant in the first temperature steps and reaches the maximum value at 500°C. At higher temperatures the ARM(T) decreases.

5.5 Discussion

5.5.1 Coercivity spectra

The room temperature MDFs of the Manicouagan samples are between 12 mT and 26 mT. When AF demagnetization is performed at 300°C, they decrease to 10 to 16 mT; the MDF(500°C, 500°C) is about 8 mT for all three samples from Manicouagan. At room temperature, the maximum field (90 mT) of the coil demagnetizes the

Obsidian samples (Va, Vb, IXd) only to 54 ± 2% of its initial TRM. Therefore calculation of the MDF is not possible, but is likely only slightly higher than the maximum field. Increasing the temperature lowers the MDF(300°C, 300°C) of the obsidians to 49-55 mT and the MDF(500°C, 500°C) to 12-16 mT. This demonstrates the temperature dependence of the coercivity of titanomagnetites.

Furthermore, figure 5.2 and table 5.2 show that the MDF of the samples is raised by a zero field heating cooling cycle before an AF demagnetization. This effect occurs, because the particles with lower coercivities also posses lower unblocking temperatures (T_{UB}), and so, the fraction of the magnetically weakest particles has already thermally been demagnetized. As a consequence, the AF demagnetization, which then can take place only on the remaining – harder – particles, becomes less efficient.

Figure 5.4 shows the derivative of the decay plots from figure 5.2. Compared to the room temperature AF demagnetization of sample M1125, the loss of magnetization is shifted towards higher demagnetizing fields, when the sample is demagnetized after it was exposed to T_n = 300°C or 500°C. The derivatives of the decay plots of sample IXd, however do not show any difference from each other caused by that treatment. In the case of AF demagnetizing the sample while kept at T_n, the coercivity spectrum is shifted and squeezed towards lower fields. While for the Manicouagan sample the maximum measured value of the derivative stays constant at 10 mT, at T_0 and T_n = 300°C the true maximum seems to lie between 10 and 15 mT, at T_n = 500°C between 5 and 10 mT. As the magnetization is now demagnetized in a smaller AF-interval, the maximum value of the derivative becomes higher. This is also true for the obsidian sample, but here, the maximum of the derivative is shifted from 25 mT at room temperature over 20 mT at 300°C to 10 mT at 500°C. This observation also confirms that in the case of the Manicouagan samples thermal demagnetization at moderate temperatures affects the same grains which were demagnetized in alternating fields up to 20 mT, and thus, apparently raises the coercivity of the sample.

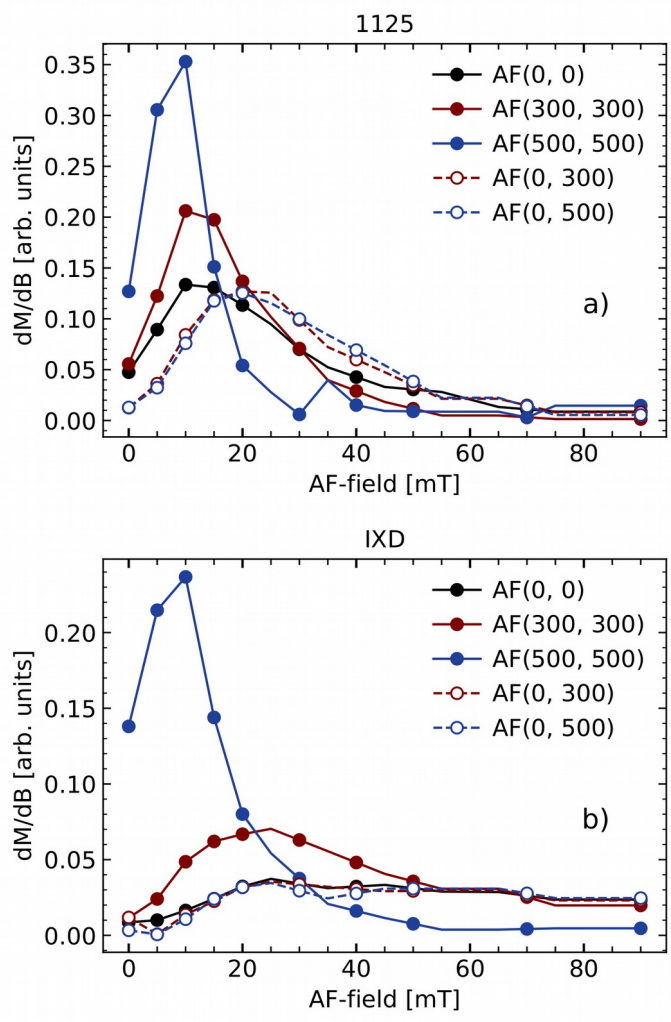

Figure 5.4: Derivatives of the AF decay plots of representative samples M1125 (a) and IXD (b) at room temperature (black), after thermal treatment (open symbols) and at temperature (solid symbols), representing the coercivity spectra of the grains with $T_b > T_i$.

5.5.2 Additivity

The dashed blue line in figure 5.3 represents the sum of the ARM(T) and pTRM(T) curves. In the case of perfect additivity of ARM and pTRM, this curve falls together with the hybrid ATRM curve. For sample M1125, both curves are in good agreement with each other, with a maximum deviation of 6.8%, disregarding the outlier at 450°C. Also in the case of the obsidian sample IXd, deviations never exceed 8.3%,

and are absent below 500°C. The differences of pTRM(T) (red) and ARM(T) (black) from the hybrid tARM measurement are shown for comparison with the ARM(T) and pTRM(T) curves, respectively. The fact that the combined additivity of pTRM and ARM is fulfilled in the samples used in our experiments, can be explained as follows: During the pTRM acquisition, all grains with a blocking temperature below the actual temperature step T_i are magnetized after cooling to room temperature (T_R). In the case of the ARM acquisition at elevated temperature, only those grains with a coercivity $B_C(T_i > T_R) < 90$ mT are magnetized, which have a blocking temperature higher than T_i, as all grains with $T_B < T_i$ stay demagnetized due to cooling to room temperature in zero field. For the hybrid tARM acquisition, however, in the ARM acquisition step, again, the grains with $B_C(T_i > T_R) < 90$ mT and $T_B > T_i$ are magnetized, but during in-field cooling to room temperature, all grains with $T_B < T_i$ are magnetized, regardless of their coercivity. Hence, the grains that acquire a pTRM plus the grains that acquire an ARM are exactly those that are magnetized in the hybrid tARM acquisition step.

5.5.3 Thermal Fluctuations

Thermal fluctuations have been described by Néel (1949) as a thermal fluctuation field, that acts on particles and reduces their coercivity. This effect can be seen by shift in coercivity spectrum towards lower fields when AF-demagnetization is done at elevated temperatures. Dunlop (1976) developed a method using thermal fluctuation analysis to calculate the magnetic grain size.

Just like the MDF one can define the field at which some percentage of the initial magnetic moment is lost (e.g., $B_{0.1}$ being the field where 10% of the initial moment is lost). When the values for the thermally demagnetized samples ($AF(T_0,T_n)$) are compared to the AF at elevated temperature ($AF(T_n,T_n)$) a linear relationship is found (figure 5.5).

In samples 525 (not shown) and 1125 (figure 5.5a) the $B_n(T_0) – B_n(T_n)$ slopes for the experiments at 300°C are the highest obtained from all analyzed samples (e.g.,

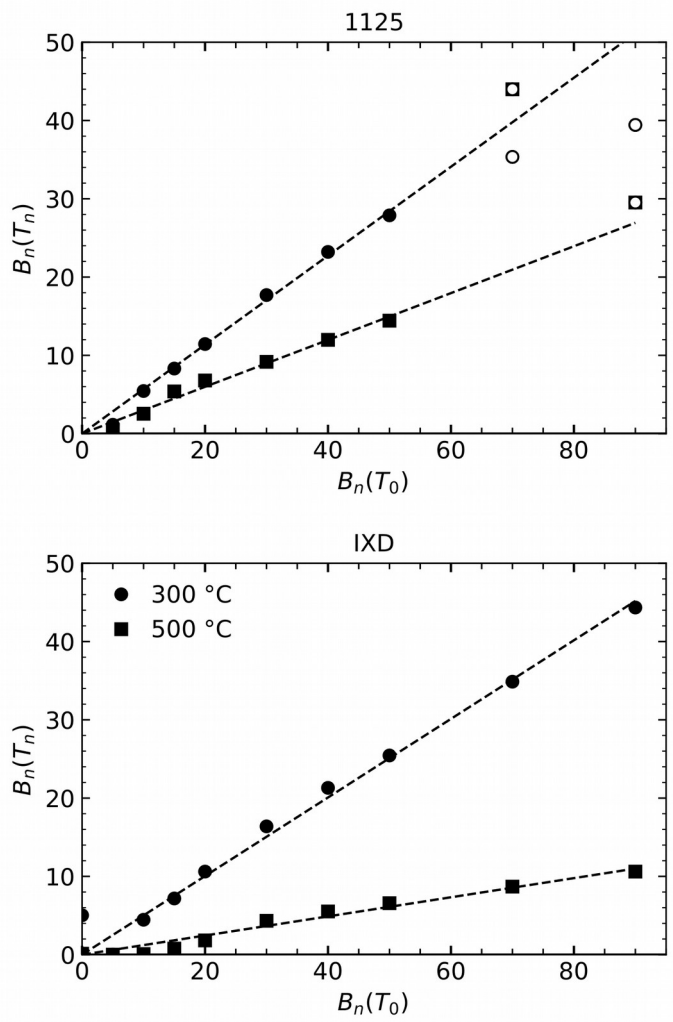

Figure 5.5: The field (in mT) needed to demagnetize the same amount of magnetic moment. The last 2 points of sample M1125 have been excluded in the linear regression line. The slope is proportional to the field needed to demagnetize the same amount of moment at elevated temperatures compared to room temperature.

0.5902 for sample 1125). Here, heating has the least influence on coercivity. Further heating to 500°C reduces the slope to 0.3001. If the slopes of sample 1524 are not forced to the origin, the lines at 300 and 500°C are nearly parallel, with the AF demagnetization at 500°C being 3 to 5% more efficient than at 300°C. The slopes of samples Va and Vb are very similar to the slope of IXd (figure 5.5b). At 300°C, the slopes are around 0,0578, which approximately corresponds to the Manicouagan samples. However, when AF demagnetization is carried out at 500°C, the slope of

sample IXd decreases to 0.1329. Hence, for AF demagnetization an increased temperature shows a stronger effect in the case of the obsidians than for the Manicouagan samples.

All of the samples, however, obtain a weak, but systematic deviation from linearity (figure 5.5). In the first demagnetizing steps, the $B_n(T_0) - B_n(T_n)$ values are below the average slope, increasing above the slope, when 20 to 50% of the initial magnetization are lost through AF demagnetization at elevated temperature. At the highest demagnetization levels, the $B_n(T_0) - B_n(T_n)$ values again fall below the average trend. Elucidation of the reason for the S-shaped form of the data curve still remains subject of research.

5.6 Conclusion

This study has successfully confirmed the reduction of coercivity with increasing temperature also for two sets of natural rock samples containing Ti-poor titanomagnetite of PSD state as shown by Dunlop and Bina (1977) for artificial magnetite bearing samples in a size range between 37 nm and 220 nm. It was shown that magnetite particles that can thermally be demagnetized at lower temperatures, are also those with lower coercivity. Furthermore, we showed that Thellier's law of additivity, which was proven to apply for thermoremanent magnetization (Thellier, 1938) as well as for anhysteretic remanent magnetization (Patton and Fitch, 1962; Yu et al., 2002a) is also valid for a combination of both kinds of magnetization.

5.7 Acknowledgments

Funding for the Project by: Deutsche Forschungsgemeinschaft, SPP 1488 (planetary magnetism). We acknowledge John Spray (Planetary and Space Science Centre, University of New Brunswick) for providing the samples from Manicouagan, and Bettina Scheu (LMU München) for providing the samples from Lipari. Fruitful discussions with Stuart Gilder (LMU München) improved the design of our experi-

ments. Part of this work was performed at the Institute for Rock Magnetism (IRM) at the University of Minnesota. The IRM is a US National Multi user Facility supported through the Instrumentation and Facilities program of the National Science Foundation, Earth Sciences Division, and by funding from the University of Minnesota.

6 Conclusions and outlook

In the framework of this study, the paleomagnetic records of the impact melts and basement rocks of two meteorite impact craters have been checked for evidence of changes of the geomagnetic field followed by the impact event. Furthermore, it includes a rock magnetic study of the effects of high temperature on the alternating field (AF) demagnetization and anhysteretic remanent magnetization (ARM) acquisition in natural titanomagnetites.

For the Rochechouart crater, stepwise demagnetization revealed three kinds of stable magnetization directions: solely normal, solely reversed and samples with multiple, nearly antipodal magnetization directions. This finding posed the question whether these antipodal magnetizations are caused by a geomagnetic field reversal, which was recorded during the time it took the impact melts and suevites to cool through their Curie temperature, or by a rock magnetic self-reversal.

In order to distinguish between the two possibilities, a series of rock magnetic, paleomagnetic, and microscopy experiments were performed. The Curie temperatures found in the rocks from the Rochechouart crater are characteristic for the different sampling localities and resemble different titanium content of the titanohematites. Nearly stoichiometric hematite was found only at Montoume, where stepwise demagnetization revealed one stable, reversely polarized, component. Samples from this locality also yield the most reliable paleointensity results. The lowest Curie temperatures are found in the Chassenon samples that bear only reversed and a few of them mixed magnetic polarities. Optical microscopy, Raman spectroscopy and chemical mapping identify titanohematite grains with multiple phases of varying titanium concentrations at Valette, where normal and mixed magnetic polarities are found. At

this sampling locality, the Curie temperatures lie between those of the other localities.

As the mineralogy found at sites with normal and mixed paleomagnetic polarity is typical of rocks bearing self-reversal behavior, Eitel et al. (2014) concluded that the variation of the magnetic polarity in the stepwise demagnetization experiments does reflect a rock magnetic self-reversal and not the record of a geomagnetic event potentially triggered by the impact. At the time of the impact, the geodynamo was in a reversed state. The virtual dipole moment as obtained from the high quality paleointensity data is relatively low, but still within uncertainty limits compared to reference data of the time of the impact. This finding also gives no support for abnormal field behavior following the impact corresponding to the conclusion for the Ries crater (Koch et al., 2012).

At the Manicouagan crater, all samples – impact melts as well as uplifted basement rocks – exhibit a single component of natural remanent magnetization during stepwise demagnetization. The magnetic polarity in the rocks is normal with the site mean direction probably averaging out secular variation. That in the records not only of the three other craters examined in the scope of the project "Planetary Magnetism" (Ries – Koch et al., 2012; Rochechouart – Eitel et al., 2014; Mistastin – Herve et al., 2015), but also of the ca. three times larger Manicouagan crater no post-impact geomagnetic event was found, gives rise to the conclusion that meteorite impacts – at least in orders of magnitude as they exist on Earth – do not provide enough energy to significantly influence the magnetic field on the surface of the Earth. Also the paleomagnetic directions recorded in the impact craters summarized in Chapter 4, show no unusual behavior. In the Manicouagan crater, the time the impact melts needed to cool through their Curie temperature ranges up to 31,000 years, which exceeds geomagnetic reversal times (Bogue and Merrill, 1992; Leonhardt and Fabian, 2007; Valet et al., 2012). Therefore, if there had been a reversal or excursion followed by the impact, this had been recorded in the crater rocks.

The virtual geomagnetic pole is consistent with two apparent polar wander paths (Torsvik et al., 2001; Besse and Courtillot, 2002) in the upper Triassic, and also the

virtual dipole moment is close to global reference data of that time, again speaking against any abnormal field behavior after the impact.

New insights into the processes of the formation of the Manicouagan crater are given from data of the anisotropy of magnetic remanence. In six out of seven site groups, the declination of the major anisotropy axis (M_1) deviates less than 45° from the radial angle of the site group within the crater. Thus, a random relationship between the data is considered improbable (5%), and it is concluded that the trend in the lineation direction is caused by the radial flow of the impact melt during crater formation. Anisotropy data are ambiguous about whether the recorded flow direction is centripetal (inward flow during the collapse of the transient crater; Dence et al., 1977) or centrifugal (outward flow from the emerging central uplift), but from field observation, centrifugal movement is the rather favored option.

In the last section of this work, the effects of thermal fluctuations in natural titanomagnetites during AF demagnetization were studied. According to the findings by Dunlop and Bina (1977) for artificial magnetite, this study reveals that thermal activation during AF demagnetization reduces the median destructive field (MDF) of the magnetic minerals and shifts the coercivity spectrum towards lower values. Moreover, it was found that if the thermal demagnetization is followed by an AF demagnetization, the MDF is increased. This is because of the fact that grains with lower unblocking temperatures also tend to be magnetically weaker, and so, AF demagnetization is only applied on the magnetically harder grains that were not affected by the high temperature treatment, and thus, becomes less effective.

Acquisition experiments of partial thermal remanent magnetization (pTRM) and ARM at elevated temperatures showed that – up to a certain point – with increasing temperature, the samples become not only thermally more magnetized, but also ARM increases due to magnetic weakening. As soon as thermal demagnetization overweights this effect, ARM acquisition is diminished and at the Curie temperature finally vanished. Then, the remaining remanence is purely thermal. The comparison of separately conducted pTRM and ARM acquisition with a hybrid tARM acquisition provides evidence for Thellier's law of additivity (Thellier, 1938) being fulfilled also

for the combination of thermal and anhysteretic remanence, as the sum of both single remanences is fairly well consistent with the hybrid tARM at the respective temperature steps.

The limits of the terrestrial impact crater repertoire make the search for structures larger than Manicouagan that might carry paleomagnetic information about a post-impact geomagnetic reversal or excursion, difficult. Any traces of craters in the Earth's crust caused by meteorite impacts during the early stages of the Earth have been completely removed by erosional and subduction processes. The remaining larger sized impact craters have been affected by severe erosion or tectonic deformation and metamorphism. Although strongly magnetized, paleomagnetic directions of most of the highly eroded, ~2.0 Ga Vredefort (South Africa) lithologies are broadly distributed (Carporzen et al., 2005). The ~1.85 Ga Sudbury (Canada) crater lost its circular shape and underwent – in parts – metamorphism and paleomagnetic overprint during syn- and post-impact orogenies (Roest and Pilkington, 1994; Spray et al., 2004). The impact melts and suevites of the ~65 Ma Chicxulub crater are buried and partly offshore (e.g., Kenkmann et al., 2004). This makes sampling for paleomagnetic purposes difficult and requires the carrying out of an expensive drilling campaign or the access to it due to the need to cover widespread parts of the structure for a systematic research for a geomagnetic event. However, paleomagnetic sampling at Chicxulub is possible (Urrutia-Fucugauchi et al., 2004a; 2004b) and due to the size of the crater, it is probably the most promising place on Earth to discover evidence for impact driven changes of the geomagnetic field.

An extension of the high temperature AF demagnetization and ARM acquisition study could be performed analogously to the experiments by Dunlop and Bina (1977), who varied the grain sizes of the magnetic carriers. In the current case, however, it would be interesting to systematically and quantitatively repeat the experiments with titanomagnetites and also titanohematites of varying titanium concentrations.

Appendix

The content of this appendix is published as "Supporting Information for A paleomagnetic and rock magnetic study of the Manicouagan impact structure: Implications for crater formation and geodynamo effects" in *Journal of Geophysical Research: Solid Earth* (Eitel et al., 2016).

This appendix consists of two data tables as discussed in chapter 3. Table A1 lists the rock magnetic data from the three deep drill cores and table A2 lists the anisotropy of anhysteretic remanent magnetization data for each site.

Table A1
Rock magnetic data for Manicouagan drill cores M0302, M0603 and M0608.

Alt. [m]	Core depth [m]	χ [10^{-6} m^3/kg]	Ms [Am^2/kg]	Mrs [Am^2/kg]	Bc [mT]	Bcr [mT]	Tc_1 [°C]	Tc_2 [°C] (rel%)
				M0302				
503	7	4.22	0.771	3.48×10^{-2}	5.38	26.21	548	
453	57	6.56	0.930	3.28×10^{-2}	4.22	24.07	549	
403	107	2.72	0.130	1.06×10^{-2}	7.19	42.40	547	
361	149	0.77	0.147	1.30×10^{-2}	8.45	51.60	544	641 (28%)
200	310	1.15	0.147	8.98×10^{-3}	7.17	65.90	541	648 (33%)
193	317	0.72	0.075	1.24×10^{-2}	13.56	79.50	559	645 (22%)
172	338		0.856	3.16×10^{-2}	4.25	23.14	550	
				M0603				
535	5	0.66	0.135	1.66×10^{-2}	13.34	52.27	558	
515	25	4.50	0.826	3.92×10^{-2}	5.21	24.45	556	
495	45	4.16	0.784	3.89×10^{-2}	6.13	25.31	565	
475	65	3.86	0.449	2.81×10^{-2}	8.15	36.69	551	
455	85	1.73	0.407	5.54×10^{-2}	18.21	42.32	550	
435	105	3.10	0.321	4.97×10^{-2}	15.82	42.53	551	
416	124	5.47	0.632	6.06×10^{-2}	8.05	27.97	537	
				M0608				
480	25	0.29	0.021	9.48×10^{-3}	52.14	304.23	543	636 (42%)
460	45	0.81	0.118	5.23×10^{-2}	47.06	83.49	551	603 (19%)
440	65	0.52	0.047	1.59×10^{-2}	33.78	141.18	553	629 (20%)
420	85	0.67	0.083	2.86×10^{-2}	38.04	95.55	554	606 (19%)
400	105	0.24	0.145	5.39×10^{-2}	41.17	88.22	559	603 (20%)
380	125	0.63	0.035	1.69×10^{-2}	78.33	162.62	555	631 (26%)
360	145	0.32	0.098	5.34×10^{-2}	79.03	129.30	553	619 (17%)
340	165	0.58	0.095	4.10×10^{-2}	57.04	119.65	556	625 (15%)
320	185	0.52	0.052	2.38×10^{-2}	63.67	127.89	559	614 (18%)
300	205	10.80	1.220	2.67×10^{-2}	2.37	15.10	544	
280	225	10.93	1.230	2.84×10^{-2}	2.57	16.02	543	
180	325	8.48	0.662	2.12×10^{-2}	3.67	16.54	549	
80	425	7.86	1.530	1.10×10^{-1}	7.22	23.24	554	
-20	525	5.03	0.727	6.23×10^{-2}	8.14	22.04	551	
-120	625	4.74	0.789	6.89×10^{-2}	8.54	27.13	552	
-320	825	7.79	0.651	4.95×10^{-2}	8.05	28.40	549	
-420	925	6.17	1.080	9.69×10^{-2}	9.84	26.68	550	
-520	1025	3.88	0.671	4.69×10^{-2}	7.95	24.66	549	
-620	1125	5.76	0.532	3.21×10^{-2}	6.53	24.44	550	
-755	1260	46.09	4.460	1.38×10^{-1}	4.27	24.07	555	
-826	1331	16.79	0.488	1.80×10^{-2}	4.63	23.73	552	
-1019	1524	60.12	5.600	2.77×10^{-1}	4.86	16.82	561	

Abbreviations are: Alt., altitude in meters; χ, mass normalized magnetic susceptibility; Ms, saturation magnetization; Mrs, saturation remanence; Bc, coercive force; Bcr, coercivity of remanence; Tc_1 and Tc_2, first (<580°C) and second (>580°C) Curie temperature, the latter with the total percentage of the two when both are present.

Table A2
Anisotropy of anhysteretic remanent magnetization results.

Site	Rock Type	N	M_1	M_2	M_3	D_1	I_1	D_2	I_2	D_3	I_3	T	P'	Ctr Az [°]
1	Impact melt	8	1.047	1.002	0.951	281.4	20.4	43.8	66.8	185.1	21.6	-0.05 ± 0.31	1.11 ± 0.08	312
2	Impact melt	6	1.029	0.999	0.972	127.0	26.1	272.0	64.7	34.2	10.3	-0.03 ± 0.19	1.06 ± 0.01	312
3	Impact melt	6	1.052	0.983	0.966	337.3	4.7	218.2	79.9	68.5	9.0	-0.59 ± 0.12	1.09 ± 0.01	312
6	Impact melt	12	1.114	0.983	0.903	101.2	1.0	62.7	72.3	187.3	15.4	-0.24 ± 0.37	1.25 ± 0.17	117
7	Impact melt	8	1.064	0.984	0.952	342.0	7.0	241.8	57.5	88.6	43.5	-0.40 ± 0.17	1.12 ± 0.03	111
8	Impact melt	8	1.047	0.997	0.956	335.2	8.2	247.3	35.1	75.4	57.0	-0.03 ± 0.53	1.10 ± 0.03	111
9	Impact melt	8	1.046	0.998	0.957	305.1	23.0	33.5	47.1	161.9	42.4	0.01 ± 0.29	1.09 ± 0.03	111
10	Anorthosite	4	1.038	1.012	0.951	319.0	12.4	228.9	14.8	83.0	67.9	0.20 ± 0.69	1.10 ± 0.06	-
11	Anorthosite	4	1.033	1.008	0.959	125.9	19.1	32.5	11.3	273.6	68.8	0.33 ± 0.22	1.08 ± 0.03	-
12	Anorthosite	4	1.018	1.004	0.978	116.7	24.0	125.9	1.3	330.7	74.4	0.40 ± 0.42	1.04 ± 0.01	-
13	Anorthosite	4	1.113	0.961	0.925	19.8	33.0	255.1	47.9	118.7	25.6	-0.54 ± 0.31	1.22 ± 0.06	-
14	Anorthosite	4	1.090	0.998	0.912	338.6	39.2	146.4	53.9	245.1	12.1	-0.17 ± 0.53	1.21 ± 0.14	-
15	Impact melt	10	1.059	1.003	0.939	130.6	38.0	333.4	48.4	231.7	16.4	0.19 ± 0.24	1.13 ± 0.09	268
16	Impact melt	14	1.051	0.993	0.956	147.0	10.3	311.0	76.6	55.7	0.5	-0.21 ± 0.29	1.10 ± 0.02	211
17	Impact melt	9	1.046	1.006	0.948	40.9	9.5	254.8	74.1	133.5	6.6	-0.02 ± 0.37	1.12 ± 0.15	159
18	Impact melt	8	1.026	1.002	0.971	150.7	40.2	31.6	35.2	272.8	33.6	0.07 ± 0.45	1.06 ± 0.03	159
19	Impact melt	7	1.027	0.993	0.980	205.8	85.6	306.4	0.3	35.5	5.7	-0.44 ± 0.30	1.05 ± 0.01	159
20	Impact melt	9	1.068	0.998	0.934	21.1	10.2	121.6	58.8	312.0	29.4	-0.02 ± 0.52	1.15 ± 0.04	62
21	Suevite	7	1.018	1.001	0.981	209.2	64.8	65.3	40.0	296.9	15.3	0.07 ± 0.33	1.04 ± 0.01	-
22	Impact melt	10	1.155	0.987	0.858	42.8	41.8	267.3	65.2	128.2	12.2	0.07 ± 0.37	1.38 ± 0.28	62
23	Impact melt	10	1.053	1.000	0.948	261.1	1.1	190.5	51.7	10.5	46.0	0.14 ± 0.45	1.11 ± 0.05	62
24	Impact melt	9	1.069	0.997	0.933	323.0	26.4	227.7	23.3	112.2	51.4	-0.01 ± 0.55	1.15 ± 0.04	62
25	Gneissic diorite	10	1.194	1.029	0.777	143.8	32.3	319.7	59.8	232.6	1.3	0.29 ± 0.24	1.56 ± 0.13	-

Abbreviations are: N, number of samples analyzed; M_1, M_2 and M_3, the major, intermediate and minor eigenvalues of the anisotropy ellipsoid; D_1 (I_1), D_2 (I_2) and D_3 (I_3), the declination (inclination) of the major, intermediate and minor axis directions of the anisotropy ellipsoid; T, shape parameter (Jelinek, 1981); P', corrected anisotropy degree (Jelinek, 1981); Ctr Az, azimuth of each impact melt site with respect to the center of the crater.

References

Abramov, O., Kring, D., 2005. Impact-induced hydrothermal activity on early Mars. J. Geophys. Res. 110, E12S09, doi:10.1029/2005JE002453.

Agarwal, A., Kontny, A., Greiling, R., 2015. Relationship among magnetic fabrics, microfractures and shock pressures at an impact crater: a case study from Lockne crater, Sweden. J. Appl. Geophys. 114, 232-243, doi:10.1016/j.jappgeo.2015.01.010.

Agarwal, A., Kontny, A., Srivastava, D., Greiling, R., 2016. Shock pressure estimates in target basalts of a pristine crater: a case study in the Lonar crater, India. Geol. Soc. Am. Bull. 128, 19-28, doi:10.1130/B31172.1.

Akimoto, S., 1962. Magnetic properties of FeO-Fe_2O_3-TiO_2 system as a basis of rock magnetism. J. Phys. Soc. Jpn. 17, 706-710.

Antoine, L., Nicolaysen, L., Niccol, S., 1990. Processed and enhanced gravity and magnetic images over the Vredefort structure and their interpretation. Tectono-physics 171, 63-74, doi:10.1016/0040-1951(90)90090-U.

Aray, Y., 1963. Secular variation in the intensity of the past geomagnetic field. M.Sc. thesis. Univ. of Tokyo.

Arif, M., Basavaiah, N., Misra, S., Deenadayalan, K., 2012. Variations in magnetic properties of target basalts with the direction of asteroid impact: Example from Lonar crater, India. Meteorit. Planet. Sci. 47, 1305-1323, doi:10.1111/j.1945-5100.2012.01395.x.

Arkani-Hamed, J., Olson, P., 2010. Giant impact stratification of the Martian core. Geophys. Res. Lett. 37, L02201, doi:10.1029/2009GL041417.

Badjukov, D., Bazhenov, M., Nazarov, M., 1989. Paleomagnetism of impactites of the Kara impact crater: preliminary results. In: Lunar and Planetary Science Conference, vol. 20.

Barr, A., Citron, R., 2011. Scaling of melt production in hypervelocity impacts from high-resolution numerical simulations. Icarus 211, 913-916, doi:10.1016/j.icarus.2010.10.022

Beard, L., 2012. Magnetic anomalies of impact craters at low magnetic latitudes. Environmental and engineering geophysical society (EEGS), 2012 symposium on the application of geophysics to engineering and environmental problems (SAGEEP) proceedings, doi:10.4133/1.4721703.

Besse, J., Courtillot, V., 2002. Apparent and true polar wander and the geometry of the geomangetic field over the last 200 Myr. J. Geophys. Res. 107, EPM 6-1 - EPM 6-31, doi:10.1029/2000JB000050.

Bezaeva, N., Swanson-Hysell, N., Tikoo, S., Badyukov, D., Kars, M., Egli, R., Chareev, D., Fairchild, L., Khakhalova, E., Strauss, B., Lindquist, A., 2016. The effects of 10 to >160 GPa shock on the magnetic properties of basalt and diabase. Geochem. Geophys. Geosyst. 17, 1-19, doi:10.1002/2016GC006583.

Biggin, A., McCormack, A., Roberts, A., 2010. Paleointensity database updated and upgraded. Eos Trans. AGU 91, 15, doi:10.1029/2010EO020003.

Biren, M., Spray, J., 2011. Shock veins in the central uplift of the Manicouagan impact structure: Context and genesis. Earth Planet. Sci. Lett. 303, 310-322, doi:10.1016/j.epsl.2011.01.003.

Biren, M., van Soest, M., Wartho, J., Spray, J., 2014. Dating the cooling of exhumed central uplifts of impact structures by the (U-Th)/He method: A case study at Manicouagan. Chem. Geol. 377, 56-71, doi:10.1016/j.chemgeo.2014.03.013.

Bischoff, L., Oskierski, W., 1987. Fractures, pseudotachylite veins and breccia dikes in the crater floor of the Rochechouart impact structure, SW-France, as indicators of crater forming processes. In: Pohl, J. (Ed.), Research in Terrestrial Impact Structures. Springer, Wiesbaden, pp. 5-29, doi:10.1007/978-3-663-01889-6_1.

Bogue, S., Merrill, R., 1992. The character of the field during geomagnetic reversals. Annu. Rev. Earth Planet. Sci. 20, 181-219, doi:10.1146/annurev.ea.20.050192.001145.

Bucur, I., 1994. The direction of the terrestrial magnetic field in France during the last 21 centuries. Recent progress. Phys. Earth Planet. Int. 87, 95-109, doi:10.1016/0031-9201(94)90024-8.

Buddington, A., Lindsley, D., 1964. Iron-titanium oxide minerals and synthetic equivalents. J. Petrol. 5, 310-357, doi:10.1093/petrology/5.2.310.

Bullard, E., Gellman, H., 1954. Homogeneous dynamos and terrestrial magnetism. Phil. Trans. Roy. Soc. London, Ser. A 247, 213-278.

Burek, P., Wänke, H., 1988. Impacts and glacio-eustacy, plate-tectonic episodes, geomagnetic reversals: a concept to facilitate detection of impact events. Phys. Earth Planet. Inter. 50, 183-194, doi:10.1016/0031-9201(88)90005-2.

Burns, C., 1990. The Australasian microtektite layer: Implication concerning its source and relationship to the Brunhes/Matuyama geomagnetic reversal. Ph.D. thesis. University of Delaware.

Bylund, G., 1974. Paleomagnetism of a probable meteoritic impact, the Dellen structure. Geologiska Föreningens i Stockholm Förhandlinger 96, 275-278, doi:10.1080/11035897409454954.

Carporzen, L., Gilder, S., Hart, R., 2005. Paleomagnetism of the Vredefort meteorite crater and implications for craters on Mars. Nature 435, 198-201, doi:10.1038/nature03560.

Carporzen, L., 2006. Magnétisme des cratères d'impact de météorite à Vredefort (Afrique du Sud) et Rochechouart (France). Thesis, Université Paris VII - Denis Diderot.

Carporzen, L., Gilder, S., 2006. Evidence for coeval Late Triassic terrestrial impacts from the Rochechouart (France) meteorite crater. Geophys. Res. Lett. 33, L19308, doi:10.1029/2006GL027356.

Carporzen, L., Gilder, S., Hart, R., 2006. Origin and implications of the Verwey transitions in the basement rocks of the Vredefort meteorite crater, South Africa. Earth Planet. Sci. Lett. 251, 305-317, doi:10.1016/j.epsl.2006.09.013.

Carporzen, L., Gilder, S., 2010. Strain memory of the Verwey transition. J. Geophys. Res. 115, B05103, doi:10.1029/2009JB006813.

Carporzen, L., Weiss, B., Gilder, S., Pommier, A.,2012. Lightning remagnetization of the Vredefort impact crater: no evidence for impact-generated magnetic fields. J. Geophys. Res. 117, E01007, doi:10.1029/2011JE003919.

Cavosie, A., Lugo Centeno, C., 2014. Shocked apatite from the Santa Fe impact structure (USA): A new accessory mineral for studies of shock metamorphism (abs.). 45th Lunar Planet. Sci. Conf., 1691.

Chèvremont, P., Floc'h, J., Ménillet, F., Stussi, J., Delbos, R., Sauret, B., Blès, J., Courbe, C., Vuaillat, D., Gravelat, C., 1996. Note explicative. In: Carte Géologique de la France (1/50000), feuille Rochechouart (687), BRGM, Orléans.

Cisowski, S., Fuller, M., 1978. The effect of shock on the magnetism of terrestrial rocks. J. Geophys. Res. 83, 3441-3458, doi:10.1029/JB083iB07p03441.

Cloete, M., Hart, R., Schmidt, H., Drury, M., Demanet, C., Sankar, K., 1999. Characterization of magnetite particles in shocked quartz by means of electron- and magnetic force microscopy: Vredefort, South Africa. Contrib. Miner. Petrol. 137, 232-245, doi:10.1007/s004100050548.

Coe, R., 1967a. Paleo-intensities of the Earth's magnetic field determined from Tertiary and Quaternary rocks. J. Geophys. Res. 72, 3247-3262, doi:10.1029/JZ072i012p03247.

Coe, R., 1967b. The determination of paleo-intensities of the Earth's magnetic field with emphasis on mechanisms which could cause non-ideal behavior in Thellier's method. J. Geomagn. Geoelectr. 19, 157-179, doi:10.5636/jgg.19.157.

Coe, R., Grommé, S., Mankinen, E.A., 1978. Geomagnetic paleointensities from radiocarbon-dated lava flows on Hawaii and the question of the Pacific nondipole low. J. Geophys. Res. 83, 1740-1756, doi:10.1029/JB083iB04p01740.

Cohen, B., Mark, D., Lee, M., Simpson, S., 2017. A new high-precision $^{40}Ar/^{39}Ar$ age for the Rochechouart impact structure: At least 5 Ma older than the Triassic–Jurassic boundary. Meteorit. Planet. Sci. 52, 1600-1611, doi:10.1111/maps.12880.

Coles, R., Clark, J., 1978. The central magnetic anomaly, Manicouagan Structure, Quebec. J. Geophys. Res. 83, 2805-2808, doi:10.1029/JB083iB06p02805.

Coles, R., Clark, J., 1982. Lake St. Martin impact structure, Manitoba, Canada: magnetic anomalies and magnetizations. J. Geophys. Res. 87, 7087-7095, doi:10.1029/JB087iB08p07087.

Colón Lugo, D., Cavosie, A., 2014. Detrital shocked muscovite from the Santa Fe impact structure (USA) (abs.). 45th Lunar Planet. Sci. Conf., 2033.

Corner, B., Durrheim, R., Nicolaysen, L., 1990. Relationships between the Vredefort structure and the Witwatersrand basin within the tectonic framework of the Kaapvaal craton as interpreted from regional gravity and aeromagnetic data. Tectonophysics 171, 49-61, doi:10.1016/0040-1951(90)90089-Q.

Currie, K., Larochelle, A.,1969. A paleomagnetic study of volcanic rocks from Mistastin Lake, Labrador. Earth Planet. Sci. Lett. 6, 309-315, doi:10.1016/0012-821X(69)90173-3.

Day, R., Fuller, M., Schmidt, V., 1977. Hysteresis properties of titanomagnetites: grain-size and compositional dependence. Phys. Earth Planet. Int. 13(4), 260-267, doi:10.1016/0031-9201(77)90108-X.

deMenocal, P., Ruddiman, W., Kent, D., 1990. Depth of post-depositional remanence acquisition in deep-sea sediments: a case study of the Brunhes–Matuyama reversal and oxygen isotopic Stage 19.1. Earth Planet. Sci. Lett. 99, 1-13, doi:10.1016/0012-821X(90)90066-7.

Dence, M., 1964. A comparative structural and petrographic study of probable Canadian meteorite craters. Meteoritics 2, 249-270.

Dence, M., Grieve, R., Robertson, 1977. Terrestrial impact structures: Principal characteristics and energy considerations. In: Roddy, D., Pepin, R., Merrill, R. (Eds.), Impact and explosion cratering. Pergamon Press, New York, pp. 247-275.

Downs, R., 2006. The RRUFF Project: an integrated study of the chemistry, crystallography, Raman and infrared spectroscopy of minerals. In: Program and Abstracts of the 19th General Meeting of the International Mineralogical Association in Kobe, Japan, O03-13.

Dulin, S., Elmore, R., 2008. Paleomagnetism of the Weaubleau structure, southwestern Missouri. In: Evans, K., Horton, J., King, J., Morrow, D. (Eds.), The sedimentary record of meteorite impacts. Volume special paper 437, pp. 55-64. Geological Society of America, Boulder.

Dunlop, D., Ozima, M., Kinoshita, H., 1969. Piezomagnetization of single-domain grains: a graphical approach. J. Geomagnet. Geoelectr. 21(2), 513-518, doi:10.5636/jgg.21.513.

Dunlop, D., 1976. Thermal fluctuation analysis: A new technique in rock magnetism. J. Geophys. Res. 81, 3511-3517, doi:10.1029/JB081i020p03511.

Dunlop, D., Bina, M., 1977. The coercive force spectrum of magnetite at high temperatures: evidence for thermal activation below the blocking temperature. Geophys. J. Roy. Astr. S. 51, 121-147.

Dunlop, D., Özdemir, Ö, 1997. Rock Magnetism. Cambridge Univ. Press, Cambridge, U. K.

Dunlop, D., 2002. Theory and application of the Day plot (Mrs/Ms versus Hcr/Hc), 1. Theoretical curves and tests using titanomagnetite data. J. Geophys. Res. 107, EPM 4-1 - EPM 4-22, doi:10.1029/2001JB000486.

Durrani, S., Khan, H., 1971. Ivory Coast microtectites: Fission track age and geomagnetic reversals. Nature 232, 320-323, doi:10.1038/232320a0.

Earth Impact Database, 2018. Available at http://www.passc.net/EarthImpactDatabase/index.html.

Eitel, M., Gilder, S., Kunzmann, T., Pohl, J., 2014. Rochechouart impact crater melt breccias record no geomagnetic field reversal. Earth Planet. Sci. Lett. 387, 97-106, doi:10.1016/j.epsl.2013.11.021.

Eitel, M., Gilder, S., Spray, J., Thompson, L., Pohl, J., 2016. A paleomagnetic and rock magnetic study of the Manicouagan impact structure: implications for crater formation and geodynamo effects. J. Geophys. Res. 121, 1-19, doi:10.1002/2015JB012577.

Eitel, M., Volk, M., in prep. AF demagnetization and ARM acquisition at elevated temperatures in natural titanomagnetite bearing rocks.

Egli, R., Lowrie, W., 2002. Anhysteretic remanent magnetization of fine magnetic particles. J. Geophys. Res.: Solid Earth 107, EPM 2-1 - EPM 2-21, doi:10.1029/2001JB000671.

El Goresy, A., 1968. Electron microprobe analysis and ore microscopic study of magnetic spherules and grains collected from the Greenland ice. Contrib. Miner. Petrol. 17(4), 331-346, doi:10.1007/BF00380743.

El Goresy, A., Fechtig, H., Ottemann, T., 1968. The opaque minerals in impactite glasses. In: French, B., Short, N. (Eds.), Shock metamorphism of natural materials. pp. 531-554. Mono Book Corporation, Baltimore.

El Goresy, A., Chao, E., 1976. Identification and significance of armalcolite in the Ries glass. Earth Planet. Sci. Lett. 30, 200-208, doi: 10.1016/0012-821X(76)90246-6.

Elbra, T., Kontny, A., Pesonen, L., Schleifer, N., Schell, C., 2007. Petrophysical and paleomagnetic data of drill cores from the Bosumtwi impact structure, Ghana. Meteorit. Planet. Sci. 42, 829-838, doi:10.1111/j.1945-5100.2007.tb01078.x.

Elming, S., Bylund, G., 1991. Paleomagnetism of the Siljan impact structure, central Sweden. Geophys. J. Int. 105, 757-770, doi:10.1111/j.1365-246X.1991.tb00810.x

Elo, S., 1997. Interpretations of the gravity anomaly map of Finland. Geophysica 33, 51-80.

Fabian, K., Miyajima, N., Robinson, P., McEnroe, S., Boffa Ballaran, T., Burton, B., 2011. Chemical and magnetic properties of rapidly cooled metastable ferri-ilmenite solid solutions: Implications for magnetic self-reversal and exchange bias, I. Fe–Ti order transition in quenched synthetic ilmenite. Geophys. J. Int. 186, 997-1014, doi:10.1111/j.1365-246X.2011.05109.x.

Fackelmann, S., Morrow, J., Koeberl, C., McElvain, T., 2008. Shatter cone and microscopic shock-alteration evidence for a post-Paleoproterozoic terrestrial impact structure near Santa Fe, New Mexico, USA. Earth Planet. Sci. Lett. 270, 290-299, doi:10.1016/j.epsl.2008.03.033.

Fairchild, L., Swanson-Hysell, N., Tikoo, S., 2016. A matter of minutes: breccia dike paleomagnetism provides evidence for rapid crater modification. Geology 44(9), 723-726, doi:10.1130/G37927.1.

Fisher, R., 1953. Dispersion on a sphere. Proc. R. Soc. Lond. A 217, 295-305, doi:10.1098/rspa.1953.0064.

Floran, R., Grieve, R., Phinney, W., Warner, J., 1978. Manicouagan impact melt, Quebec, 1, stratigraphy, petrology, and chemistry. J. Geophys. Res. 83, 2737-2759, doi:10.1029/JB083iB06p02737.

French, B., 1998. Traces of Catastrophe: A Handbook of Shock Metamorphic Effects in Terrestrial Meteorite Impact Structures. LPI Contribution 954, 120 pp., Lunar and Planetary Institute, Houston.

Fregerslev, S., Carstens, H., 1976. FeNi metal in impact melt rocks of Lake Lappä-jarvi, Finland. Contrib. Miner. Petrol. 55(3), 255-263, doi:10.1007/BF00371336.

Gallet, Y., Krystyn, L., Marcoux, J., Besse, J., 2007. New constraints on the End-Triassic (Upper Norian–Rhaetian) magnetostratigraphy. Earth Planet. Sci. Lett. 255, 458-470, doi:10.1016/j.epsl.2007.01.004.

Gattacceca, J., Lamali, A., Rochette, P., Boustie, M., Berthe, L., 2007. The effects of explosive-driven shocks on the natural remanent magnetization and the magnetic properties of rocks. Phys. Earth Planet. Int. 162, 85-98, doi:10.1016/j.pepi.2007.03.006.

Gattacceca, J., Berthe, L., Boustie, M., Vadeboin, F., Rochette, P., De Resseguier, T., 2008. On the efficiency of shock magnetization processes. Phys. Earth Planet. Int. 166, 1-10, doi:10.1016/j.pepi.2007.09.005.

Gattacceca, J., Boustie, M., Lima, E., Weiss, B., Lamali, A., De Resseguier, T., Cuq-Lelandais, J., 2010. Unraveling the simultaneous shock magnetization of rocks. Phys. Earth Planet. Int. 182, 42-49, doi:10.1016/j.pepi.2010.06.009.

Gilder, S., Le Goff, M., Chervin, J., 2006. Static stress demagnetization of single and multidomain magnetite with implications for meteorite impacts. High Pressure Res. 26, 539-547, doi:10.1080/08957950601092085.

Gilder, S., Pohl, J., Eitel, M., 2018. Magnetic signatures of terrestrial meteorite impact craters: A summary. In: Lühr, H., Wicht, J., Gilder, S., Holschneider, M. (Eds.), Magnetic fields in the solar system. Springer, Cham, pp. 357-382, doi:10.1007/978-3-319-64292-5_13.

Gillingham, D., and Stacey, F., 1971. Anhysteretic remanent magnetization (ARM) in magnetite grains. Pure Appl. Geophys. PAGEOPH 91, 160-165, doi:10.1007/bf00879565.

Giroux, L., Benn, K., 2005. Emplacement of the Whistle dike, the Whistle embayment and hosted sulfides, Sudbury impact structure, based on anisotropies of magnetic susceptibility and magnetic remanence. Econ. Geol. 100, 1207-1227, doi:10.2113/gsecongeo.100.6.1207.

Glass, B., Heezen, B., 1967. Tektites and geomagnetic reversals. Nature 214, 372, doi:10.1038/214372a0.

Glass, B., Zwart, P., 1979. The Ivory Coast microtektite strewnfield: New data. Earth Planet. Sci. Lett. 43, 336-342, doi:10.1016/0012-821X(79)90220-6.

Glass, B., Kent, D., Schneider, D., Tauxe, L., 1991. Ivory Coast microtektite strewn field: description and relation to the Jaramillo geomagnetic event. Earth Planet. Sci. Lett. 107, 182-196, doi:10.1029/GL017i002p00163.

Glass, B., Lee, P., Osinski, G., 2002. Airborne geomagnetic investigations at the Haughton impact structure, Devon Island, Nunavut, Canada: New results. In: Lunar and Planetary Science Conference, vol. 33, p. 2008.

Glass, B., Domville, S., Lee, P., 2005. Further geophysical studies of the Haughton impact structure. In: Lunar and Planetary Science Conference, vol. 36, p. 2398.

Grieve, R., Robertson, P., Dence, M., 1981. Constraints on the formation of ring impact structures, based on terrestrial data. In: Schultz, P., Merrill, R. (Eds.) Multi-ring Basins, Proc. Lunar Planet. Sci., vol. 12A, pp. 37-57, Pergamon Press, New York, Oxford.

Grieve, R., Head, J., 1983. The Manicouagan impact structure: An analysis of its original dimensions and form. J. Geophys. Res. 88, A807-A818, doi:10.1029/JB088iS02p0A807.

Grieve, R., 1991. Terrestrial impact: The record in the rocks. Meteoritics 26, 175-194, doi:10.1111/j.1945-5100.1991.tb01038.x.

Grieve, R., Pesonen, L., 1992. The terrestrial impact cratering record. Tectonophysics 216, 1-30, doi:10.1016/0040-1951(92)90152-V.

Grieve, R., 2006. Impact Structures in Canada, 210 pp., Geol. Assoc, Canada.

Gucsik, A., 2009. Shock metamorphism of terrestrial impact structures and its application in the Earth and planetary sciences. In: Gucsik, A. (Ed.), Cathodoluminescence and its application in the planetary sciences. Springer, Berlin, Heidelberg, pp. 23-43, doi:10.1007/978-3-540-87529-1.

Halls, H., 1979. The Slate Islands meteorite impact site: a study of shock remanent magnetization. Geophys. J. R. Astron. Soc. 59, 553-559, doi:10.1111/j.1365-246X.1979.tb02573.x.

Hamano, Y., 1983. Experiments on the stress sensitivity of natural remanent magnetization. J. Geomagn. Geoelectr. 35, 155-172, doi:10.5636/jgg.35.155.

Hargraves, R., Perkins, W., 1969. Investigations of the effect of shock on natural remanent magnetism. J. Geophys. Res. 74, 2576-2589, doi:10.1029/JB074i010p02576.

Hargraves, R., 1970. Paleomagnetic evidence relevant to the origin of the Vredefort ring. J. Geol. 78, 253-263, doi:10.1086/627516.

Hargraves, R., Petersen, N., 1971. Notes on the correlation between petrology and magnetic properties of basaltic rocks, Zeitschrift für Geophys. 37, 367-382.

Hart, R., Andreoli, M., Reimold, W., Tredoux, M., 1991. Aspects of the dynamic and thermal metamorphic history of the Vredefort cryptoexplosion structure: implications for its origin. Tectonophysics 192, 313-331, doi:10.1016/0040-1951(91)90106-3.

Hart, R., Hargraves, R., Andreoli, M., Tredoux, M., Doucoure, C., 1995. Magnetic anomaly near the center of the Vredefort structure: implications for impact-related magnetic signatures. Geology 23, 277-280, doi:10.1130/0091-7613(1995)023<0277:MANTCO>2.3.CO;2.

Hartl, P., Tauxe, L., 1996. A precursor to the Matuyama/Brunhes transition-field instability as recorded in pelagic sediments. Earth Planet. Sci. Lett. 138, 121-135, doi:10.1016/0012-821X(95)00231-Z.

Hawke, P., 2003. Geophysical Investigation of the Wolfe Creek Meteorite Crater. Geological Survey of Western Australia, Perth.

Hawke, P., 2004. The geophysical signatures and exploration potential of Australia's meteorite impact structures. Thesis, University of Western Australia.

Henkel, H.,1992. Geophysical aspects of meteorite impact craters in eroded shield environment, with special emphasis on electric resistivity. Tectonophysics 216, 63-89, doi:10.1016/0040-1951(92)90156-Z.

Hervé, G., Chauvin, A., Lanos, P., 2013. Geomagnetic field variations in Western Europe from 1500 BC to 200 AD. Part I: Directional secular variation curve. Phys. Earth Planet. Inter. 218, 1-13, doi:10.1016/j.pepi.2013.02.002.

Hervé, G., Gilder, S., Marion, C., Osinski, G., Pohl, J., Petersen, N., Sylvester, P., 2015. Paleomagnetic and rock magnetic study of the Mistastin Lake impact structure (Labrador, Canada): Implications for geomagnetic perturbation and shock effects. Earth Planet. Sci. Lett. 417, 151-163, doi:10.1016/j.epsl.2015.02.011.

Hirt, A., Lowrie, W., Clendenen, W., Kligfield, R., 1993. Correlation of strain and the anisotropy of magnetic susceptibility in the Onaping formation: evidence for a near-circular origin of the Sudbury Basin. Tectonophysics 225, 231-254, doi:10.1016/0040-1951(93)90300-9.

Hodych, J., Dunning, G., 1992. Did the Manicouagan impact trigger end-of-Triassic mass extinction? Geology 20, 51-54, doi:10.1130/0091-7613(1992)020<0051:DTMITE>2.3.CO;2.

Hoffmann, V., Fehr, K., 1996. Micromagnetic, rock magnetic and mineralogical studies on dacitic pumice from the Pinatubo eruption (1991, Philippines) showing self-reversed TRM. Geophys. Res. Lett. 23, 2835-2838, doi:10.1029/96GL01317.

Hood, L., Richmond, N., Pierazzo, E., Rochette, P., 2003. Distribution of crustal magnetic fields on Mars: Shock effects of basin-forming impacts. Geophys. Res. Lett. 30, 1281, doi:10.1029/2002GL016657.

Jackson, G., 1992. Paleomagnetic study and magnetic modeling of the Vredefort Dome. PhD dissertation, University of Witwatersrand.

Jackson, M., Van der Voo, R., 1998. A paleomagnetic estimate of the age and thermal history of the Kentland, Indiana cryptoexplosion structure. J. Geol. 94, 713-723, doi:10.1086/629076.

Jahn, B., Floran, R., Simonds, C., 1978. Rb-Sr isochron age of the Manicouagan melt sheet, Quebec, Canada. J. Geophys. Res. 83, 2799-2803, doi:10.1029/JB083iB06p02799.

Jahnke, G., 2010. Methods for seismic wave propagation on local and global scales with finite differences. Dissertation. LMU München.

Jelinek, V., 1981. Characterization of the magnetic fabric of rocks. Tectonophysics 79, T63-T67, doi:10.1016/0040-1951(81)90110-4.

Jovane, L., Yokoyama, E., Seda, T., Burmester, R., Trindade, R., Housen, B., 2011. Rock magnetism of hematitic “bombs” from the Araguainha impact structure, Brazil. Geochem. Geophys. Geosyst. 12, Q12Z34, doi:10.1029/2011GC003758.

Kakol, Z., Sabol, J., Stickler, J., Kozlowski, A., Honig, J., 1994. Influence of titanium doping on the magnetocrystalline anisotropy of magnetite. Phys. Rev. B, 49, 12767-12772, doi:10.1103/PhysRevB.49.12767.

Kelley, S., Spray, J., 1997. A late Triassic age for the Rochechouart impact structure, France. Meteorit. Planet. Sci. 32, 629-636, doi:10.1111/j.1945-5100.1997.tb01548.x.

Kenkmann, T., Wittmann, A., Scherler, D., 2004. Structure and impact indicators of the Cretaceous sequence of the ICDP drill core Yaxcopoil-1, Chicxulub impact crater, Mexico. Meteorit. Planet. Sci. 39, 1069-1088, doi:10.1111/j.1945-5100.2004.tb01129.x.

Kent, D.V., 1998. Impacts on Earth in the Late Triassic. Nature 395, 126, doi:10.1038/25874.

Kent, D., Olsen, P., 1999. Astronomically tuned geomagnetic polarity timescale for the Late Triassic. J. Geophys. Res. 104, 12,831-12,841, doi:10.1029/1999JB900076.

Kirschvink, J., 1980. The least-squares line and plane and the analysis of palaeomagnetic data. Geophys. J. R. Astron. Soc. 62, 699-718, doi:10.1111/j.1365-246X.1980.tb02601.x.

Koch, S., Gilder, S., Pohl, J., Trepmann, C., 2012. Geomagnetic field intensity recorded after impact in the Ries meteorite crater, Germany. Geophys. J. Int. 189, 383-390, doi:10.1111/j.1365-246X.2012.05399.x.

Kontny, A., Elbra, T., Just, J., Pesonen, L., Schleicher, A., Zolk, J., 2007. Petrography and shock-related remagnetization of pyrrhotite in drill cores from the Bosumtwi impact crater drilling project, Ghana. Meteorit. Planet. Sci. 42, 811-827, doi:10.1111/j.1945-5100.2007.tb01077.x.

Krása, D., Shcherbakov, V., Kunzmann, T., Petersen, N., 2005. Self-reversal of remanent magnetization in basalts due to partially oxidized titanomagnetites. Geophys. J. Int. 162, 115-136, doi:10.1111/j.1365-246X.2005.02656.x.

Kraut, F., French, B., 1971. The Rochechouart meteorite impact structure, France: Preliminary geological results. J. Geophys. Res. 76, 5407-5413, doi:10.1029/JB076i023p05407.

Kring, D., 2017. Guidebook to the geology of Barringer Meteorite Crater, Arizona (a.k.a. Meteor Crater). 2nd edition, LPI Contribution 2040, 272 pp., Lunar and Planetary Institute, Houston.

Koeberl, C., 1994. African meteorite impact craters: characteristic and geological importance. J. Afr. Earth Sci. 18, 263-295, doi:10.1016/0899-5362(94)90068-X.

Kukkonen, I., Kivekäs, L., Paananen, M., 1992. Physical properties of kärnäite (impact melt), suevite and impact breccia in the Lappajärvi meteorite crater, Finland. Tectonophysics 216, 111-122, doi:10.1016/0040-1951(92)90159-4.

Lambert, P., 1974. La structure d'impact de météorite géante de Rochechouart. Ph.D. thesis. Université de Paris-Sud.

Lambert, P., 1977a. The Rochechouart crater: Shock zoning study. Earth Planet. Sci. Lett. 35, 258-268, doi:10.1016/0012-821X(77)90129-7.

Lambert, P., 1977b. Rochechouart impact crater: Statistical geochemical investigations and meteoritic contamination. In: Roddy, D., Pepin, R., Merrill, R. (Eds.), Impact and Explosion Cratering. Pergamon, New York, pp. 449-460.

Lambert, P., 2010. Target and impact deposits at Rochechouart impact structure, France. Spec. Pap., Geol. Soc. Am. 465, 509-541, doi:10.1130/2010.2465(25).

Larochelle, A., Currie, K., 1967. Paleomagnetic study of igneous rocks from the Manicouagan structure, Quebec. J. Geophys. Res. 72, 4163-4169, doi:10.1029/JZ072i016p04163.

Le Bars, M., Wieczorek, M., Karatekin, Ö., Cébron, D., Laneuville, M., 2011. An impact-driven dynamo for the early Moon. Nature 479, 215-218, doi:10.1038/nature10565.

Leonhardt, R., Heunemann, C., Krása, D., 2004. Analyzing absolute paleointensity determinations: Acceptance criteria and the software ThellierTool4.0. Geochem. Geophys. Geosyst. 5, Q12016, doi:10.1029/2004GC000807.

Leonhardt, R., Matzka, J., Nichols, A.R.L., Dingwell, D.B., 2006. Cooling rate correction of paleointensity determination for volcanic glasses by relaxation geospeedometry. Earth Planet. Sci. Lett. 243, 282-292, doi:10.1016/j.epsl.2005.12.038.

Leonhardt, R., Fabian, K., 2007. Paleomagnetic reconstruction of the global geomagnetic field evolution during the Matuyama/Brunhes transition: Iterative Bayesian inversion and independent verification. Earth Planet. Sci. Lett. 253, 172-195, doi:10.1016/j.epsl.2006.10.025.

Levi, S., 1979. The additivity of partial thermal remanent magnetization in magnetite. Geophys. J. Int. 59, 205-218, doi:10.1111/j.1365-246x.1979.tb02561.x.

Lillis, R., Robbins, S., Manga, M., Halekas, J., Frey, H., 2013. Time history of the Martian dynamo from crater magnetic field analysis. J. Geophys. Res. Planets 118, 1-24, doi:10.1002/jgre.20105.

Lipman, P., 1971. Iron-titanium oxide phenocrysts in compositionally zoned ash-flow sheets from southern Nevada. J. Geol. 79, 438-456.

Loper, D., McCartney, K., 1990. On impacts as a cause of geomagnetic field reversals or flood basalts. Spec. Pap., Geol. Soc. Am. 247, 19-26.

Louzada, K., Weiss, B., Maloof, A., Stewart, S., Swanson-Hysell, N., Soule, S., 2008. Paleomagnetism of Lonar impact crater, India. Earth Planet. Sci. Lett. 275, 308-318, doi:10.1016/j.epsl.2008.08.025.

Louzada, K., Stewart, S., Weiss, B., Gattacceca, J., Bezaeva, N., 2010. Shock and static pressure demagnetization of pyrrhotite and implications for the Martian crust. Earth Planet. Sci. Lett. 290, 90-101, doi:10.1016/j.epsl.2009.12.006.

Lugo Centeno, C., Cavosie, A., First report of shocked zircon at the Santa Fe impact structure (USA) (abs.). 45th Lunar Planet. Sci. Conf., 1839.

Macdonald, F., Wingate, M., Mitchell, K., 2005. Geology and age of the Glikson impact structure, Western Australia. Aust. J. Earth Sci. 52, 641-651, doi:10.1080/08120090500170419.

Mang, C., Kontny, A., Harries, D., Langenhorst, F., Hecht, L., 2012. Iron deficiency in pyrrhotite of suevites from the Chespeake Bay impact crater, USA. A consequence of shock metamorphism? Meteorit. Planet. Sci. 47, 277-295, doi:10.1111/j.1945-5100.2012.01329.x.

Master, S., Reimold, W., Brandt, D., Koeberl, C., Robertson, D., Antoine, L., 1994. The Highbury structure, a new impact crater in N.W. Zimbabwe (abs.). Lunar Planet. Sci. XXV, 847-848.

Melero-Asensio, I., Martín-Hernández, F., Ormö, J., 2015. A rock magnetic profile through the ejecta flap of the Lockne impact crater (central Sweden) and implications for the impact excavation process. J. Appl. Geophys. 112, 91-105, doi:10.1016/j.jappgeo.2014.11.009.

Melosh, H., Ivanov, B., 1999. Impact crater collapse. Annu. Rev. Earth Planet. Sci. 27, 385-415, doi:10.1146/annurev.earth.27.1.385.

Misra, S., Arif, M., Basavaiah, N., Srivastava, P., Dube, A., 2010. Structural and anisotropy of magnetic susceptibility (AMS) evidence for oblique impact on terrestrial basalt flows: Lonar crater, India. Geol. Soc. Am. Bull. 122, 563-574, doi:10.1130/B26550.1.

Morris, R., Golden, D., Bell, J., Lauer, H., 1995. Hematite, pyroxene, and phyllosilicates on Mars: Implications from oxidized impact melt rocks from Manicouagan Crater, Quebec, Canada. J. Geophys. Res. 100, 5319-5328, doi:10.1029/94JE01500.

Moskowitz, B., Frankel, R., Bazylinski, D., 1993. Rock magnetic criteria for the detection of biogenic magnetite. Earth Planet. Sci. Lett. 120, 283-300, doi:10.1016/0012-821X(93)90245-5.

Muller, R., Morris, D., 1986. Geomagnetic reversals from impacts on the Earth. Geophys. Res. Lett. 13, 1177-1180, doi:10.1029/GL013i011p01177.

Muundjua, M., Hart, R., Gilder, S., Carporzen, L., Galdeano, A., 2007. Magnetic imaging of the Vredefort impact crater, South Africa. Earth Planet. Sci. Lett. 261, 456-468, doi:10.1016/j.epsl.2007.07.044.

Nagata, T., 1953. Self-reversal of thermo-remanent magnetization of igneous rocks. Nature 172, 850-852, doi:10.1038/172850a0.

Nakamura, N., Iyeda, Y., 2005. Magnetic properties and paleointensity of pseudotachylites from the Sudbury structure, Canada: petrologic control. Tectonophysics 402, 141-152, doi:10.1016/j.tecto.2004.10.015.

Natural Resources of Canada, Geoscience Data Repository for Geophysical Data, 2014. Available at http://gdr.agg.nrcan.gc.ca/gdrdap/dap/search-eng.php.

Néel, L., 1949. Théorie du traînage magnétique des ferromagnétiques en grains fins avec applications aux terrescuites. Ann. Géophys. 55, 99-136.

Néel, L., 1951. L'inversion de l'aimentation permanente des roches. Ann. Geophys. 7, 90-102.

Nishioka, I., Funaki, M., 2008. Irreversible changes in anisotropy of magnetic susceptibility. Study of basalts from lunar crater and experimentally impacted basaltic andesite. In: Meteoritics & Planetary Science, vol. 43, p. A116. Meteoritical Society, Chantilly.

O'Connell-Cooper, C., Spray, J., 2011. Geochemistry of the impact-generated melt-sheet at Manicouagan: Evidence for fractional crystallization. J. Geophys. Res. 116, B06204, doi:10.1029/2010JB008084.

O'Connell-Cooper, C., Dickin, A., Spray, J., 2012. The Manicouagan impact melt sheet: Evidence for isotopic homogenization with limited assimilation. Earth Planet. Sci. Lett. 335–336, 48-58, doi:10.1016/j.epsl.2012.04.033.

Öhman, T., Lorenz, K., Pesonen, L., Badjukov, D., Raitala, J., Elo, S., Ojala, K., Nishioka, I., Funaki, M., 2003. Kara impact structure, Russia: Recent developments in petrophysical and geochemical studies. In: Large Meteorite Impacts, p. 4071.

Onorato, P., Uhlmann, D., Simonds, C., 1978. The thermal history of the Manicouagan impact melt sheet, Quebec. J. Geophys. Res. 83, 2789-2798, doi:10.1029/JB083iB06p02789.

Osinski, G., Spray, J., Lee, P., 2001. Impact-induced hydrothermal activity within the Haughton impact structure, arctic Canada: Generation of a transient, warm, wet oasis. Meteorit. Planet. Sci. 36, 731-745, doi:10.1111/j.1945-5100.2001.tb01910.x.

Osinski, G., Spray, J., 2006. Shatter cones of the Haughton impact structure, Canada. Proceedings of the 1st International Conference on Impact Cratering in the Solar System, European Space Agency Special Publication SP-612, 95-99.

Osinski, G., Ferriere, L., 2016. Shatter cones: (mis)understood? Sci. Adv. 2, e1600616, doi:10.1126/sciadv.1600616.

Pal, P., Creer, K., 1986. Geomagnetic reversal spurts and episodes of extraterrestrial catastrophism. Nature 320, 148-150, doi:10.1038/320148a0.

Patton, B., Fitch, J., 1962. Anhysteretic remanent magnetization in small steady fields. J. Geophys. Res. 67, 307-311, doi:10.1029/JZ067i001p00307.

Pesonen, L., Marcos, N., Pipping, F., 1992. Palaeomagnetism of the Lappajärvi impact structure, western Finland. Tectonophysics 216, 123-142, doi:10.1016/0040-1951(92)90160-8.

Phinney, W., Simonds, C., 1977. Dynamical implications of the petrology and distribution of impact melt rocks. In: Roddy, D., Pepin, R., Merrill, R. (Eds.), Impact and explosion cratering. Pergamon Press, New York, pp. 771-790.

Pierazzo, E., Vickery, A., Melosh, H., 1997. A reevaluation of impact melt production. Icarus 127, 408-423, doi:10.1006/icar.1997.5713.

Pierazzo, E., Melosh, H., 2000. Melt production in oblique impact. Icarus 145, 252-261, doi:10.1006/icar.1999.6332

Pierazzo, E., Melosh, H., 2013. Environmental effects of impact events. In: Osinski, G., Pierazzo, E. (Eds.), Impact cratering: Processes and products. Blackwell, Oxford, pp. 146-156.

Pilkington, M., Grieve, R., 1992. The geophysical signature of terrestrial impact craters. Rev. Geophys. 30, 161-181, doi:10.1029/92RG00192.

Pilkington, M., Hildebrand, A., 2000. Three-dimensional magnetic imaging of the Chicxulub crater. J. Geophys. Res. 105, 23479-23491, doi:10.1029/2000JB900222.

Pilkington, M., Ames, D., Hildebrand, A., 2004. Magnetic mineralogy of the Yaxcopoil-1 core, Chicxulub. Meteorit. Planet. Sci. 39, 831-841, doi:10.1111/j.1945-5100.2004.tb00933.x.

Plado, J., Pesonen, L., Puura, V., 1999. Effect of erosion on gravity and magnetic signatures of complex impact structures: geophysical modeling and applications. In: Dressler, B., Sharpton, V. (Eds.), Large Meteorite Impacts and Planetary Evolution II, volume special paper 339, pp. 229-239. Geological Society of America, Boulder.

Plado, J., Pesonen, L., Koeberl, C., Elo, S., 2000. The Bosumtwi meteorite impact structure, Ghana: a magnetic model. Meteorit. Planet. Sci. 35, 723-732, doi:10.1111/j.1945-5100.2000.tb01456.x.

Pohl, J., 1965. Die Magnetisierung der Suevite des Rieses. Neues Jahrb. Miner. Monatsh. 1965, 268-276.

Pohl, J., Soffel, H., 1971. Paleomagnetic age determination of the Rochechouart impact structure (France). Z. Geophys. 37, 857-866.

Pohl, J., Bleil, U., Hornemann, U., 1975. Shock magnetization and demagnetization of basalt by transient stress up to 10 kbar. J. Geophys. 41, 23-41.

Pohl, J., 1977. Paläomagnetische und gesteinsmagnetische Untersuchungen an den Kernen der Forschungsbohrung Nördlingen 1973. Geol. Bavarica 75, 329-348.

Pohl, J., Stoffler, D., Gall, H., Ernston, K., 1977. Impact and explosion cratering. In: Roddy, D., Pepin, R., Merrill, R. (Eds.), Impact and Explosion Cratering, pp. 343-404. Pergamon Press, Oxford.

Pohl, J., Eckstaller, A., Robertson, P., Hajnal, Z., 1985. First results of a multidisciplinary analysis of the Haughton Dome impact structure, Devon Island, Canada. In: Lunar and Planetary Science Conference, vol. 16, pp. 669-670.

Pohl, J., Eckstaller, A., Robertson, P., 1988. Gravity and magnetic investigations in the Haughton impact structure, Devon Island, Canada. Meteoritics 23, 235-238.

Pohl, J., Ernstson, K., 1994. Gravity investigations in the Rochechouart impact structure (abstract). In: European Science Foundation, Third International Workshop on shock wave behaviour of solids in nature and experiments. Limoges, France.

Prévot, M., Hoffman, K., Goguitchaichvili, A., Doukhan, J., Shcherbakov, V., Bina, M., 2001. The mechanism of self-reversal of thermoremanence in natural hemoilmenite crystals: new experimental data and model. Phys. Earth Planet. Inter. 126, 75-92, doi:10.1016/S0031-9201(01)00245-X.

Quesnel, Y., Gattacceca, J., Osinski, G., Rochette, P., 2013. Origin of the central magnetic anomaly at the Haughton impact structure, Canada. Earth Planet. Sci. Lett. 367, 116-122, doi:10.1016/j.epsl.2013.02.032.

Quintana, S., Crawford, D., Schultz, P., 2015. Analysis of impact melt and vapor production in CTH for planetary applications. Proc. Eng. 103, 499-506, doi:10.1016/j.proeng.2015.04.065.

Raiskila, S., Salminen, J., Elbra, T., Pesonen, L., 2011. Rock magnetic and paleomagnetic study of the Keurusselkä impact structure, central Finland. Meteorit. Planet. Sci. 46, 1670-1687, doi:10.1111/j.1945-5100.2011.01255.x.

Rao, G., Bhalla, M., 1984. Lonar Lake: palaeomagnetic evidence of shock origin. Geophys. J. Int. 77, 847-862, doi:10.1111/j.1365-246X.1984.tb02225.x.

Rebolledo-Vieyra, M., Urrutia-Fucugauchi, J., 2004. Magnetostratigraphy of the impact breccias and post-impact carbonates from borehole Yaxcopoil-1, Chicxulub impact crater, Yucatan, Mexico. Meteorit. Planet. Sci. 39, 821-829, doi:10.1111/j.1945-5100.2004.tb00932.x.

Rebolledo-Vieyra, M., Urrutia-Fucugauchi, J., López-Loera, H., 2010. Aeromagnetic anomalies and structural model of the Chicxulub multiring impact crater, Yucatan, Mexico. Rev. Mex. Cienc. Geol. 27, 185-195,

Reimold, W., Bischoff, L., Oskierski, W., Schäfer, H., 1984. Genesis of pseudotachylite veins in the basement of the Rochechouart impact crater, France. I. Geological and petrographical evidence (abs.). Lunar Planet. Sci. XV, 683-684.

Reimold, W., Master, S., Koeberl, C., Robertson, D., 1994. The 1993 Zimbabwe impact crater and meteorite expedition (abs.). Meteorit. 29, 521-522.

Reimold, W., Koeberl, C., 2014. Impact structures in Africa: A review. J. Afr. Earth Sci. 93, 57-175, doi:10.1016/j.jafrearsci.2014.01.008.

Reznik, B., Kontny, A., Fritz, J., Gerhards, U., 2016. Shock-induced deformation phenomena in magnetite and their consequences on magnetic properties. Geochem. Geophys. Geosyst. 17, 393-396, doi:10.1002/2016GC006338.

Rice, A., Creer, K., 1989. Geomagnetic polarity reversals: Can meteor impacts cause spall disruption into the outer core? In: Lowes, F., Collinson, D., Parry, J., Runcorn, S., Tozer, D., Soward, A. (Eds.), Geomagnetism and Palaeomagnetism, pp. 227-230. Springer Science, Dordrecht, doi:10.1007/978-94-009-0905-2_16.

Riisager, P., Riisager, J., 2001. Detecting multidomain magnetic grains in Thellier palaeointensity experiments. Phys. Earth Planet. Inter. 125, 111-117, doi:10.1016/s0031-9201(01)00236-9.

Roberts, J., Lillis, R., Manga, M., 2009. Giant impacts on early Mars and the cessation of the Martian dynamo. J. Geophys. Res. 114, E04009, doi:10.1029/2008JE003287.

Robertson, P., Mason, G., 1975. Shatter cones from Haughton Dome, Devon Island, Canada. Nature 255, 393-394, doi:10.1038/255393a0.

Robertson, W., 1967. Manicouagan, Quebec, paleomagnetic results. Can. J. Earth Sci. 4, 641-649.

Roest, W., Pilkington, M., 1994. Restoring post-impact deformation at Sudbury: A circular argument. Geophys. Res. Lett. 21, 959-962, doi:10.1029/93GL02044.

Salminen, J., Pesonen, L., Reimold, W., Donadini, F., Gibson, H., 2009. Paleomagnetic and rock magnetic study of the Vredefort impact structure and the Johannesburg Dome, Kaapvaal craton, South Africa – implications for the apparent polar wander path of the Kaapvaal craton during the Mesoproterozoic. Precambrian Res. 168, 167-184, doi:10.1016/j.precamres.2008.09.005.

Salminen, J., Pesonen, L., Lahti, K., Kannus, K., 2013. Lightning-induced remanent magnetization – the Vredefort impact structure, South Africa. Geophys. J. Int. 195, 117-129, doi:10.1093/gji/ggt230.

Schmieder, M., Buchner, E., Schwarz, W., Trieloff, M., Lambert, P., 2010. A Rhaetian $^{40}Ar/^{39}Ar$ age for the Rochechouart impact structure (France) and implications for the latest Triassic sedimentary record. Meteorit. Planet. Sci. 45, 1225-1242, doi:10.1111/j.1945-5100.2010.01070.x.

Schneider, D., Kent, D., 1990. Ivory Coast microtectites and geomagnetic reversals. Geophys. Res. Lett. 17,163-166, doi: 10.1029/GL017i002p00163.

Schneider, D., Kent, D., Mello, G., 1992. A detailed chronology of the Australasian impact event, the Brunhes-Matuyama geomagnetic polarity reversal, and global climate change. Earth Planet. Sci. Lett. 111, 395-405, doi:10.1016/0012-821X(92)90192-X.

Schult, A., 1968. Self-reversal of magnetization and chemical composition of titano-magnetites in basalts. Earth Planet. Sci. Lett. 4, 57-63, doi:10.1016/0012-821X(68)90054-X.

Schwarzschild, B., 1987. Do asteroid impacts trigger geomagnetic reversals? Phys. Today 40, 17, doi:10.1063/1.2819902.

Scott, R., Grieve, R., Pilkington, M., 1996. Petrographic and rock magnetic study of the central magnetic anomaly, Manicouagan impact structure, Canada (abstract). Lunar Planet. Sci. XXVII, 1163-1164.

Scott, R., Pilkington, M., Tanczyk, E., 1997. Magnetic investigations of the West Hawk, Deep Bay and Clearwater impact structures, Canada. Meteorit. Planet. Sci. 32, 293-308, doi:10.1111/j.1945-5100.1997.tb01267.x.

Scott, R., Spray, J., 1999. Magnetic fabric constraints on friction melt flow regimes and ore emplacement direction within the South Range breccia belt, Sudbury impact structure. Tectonophysics 307, 163-189, doi:10.1016/S0040-1951(99)00124-9.

Selkin, P.A., Gee, J.S., Tauxe, L., Meurer, W.P., Newel, A.J., 2000. The effect of remanence anisotropy on paleointensity estimates: A case study from the Archean Stillwater Complex. Earth Planet. Sci. Lett. 183, 403-416, doi:10.1016/S0012-821X(00)00292-2.

Shcherbakov, V., Shcherbakova, V., 2001. On the suitability of the Thellier method of palaeointensity determinations on pseudo-single-domain and multidomain grains. Geophys. J. Int. 146, 20-30, doi:10.1046/j.0956-540x.2001.01421.x.

Shcherbakova, V., Shcherbakov, V., Heider, F., 2000. Properties of partial thermoremanent magnetization in pseudosingle domain and multidomain magnetite grains. J. Geophys. Res.: Solid Earth 105, 767-781, doi10.1029/1999jb900235.

Shoemaker, E., 1977. Why study impact craters? In: Roddy, D., Pepin, R., Merrill, R. (Eds.), Impact and Explosion Cratering, Pergamon, New York, pp. 1-10.

Shoemaker, E., Shoemaker, C., 1997. Glikson, a probable impact structure, western Australia. In: Lunar and Planetary Science XXVIII, p. 1669.

Spray, J., Kelley, S., Rowley, D., 1998. Evidence for a late Triassic multiple impact event on Earth. Nature 392, 171-173, doi:10.1038/32397.

Spray, J., Butler, H., Thompson, L., 2004. Tectonic influences on the morphometry of the Sudbury impact structure: Implications for terrestrial cratering and modeling. Meteorit. Planet. Sci. 39, 287-301, doi:10.1111/j.1945-5100.2004.tb00341.x.

Spray, J., Thompson, L., 2008. Constraints on central uplift structure from the Manicouagan impact crater. Meteorit. Planet. Sci. 43, 2049-2057, doi:10.1111/j.1945-5100.2008.tb00660.x.

Spray, J., Thompson, L., Biren, M., O'Connell-Cooper, C., 2010. The Manicouagan impact structure as a terrestrial analogue site for lunar and martian planetary science. Planet. Space Sci. 58, 538-551, doi:10.1016/j.pss.2009.09.010.

Stacey, F., 1963. The physical theory of rock magnetism. Adv. Phys. 12 , 45-133, doi:10.1080/00018736300101263.

Steiger, R., Jäger, E., 1978. Subcommission on geochronology: Convention on the use of decay constants in geo- and cosmochronology. In: Cohee, G., Glaessner, M., Hedberg, H. (Eds.), AAPG Special Volume SG6: Contributions to the Geologic Time Scale, pp. 67-71, Am. Assoc. of Pet. Geol., Sydney.

Steiner, M., 1996. Implications of magneto-mineralogic characteristics of the Manson and Chicxulub impact craters. In: Ryder, G., Fastovski, D., Gartner, S. (Eds.), The Cretaceous-Tertiary Event and Other Catastrophes in Earth History, volume special paper 307, pp. 89-104. Geological Society of America, Boulder.

Stevenson, J., Stevenson, L., 1980. Sudbury, Ontario, and the meteorite theory. Geosci. Can. 7, 103-108.

Sugiura, N., 1979. ARM, TRM and magnetic interactions: Concentration dependence. Earth Planet. Sci. Lett. 42, 451-455, doi:10.1016/0012-821x(79)90054-2.

Swanson-Hysell, N., Feinberg, J., Berquó, T., Maloof, A., 2011. Self-reversed magnetization held by martite in basalt flows from the 1.1-billion-year-old Keweenawan rift, Canada. Earth Planet. Sci. Lett. 305, 171-184, doi:10.1016/j.epsl.2011.02.053.

Tauxe, L., Pick, T., Kok, Y., 1995. Relative paleointensity in sediments: A pseudo-Thellier approach. Geophys. Res. Lett. 22, 2885-2888, doi:10.1029/95gl03166.

Taylor, S., 2001. Solar System Evolution: A New Perspective. 460 pp., Cambridge Univ. Press, Cambridge, New York, Oakleigh, Madrid and Cape Town.

Thellier, E., 1938. Sur l'aimantation des terres cuites et ses applications géophysiques. PhD thesis, IPGP, Université de Paris.

Thellier, E., Thellier, O., 1959. Sur l'intensité du champ magnétique terrestre dans le passé historique et géologique. Ann. Geophys. 15, 285-376.

Tikoo, S., Gattacceca, J., Swanson-Hysell, N., Weiss, B., Suavet, C., Cournède, C., 2015. Preservation and detectability of shock-induced magnetization. J. Geophys. Res. 120, 1461-1475, doi:10.1002/2015JE004840.

Torsvik, T., Van der Voo, R., Meert, J., Mosar, J., Walderhaug, H., 2001. Reconstruction of the continents around the North Atlantic at about the 60th parallel. Earth Planet. Sci. Lett. 187, 55-69, doi:10.1016/S0012-821X(01)00284-9.

Torsvik, T., Müller, D., Van der Voo, R., Steinberger, B., Gaina, C., 2008. Global plate motion frames: Toward a unified model. Rev. Geophys. 46. RG3004, doi:10.1029/2007RG000227.

Trepmann, C., 2008. Shock effects in quartz: Compression versus shear deformation – An example from the Rochechouart impact structure, France. Earth Planet. Sci. Lett. 267, 322-332, doi:10.1016/j.epsl.2007.11.035.

Turcotte, D., Schubert, G., 1982. Geodynamics – Applications of Continuum Physics to Geological Problems. John Wiley, New York.

Ugalde, H., Artemieva, N., Milkereit, B., 2005. Magnetization on impact structures - constraints from numerical modelling and petrophysics. In: Kenkmann, T., Hörz, F., Deutsch, A. (Eds.), Large Meteorite Impacts III, volume special paper 384, pp. 24-42. Geological Society of America, Boulder.

Urrutia-Fucugauchi, J., Marin, L., Sharpton, V., 1994. Reverse polarity magnetized melt rocks from the Cretaceous/Tertiary Chicxulub structure, Yucatan peninsula, Mexico. Tectonophysics 237, 105-112, doi:10.1016/0040-1951(94)90161-9.

Urrutia-Fucugauchi, J., Soler-Arechalde, A., Rebolledo-Vieyra, M., Vera-Sanchez, P., 2004a. Paleomagnetic and rock magnetic study of the Yaxcopoil-1 impact breccia sequence, Chicxulub impact crater (Mexico). Meteorit. Planet. Sci. 39, 843-856, doi:10.1111/j.1945-5100.2004.tb00934.x.

Urrutia-Fucugauchi, J., Morgan, J., Stöffler, D., Claeys, P., 2004b. The Chicxulub Scientific Drilling Project (CSDP). Meteorit. Planet. Sci. 39, 787-790, doi:10.1111/j.1945-5100.2004.tb00928.x.

Valeev, K., Absalyamov, S., 2000. Remanent magnetization of magnetite under high pressures and shear loads. Izv. Phys. Solid Earth 36, 241-245.

Valet, J., Fournier, A., Courtillot, V., Herrero-Bervera, E., 2012. Dynamical similarity of geomagnetic field reversals. Nature 490, 89-93, doi:10.1038/nature11491.

van Soest, M., Hodges, K., Wartho, J., Biren, M., Montelone, B., Ramezani, J., Spray, J., Thompson, L., 2011. (U-Th)/He dating of terrestrial impact structures: The Manicouagan example. Geochem. Geophys Geosyst. 12, Q0AA16, doi:10.1029/2010GC003465.

Velasco-Villareal, M., Urrutia-Fucugauchi, J., Rebolledo-Vieyra, M., Perez-Cruz, L., 2011. Paleomagnetism of impact breccias from the Chicxulub crater: implications for ejecta emplacement and hydrothermal processes. Phys. Earth Planet. Inter. 186, 154-171, doi:10.1016/j.pepi.2011.04.003.

Verhoogen, J., 1956. Ionic ordering and self-reversal of magnetization in impure magnetites. J. Geophys. Res. 61, 201-209, doi:10.1029/JZ061i002p00201.

Volk, M., Gilder, S., 2016. Effect of static pressure on absolute paleointensity recording with implications for meteorites. J. Geophys. Res.: Solid Earth 121, 5596-5610, doi:10.1002/2016jb013059.

Wack, M., 2010. A new software for the measurement of magnetic moments using SQUID and spinner magnetometers. Comput. Geosci. 36, 1178-1184, doi:10.1016/j.cageo.2010.05.002.

Wack, M., 2012. Anisotropy of magnetic remanence: development of an automated system and application to natural sediments. PhD Dissertation. LMU München, Faculty of Geosciences.

Wack, M., Gilder, S., 2012. The SushiBar: An automated system for paleomagnetic investigations. Geochem. Geophys. Geosyst. 13, Q12Z38, doi:10.1029/2011GC003985.

Wei, Q., Gilder, S., Maier, B., 2014. Pressure dependence on the remanent magnetization of Fe-Ni alloys and Ni metal. Phys. Rev. B 90, 144425-1 - 144425-8, doi:10.1103/PhysRevB.90.144425.

Wolfe, S., 1971. Potassium-argon ages of the Manicouagan-Mushalagan lakes structure. J. Geophys. Res. 76, 5424-5436, doi:10.1029/JB076i023p05424.

Won, I., Kuo, J., 1973. Oscillation of the Earth's inner core and its relation to the generation of geomagnetic field. J. Geophys. Res. 78, 905-911, doi:10.1029/JB078i005p00905.

Yokoyama, E., Brandt, D., Tohver, E., Trindade, R., 2014. Palaeomagnetism of the Permo-Triassic Araguainha impact structure (central Brazil) and implications for Pangean reconstructions. Geophys. J. Int. 198, 154-163, doi:10.1093/gji/ggu125.

Yokoyama, E., Nédélec, A., Baratoux, D., Trindade, R., Fabre, S., Berger, G., 2015. Hydrothermal alteration in basalts from Vargeao impact structure, south Brazil, and implications for recognition of impact-induced hydrothermalism on Mars. Icarus 252, 347-365, doi:10.1016/j.icarus.2015.02.001.

Yu, Y., Dunlop, D., Özdemir, Ö., 2002a. Partial anhysteretic remanent magnetization in magnetite, 1. additivity. J. Geophys. Res.: Solid Earth 107, EPM 7-1 - EPM 7-9, doi:10.1029/2001jb001249.

Yu, Y., Dunlop, D., Özdemir, Ö., 2002b. Partial anhysteretic remanent magnetization in magnetite, 2. reciprocity. J. Geophys. Res.: Solid Earth, 107, EPM 8-1 - EPM 8-9, doi:10.1029/2001jb001269.

Yu, Y., Dunlop, D., Özdemir, Ö., 2003. Are ARM and TRM analogs? Thellier analysis of ARM and pseudo-Thellier analysis of TRM. Earth Planet. Sci. Lett. 205, 325-336, doi:10.1016/s0012-821x(02)01060-9.

Yu, Y., Tauxe, L., 2005. Testing the IZZI protocol of geomagnetic field intensity determination. Geochem. Geophys. Geosyst. 6, Q05H17, doi:10.1029/2004GC000840.

Zylberman, W., Gattacceca, J., Quesnel, Y., Rochette, P., Osinski, G., Demory, F., 2015. Paleomagnetism in complex impact structures: examples from the Haughton and West Clearwater impacts, Canada. LPI Contributions 1861, 1101.

Acknowledgments

First of all, I wish to express my thanks to my adviser, Stuart Gilder, to give me the opportunity to work on this highly interesting research topic. I also thank him for his advice, help and ideas, of which this dissertation took a lot of profit, as well as for his patience.

The DFG (Deutsche Forschungsgsmeinschaft) is thanked for financing most of this thesis through Schwerpunktprogramm SPP 1488 “Planetary Magnetism”.

I am very grateful of Jean Pohl, of whose expertise in meteorite impact craters I was profiting a lot. Nikolai Petersen is acknowledged for his help with the VFTB and with the interpretations of our rock magnetic results. Michael Wack is thanked for making the SushiBar available and explaining me how to use it. I thank Melanie Kaliwoda for her help with the use of the Raman spectrometer.

Thomas Kunzmann is thanked a lot for his patience with me at the electron microprobe as well as for the great field trip to Namibia. Many thanks to Mike Volk and Vasyl Gyshchyn for the funny field trip(s) to the Siljan crater. Mike is also acknowledged for our common work that forms the last chapter of this thesis.

I thank Manuela Weiß a lot for her indispensable introduction into, advice for, and help with the instruments situated in Niederlippach. Denise Schmid is acknowledged for lab measurements. I express my thanks Markus Sieber, Günter Hesberg and the workshop team for preparing various mechanical parts.

I am grateful to my former and current office mates and all the colleagues at the department who made my days at the institute more pleasant.

Last, but not least, I thank my parents and all my friends including the lunch group.